

DIFFUSION OF HE³
IN SUPERFLUID BACKGROUND

by

George Arthur Herzlinger

S.B. Massachusetts Institute of Technology (1965)

Submitted in Partial Fulfillment

of the Requirements for the

Degree of

Doctor of Philosophy

at the

Massachusetts Institute of Technology

August, 1971

Signature of Author.....
Department of Physics
August 16, 1971

Certified by.....
Thesis Supervisor

Accepted by.....
Chairman,
Departmental Committee on Graduate Students

Archives



ABSTRACT

Diffusion of He^3 in Superfluid Background

George Arthur Herzlinger

Submitted to the Department of Physics on August 16, 1971 in partial fulfillment of the requirement for the degree of Doctor of Philosophy.

The diffusion constant has been measured in dilute $\text{He}^3\text{-He}^4$ solutions at temperatures from 1.27° to 1.69°K , at concentrations of the order of 10^{-4} . Under these conditions, the diffusion is determined by the interaction between the He^3 solute "quasiparticles" and the roton excitations of the He^4 . The experiment constitutes the first direct (in the sense of measuring the time decay of a concentration gradient) measurement of diffusion in $\text{He}^3\text{-He}^4$ solutions.

The concentration gradients were produced by exploiting the "heat flush" effect, and could be carefully controlled. The He^3 concentration was monitored continuously by sampling the vapor just above the mixture with a small capillary tube leading to a high vacuum system and a mass spectrometer. The effect of the measuring process on the diffusion was negligible.

The measurements indicate that D varies by a factor of 10 over the temperature range of the experiment. The observed temperature dependence is due primarily to the roton number density, but also indicates that the He^3 -roton cross section is energy dependent. The effective cross section was computed, and found to increase with temperature, ranging from about 160 \AA^2 at 1.27° to about 240 \AA^2 at 1.69° . This behavior is unlike that seen in gaseous helium mixtures, and unlike that predicted by the delta function interaction usually assumed for He^3 -roton collisions.

The results for values of D are compared with those predicted by the theory of Khalatnikov and Zharkov, and with those obtained by other methods of measurement. Finally, a model indicating how an energy-dependent interaction might arise is presented.

Thesis Supervisor: John G. King
Title: Professor of Physics

TABLE OF CONTENTS

CHAPTER 1	INTRODUCTION AND DESCRIPTION OF THE EXPERIMENT.....	6
I.	Introduction.....	7
II.	The Experiment.....	9
	References for Chapter 1.....	12
CHAPTER 2	APPARATUS AND PROCEDURE.....	13
I.	Diffusion Chamber.....	14
II.	"Sniffer" Capillary.....	17
III.	Mass Spectrometer.....	18
	A. Operation and Circuitry	
	B. Omegatron Linearity	
IV.	Low Temperature Thermometry and Temperature Regulation.....	23
V.	Procedure for a Given Run.....	27
	References for Chapter 2.....	29
CHAPTER 3	FORMAL SOLUTION TO THE DIFFUSION PROBLEM, AND CONSIDERATION OF EXPERIMENTAL CONDITIONS.....	30
I.	Solution to the Diffusion Equation - Ideal Case.....	31
II.	Correction to the Ideal Case - Geometry.....	33
III.	The Effect of the Finite Diffusion Time in the Vapor.....	36
IV.	The Effect of the Finite Amount of He ³ in the Vapor.....	41
V.	Effects Due to the Sniffer Capillary.....	44
	A. Pumping Effects	
	B. Transmission of the Vapor	
VI.	Method for Determining D.....	50
	References for Chapter 3.....	51
CHAPTER 4	SOME THEORETICAL CONSIDERATIONS.....	52
I.	Relation of the Diffusion Coefficient to the Cross Section..	53
II.	Temperature Dependence of D.....	55
	A. Khalatnikov and Zharkov Calculation of the Cross Section	
	B. Evaluation of (ρ_{no} / ρ_n)	
III.	Spatial Distribution of Rotons.....	58
IV.	Concentration Effects in Mixtures.....	60
	References for Chapter 4.....	63
CHAPTER 5	DATA AND DATA ANALYSIS.....	64
I.	General Observations (Plots of the Diffusion Runs are Included in this Section).....	65
II.	Determination of Diffusion Constant and Discussion of Sources of Error.....	77
	A. Method for Determining D From the Data	
	B. Additional Sources of Error	
III.	Temperature Dependence of the Diffusion Coefficient and Effective Scattering Cross Section.....	86

A.	Diffusion Constant	
B.	He^3 -Roton Scattering Cross Section	
IV.	Concentration Dependence of the Diffusion Coefficient.....	90
V.	Steady State Data.....	93
	References for Chapter 5.....	95
CHAPTER 6	COMPARISON OF RESULTS WITH OTHER METHODS OF MEASUREMENT....	96
I.	Thermal Conduction Measurements.....	97
A.	Relation of Effective Thermal Conductivity to D	
B.	Results of Measurements	
II.	Nuclear Magnetic Resonance Diffusion Measurements.....	101
A.	Spin Echo Measurements	
1.	Description of the Method	
2.	Experimental Results	
B.	Nuclear Relaxation	
References for Chapter 6.....		107
CHAPTER 7	A POSSIBLE MODEL FOR THE He^3 -ROTON INTERACTION.....	108
Reference for Chapter 7.....		115
APPENDIX I	SOME PROPERTIES OF LIQUID He^4 AND OF LIQUID He^3 - He^4	
	MIXTURES.....	116
I.	Liquid He^4	
A.	Roton Number Densities	
B.	Numbers of Phonons	
C.	Fountain Pressure in Liquid Helium as a Roton Kinetic Pressure (a new interpretation)	
II.	Dilute He^3 - He^4 Mixtures.....	120
A.	Phase Separation	
B.	Osmotic Pressure	
C.	Vapor-Liquid Equilibrium	
D.	Spectrum of Solute He^3 Atoms	
E.	"Heat Flush"	
References for Appendix I.....		126

LIST OF FIGURES

<u>Figure</u>	<u>Page</u>
1. Diffusion Chamber	15
2. Omegatron Mass Spectrometer and Circuitry	19
3. Omegatron Linearity	22
4. Temperature Regulation Unit	26
5. Initial Concentration Distributions for a Typical Run	34
a. Ideal Geometry	
b. Non-ideal (Actual) Case	
6. Sniffer Function	48
7 through 17: Diffusion Runs - $\text{Log}[h(t) - n_{\infty}]$ is plotted versus time, for 11 runs.	66 - 76
18. Error Analysis - The Effect of Uncertainty in n_{∞}	79
19. Temperature Dependence of D	85
20. He^3 -Roton Cross Section	89
21. Temperature Dependence of D - Comparison of Results with Other Measurements	100
22. Vapor Enhancement - Summary of Data for 2 Temperatures	123
23. Composite Vapor Enhancement Data at Low Concentration	124

ACKNOWLEDGEMENT

My primary thanks must go to Professor John King, not out of propriety, but from a sense of gratitude. The opportunity to work under his supervision enabled me to benefit from his creative intellect, and his insight into all aspects of physics, and, for that matter, into many aspects of life.

I would also like to thank Mr. Frank O'Brien for assistance with the mechanical design of the apparatus, and for assisting me in developing some measure of skill in the mechanical fabrication of apparatus. In addition, I would like to acknowledge the assistance of Mr. Arthur Berg in dealing with electronics problems. Other technical help was received from Mr. John McLean, and Mr. Patrick Nerpouni.

Advice and assistance of various sorts was also received from Dr. James Weaver, Dr. Robert Pandorf and Dr. James Clow, and from the graduate students in the Molecular Beams Laboratory during the past few years: John McWane, Dan Oates, Truman Brown, Sam Cohen and Bill Davis. Anita Hucksam graciously assisted with the typing of the manuscript.

Finally, I would like to thank my wife, Regi, who has been a very good sport about the whole thing.

CHAPTER 1
Introduction and Description
of the Experiment

I. Introduction

The model for He II as a gas of excitations in an inert superfluid "ether" has been successful in explaining the thermodynamic and hydrodynamic properties of the liquid. At temperatures below about 1.7°, the thermodynamic quantities are determined primarily by two regions in the excitation spectrum, the low energy phonon region, where the excitation energy is proportional to the momentum, $\epsilon = c\hbar k$ and the roton region, where $\epsilon = (\hbar^2/2\mu)(k - k_0)^2 + \Delta$. If a small amount of He³ is dissolved in the He II to form a dilute solution, then the He³ solute atoms can be thought of as an additional excitation gas having the spectrum $\epsilon = -\epsilon_0 + \frac{\hbar^2}{2m^*} k^2$ where ϵ_0 is a binding energy, and m^* represents a hydrodynamic effective mass which takes into account that motion of a He³ atom involves backflow of the surrounding superfluid. Measurements of specific heat and the velocity of second sound in solutions confirm the validity of this spectrum, and the picture of a dilute He³-He⁴ solution as a gas of phonon, roton, and He³ excitations all moving in a superfluid background.⁺

Experiments involving He³-He⁴ mixtures are generally of two types. In one type of experiment the bulk properties of the solute He³ atoms are of interest, primarily because He³-He⁴ solutions are unique in that both Fermi-Dirac and classical properties can be observed in different temperature and concentration ranges. In another type of experiment

⁺ The properties of liquid He⁴ and He³-He⁴ mixtures are discussed in more detail in Appendix I.

the He^3 solute atoms are used to investigate the properties of the He II. This work is of the latter type and involves the measurement of the interaction between the semi-classical He^3 quasi-particles and the roton excitations of the Helium II. This is accomplished by measuring the diffusion constant D in very dilute solutions at moderately high temperatures where the effects due to phonons are small. Since D is a direct measure of the mean free path of a He^3 solute atom, the measurements give values for the He^3 -roton cross section. These measurements, it is hoped, will lead to a clearer understanding of the nature of the roton.

The measurements involve monitoring the time decay of an applied He^3 concentration gradient in the solution and constitute a direct measurement of D . A previous attempt at a "direct" (in the sense of measuring the time decay of a concentration difference) measurement has been reported,⁽¹⁾ but no results for He^3 - He^4 mixtures below the superfluid transition temperature were achieved before the effort was abandoned. The diffusion constant has been previously obtained by monitoring the decay of a nuclear polarization in a mixture, using the spin-echo technique, and from thermal conductivity measurements. The spin-echo measurements have, in general, been carried out in the regime where He^3 - He^3 interactions play a significant role in the diffusion, enabling the contribution due to He^3 -roton interactions to be determined only indirectly. In the present work, the effect of He^3 - He^3 interactions is negligible, and the He^3 -roton interaction determines the diffusion.

II. The Experiment

In the experiment, the diffusion constant was measured directly by establishing a He^3 concentration gradient in the solution and monitoring the decay of the gradient under known boundary conditions.

At first it might seem that the initial concentration difference could be produced by mechanically injecting a small amount of He^3 into a solution of pure He^4 . One configuration for accomplishing this was considered in the course of the experiment. A He^3 - He^4 mixture was condensed on one side of a superfluid-tight valve^{*}; at $t=0$ the valve was opened to one side of a U-tube filled with pure He^4 . The build up of the He^3 signal on the other side of the U-tube was then observed as a function of time. This method suffered from difficulties which characterize most injection schemes:

1. The large vapor pressure difference between even dilute He^3 - He^4 mixtures and pure liquid He^4 implies a pressure difference across the U-tube. Thus the diffusion is plagued by initial turbulence and a changing level difference.

2. Opening a valve involves the generation of a substantial amount of heat at the valve seat, leading to a spurious heat flush effect.

^{*} A working superfluid-tight valve, designed by Mr. Frank O'Brien of the Molecular Beam Laboratory, was incorporated into an early version of the apparatus.

3. If pure He^3 liquid were to be used, the pressure difference referred to in (1) would be enormous, and in addition, heat flush due to the substantial "heat of mixing" of the two liquid isotopes would be present. The above difficulties are severe, and rather than overcoming them, a new method was developed.

The method finally adopted for producing initial concentration distributions does not require external injection of He^3 into the He^4 solution, but rather the "heat flush" effect is exploited in a controlled way to produce the initial gradient internally. A plane heater at the bottom of the diffusion chamber produces a steady convective current of thermal excitations. The current interacts with the He^3 atoms, forcing them to the region near the top of the apparatus. When a steady state has been reached, the flow of He^3 atoms due to the thermal current just equals the "back flow" current produced by gradient of the concentration distribution. If it is assumed that:

1. The current of He^3 atoms is characterized by V_n , the velocity of thermal current. $V_n = Q/\rho s T$, where Q =heat applied/ cm^2 , S =entropy per unit mass.

2. All of the heat is propagated via the convective process.

Then for 1-dimensional geometry:

$$J = v_n n_3 = D \frac{\partial n_3}{\partial z}$$

implying an exponential distribution $n_3 \sim \exp(V_n Z/D)$. In analyzing the experiment, an initial exponential distribution is assumed, $n_3 \sim \exp(\alpha Z)$, but no assumption as to the value of α is made.

After the steady state has been established, the heater is turned off, and the exponential distribution decays into a uniform distribution as the He^3 atoms diffuse through the superfluid in the chamber. During this process the He^3 concentration is monitored as a function of time by continuously sampling the vapor just above the liquid by means of a small capillary "sniffer" which is connected to a high vacuum system and a mass spectrometer.

The vapor concentration monitored in this way follows the decay of the concentration in the liquid, since

1. The diffusion times the vapor are much smaller than those in the liquid. (See Chapter 3, Section III.)

2. The vapor concentration of sufficiently dilute solutions is proportional to the concentration at the liquid surface. (See Appendix 1, Section IIC.)

From the measured decay of the He^3 concentration at the liquid surface the diffusion constant is derived.

References for Chapter 1

1. G. Careri, J. Reuss, and J. J. M. Beenakker, *Nuovo Cimento* 13: 148 (1959).

CHAPTER 2

Apparatus and
Procedure

I. Diffusion Chamber

The diffusion occurs in an inner cylindrical chamber which is surrounded by a vacuum space between it and an outer brass shell. (See Fig. 1). At the liquid level, near the top of the inner chamber is a thin perforated copper block which provides a good thermal link to the outer helium bath. A 51 Ω plane heater consisting of about 12" of .004" diameter evanohm wire wound in a plane configuration on a thin teflon disc is at the bottom of the chamber. The vacuum space between the chamber and the outer shell provides thermal isolation, so that the only thermal connection between the liquid mixture and the bath is via the copper block. Since the heat flow through the .010" stainless steel walls of the chamber is negligible, nearly all of the heat current flows from the heater through the He³-He⁴ mixture to the outer bath via the copper block. The interior part of the block is about .04" thick, and is perforated by 28 holes, about 12% of its total area. The exterior part of the block is roughened to increase its effective surface area.

The chamber is filled with "crinkly" and plane .001" thick stainless steel foil coiled together to form numerous vertical channels about .05" in diameter, as illustrated in fig. 1. The purpose of the channels is to maintain a one-dimensional geometry, and to eliminate

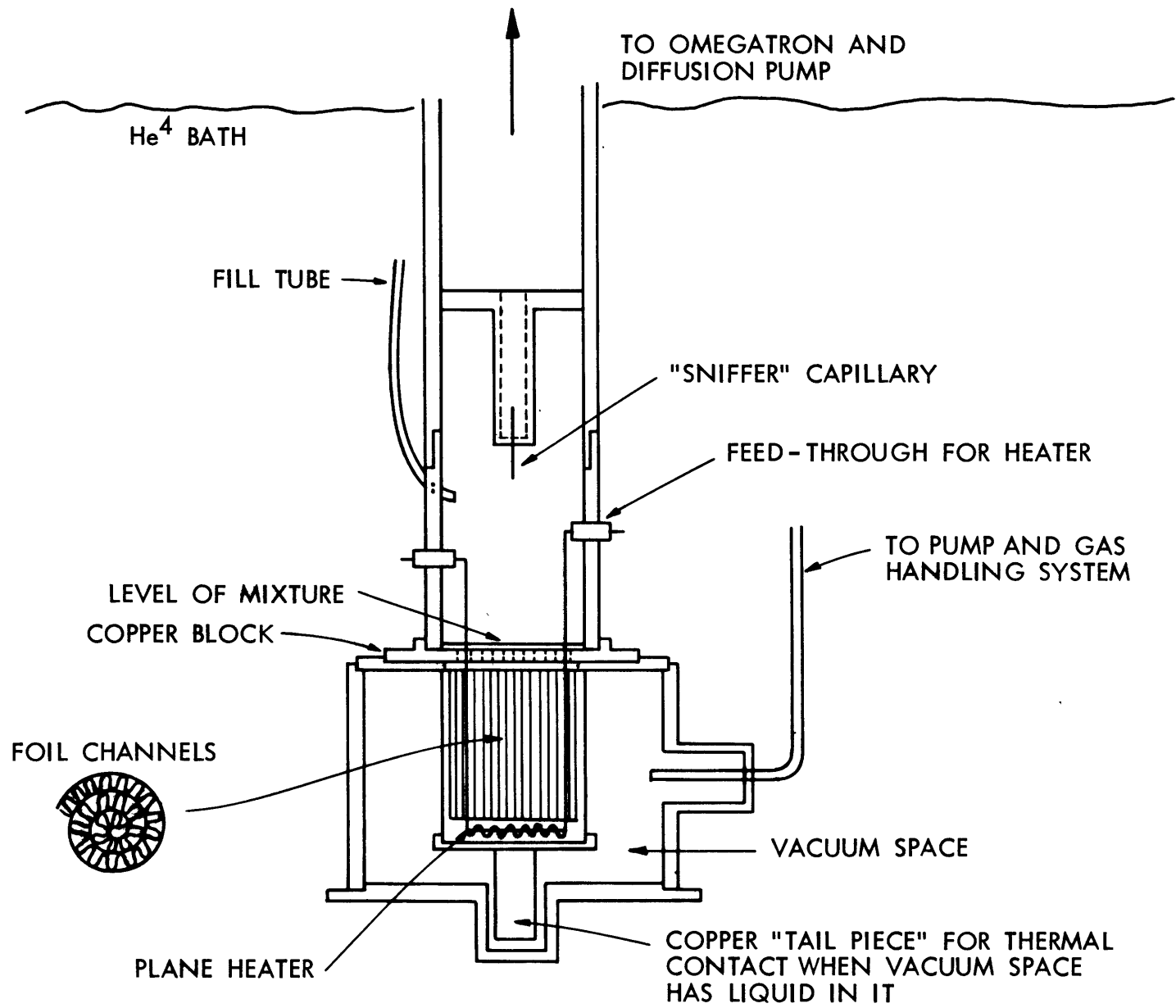


Figure 1 - Diffusion Chamber

any secondary convection when the thermal current is applied.

The mixture is condensed into the chamber by means of a .029" i.d. capillary, and filled to just above the copper block. When the apparatus was first tried, the condensing liquid produced a large pressure in the chamber, overloading the vacuum system. This was due to the thermal isolation of the liquid which had not yet reached the copper block. This problem was solved by adding the copper tail piece to the bottom of the inner chamber, and partially filling the "vacuum space" with a few c.c.'s of superfluid helium, thus maintaining thermal contact with the outer bath until the liquid level had reached the copper block. Once the condensation in the inner chamber was complete, the liquid in the vacuum space was pumped away, restoring the thermal isolation. The amount of helium liquid needed for this process was minimized by the small volume formed by the copper tail piece and the well at the bottom of the outer shell.

One feature of the diffusion chamber design is that any spurious heat inputs propagating through the vapor from above the chamber flow through the copper block to the bath, rather than through the liquid $\text{He}^3\text{-He}^4$ mixture. Several papers dealing with $\text{He}^3\text{-He}^4$ mixtures refer to a spurious heat flash effect arising from the evaporation of the mobile helium film at a warm part of the apparatus,

and the subsequent condensation at the liquid surface. (1), (2)
 This effect was probably not present in the apparatus since the level of the outer bath was always well above the diffusion chamber, and the only path for the film to flow to a warmer region was through the .029" fill capillary. Any surge of vapor originating from the higher, warmer part of the capillary must then pass through a length of cold capillary, having a large surface to volume ratio, so that most of the surge would condense out before reaching the diffusion chamber. But even if the film effect were present, the fact that the thermal path is through the copper block to the bath, rather than through the He^3 - He^4 mixture, means that the concentration distribution in the liquid would be unaffected.

II. "Sniffer" Capillary

The experiment was performed at temperatures ranging from 1.27° to 1.69° . At these temperatures, the vapor pressure ranged from about 1mm to about 10mm of mercury. The .002" i.d. "sniffer" capillary tube is used to limit the flow rate from this relatively high pressure vapor to the high vacuum system. Since the "sniffer" is located just above the surface of the superfluid mixture, and it too is at the temperature of the He^4 bath, there is a continual flow of superfluid film through the "sniffer". As, 1) the He^3 does not participate in superfluid flow, (3) and 2) the film flow is considerable, for a smooth tube

the number of atoms/second⁽⁴⁾ $\frac{dN}{dt} \approx (2\pi r) \cdot 1.5 \cdot 10^{18}$

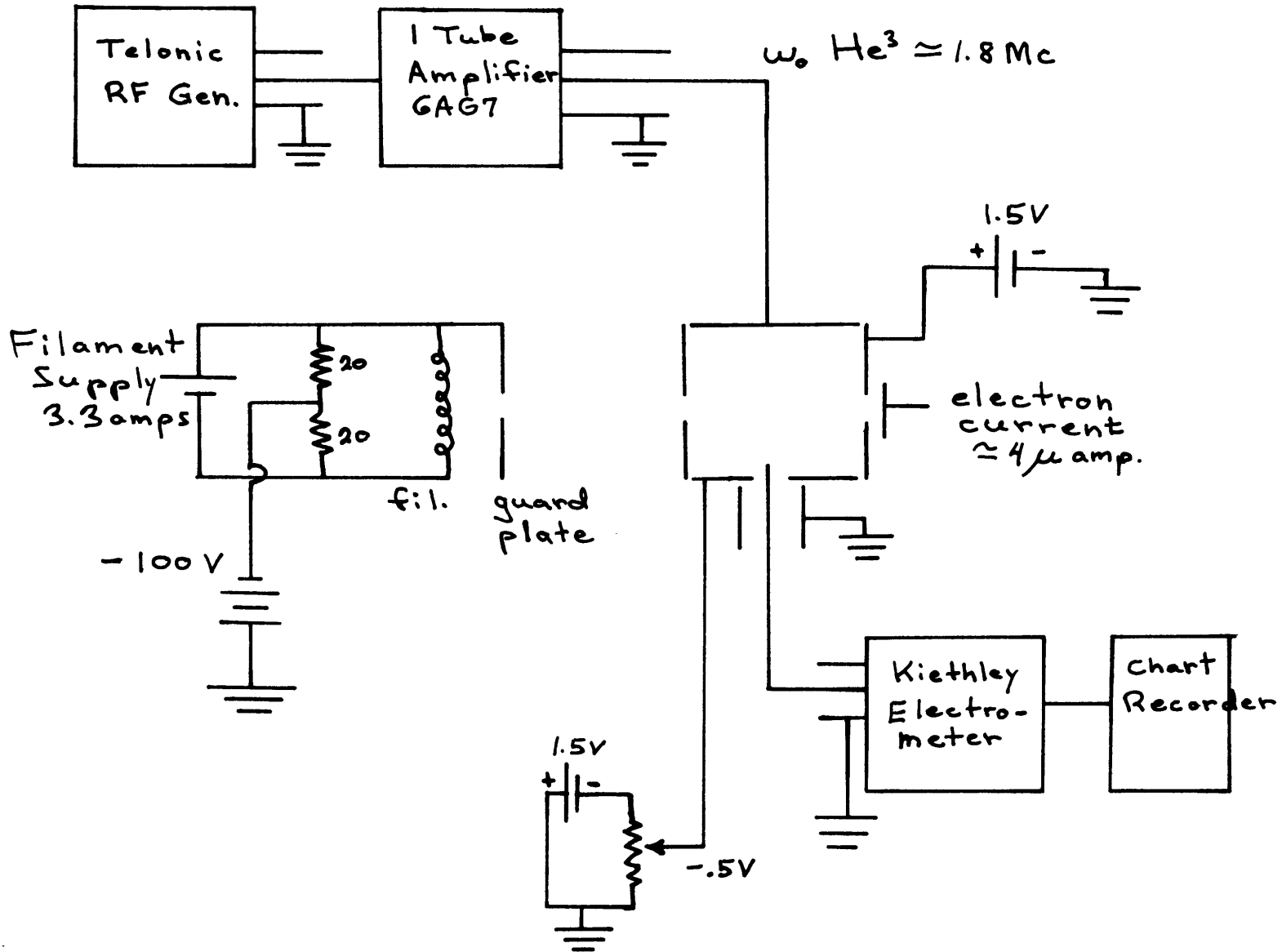
(r=radius of tube), the film flow produces a large irrelevant He⁴ background pressure in the vacuum system, and hence in the omegatron. In the experiment, the superfluid film flow through the "sniffer" was, in fact, about 10 times that of the gas flow. This effect could not have been reduced merely by reducing the "sniffer" diameter since the film flow is proportional to the radius of the tube, while the gas flow (Poiseuille viscous flow) is proportional to r⁴. The film flow effect, although unwanted, was not serious, for it was still possible to use the mass spectrometer to detect low concentrations of He³.

III. Mass Spectrometer

A. Operation and Circuitry

The omegatron mass spectrometer and associated biasing and detecting circuitry are shown schematically in Fig. 2. Details of the operation of omegatrons are discussed in the literature (see for example Ref. 5). Briefly, the operation of the omegatron is as follows: electrons are accelerated through 95-100 volts as they pass from the filament to the box-like region. Ions produced in the box spiral around the 3.8 kilogauss magnetic field which is oriented along the path of the electron beam. An rf electric field applied to top plate of the box at the

Figure 2 - Omegatron Electronics



cyclotron frequency of the relevant spiraling ion causes the ion to gain energy and hence increase the radius of its spiral until it is collected at the internal collector electrode just above the bottom plate.

Background ions whose cyclotron frequency differs from the applied rf field are alternately in and out of phase with the electric field and receive no net acceleration. The collected ion current is transmitted by a short shielded coaxial cable to an electrometer. The electrometer is used in the "fast" position, and operates as a unity gain voltage follower between the 10^7 to 10^{10} input impedance and a low impedance 100 to 1000 Ω strip chart recorder.

In the present experiment, He^3 partial pressures of the order of 10^{-9} to 10^{-8} mm of mercury are detected in the presence of about 4 to 7 $\times 10^{-5}$ mm of He^4 . The absolute value of the total pressure is obtained from a Bayert Alpert ionization gauge, corrected for the reduced helium efficiency. Because of this relatively large background pressure, the spiraling beam of resonant He^3 ions is attenuated if the total path length is too long. Thus, relatively large rf electric fields are required. Neglecting space charge effects, the equations of motion for the resonant ions:

$$m \ddot{x} = q \dot{y} B_0, \quad m \ddot{y} = -q \dot{x} B_0 + q E_0 \sin \omega t$$

where $\vec{B} = B_0 \hat{z}$, are easily solved.

For $\omega = \omega_0 = \frac{qB}{m}$, one finds that $r = \sqrt{x^2 + y^2} = \left(\frac{E_0}{2\beta_0}\right)t$

plus a small oscillating term. For $r=r_0$ the distance to the collector, the number of revolutions

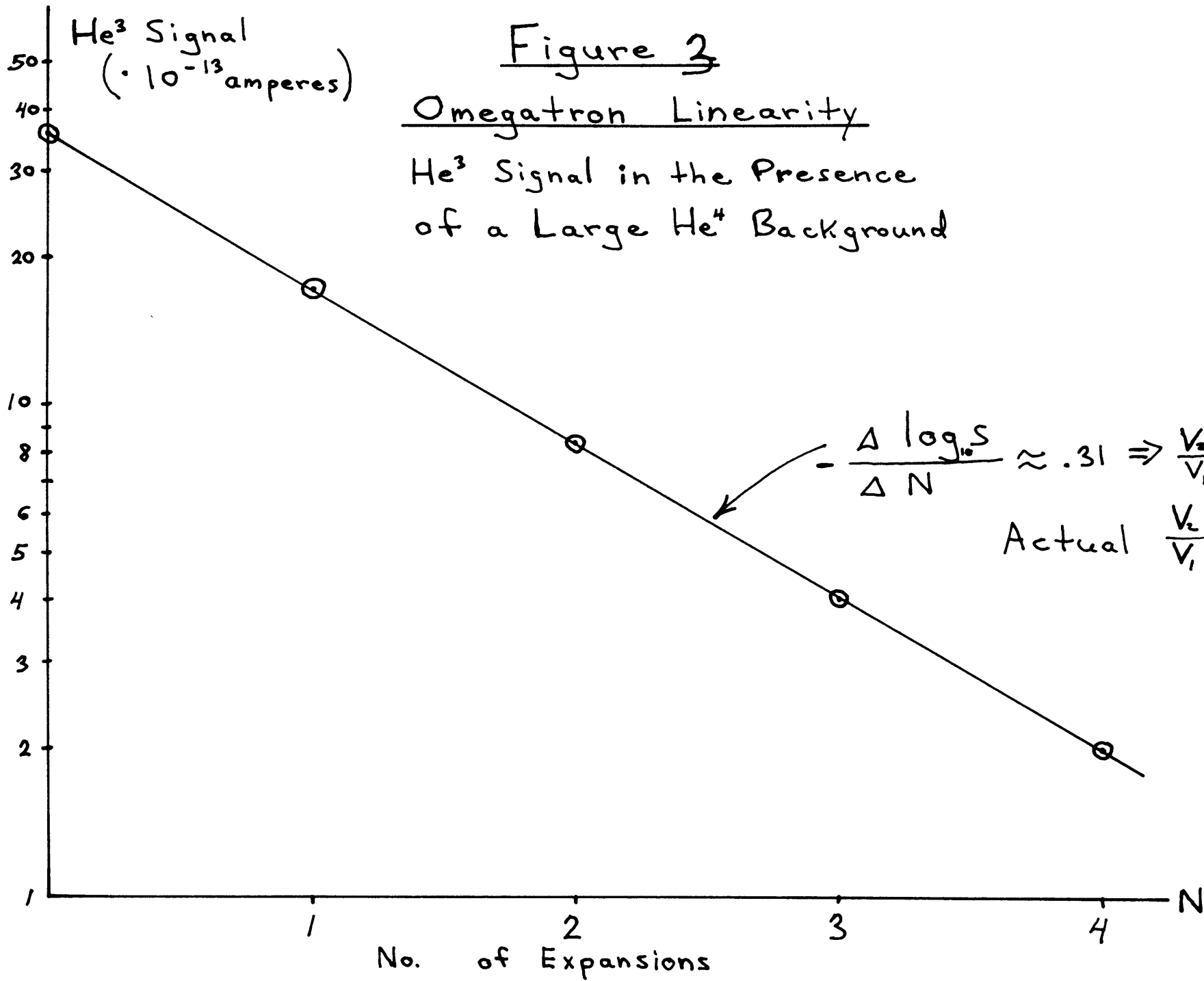
$$N = \frac{\omega_0 t}{2\pi} = \frac{\omega_0 B_0 r_0}{\pi E_0} = \frac{m\omega_0^2 r_0^2}{\pi q V}$$

For the 45 peak to peak voltage used in the experiment, this gives about 7 revolutions rather than the 500 or so conventionally used. The He^3 and He^4 spectral lines are still well separated despite the loss in resolution inherent in reducing the total path length, and the large difference in the partial pressures.

The filament current was regulated by floating the guard plate just in front of the filament at -95 volts, a few volts above the filament. This resulted in an electron current which was limited by the space charge present between the filament and the guard plate, and was relatively insensitive to changing filament conditions. It was empirically found that maintaining the sides of the box slightly above ground, and the bottom plate slightly below ground improved the omegatron sensitivity. It was also found that when detecting He^3 in the presence of the large He^4 background that floating the electron collector, which quickly charged up to -90v, also improved sensitivity.

III. B. Omegatron Linearity

The linearity of the omegatron in detecting He^3 in the presence of 10^4 times as much non-resonant He^4 was



verified as follows: A gaseous $\text{He}^3\text{-He}^4$ mixture having He^3 concentration of about 10^{-3} contained in a volume in the external gas handling system used in the experiment was expanded into a larger volume and then into the diffusion chamber where it was sampled by the "sniffer" and detected by the omegatron. The omegatron signal was noted, the first volume closed off, and the gas in the second volume and diffusion chamber pumped away. He^4 was then added to the first volume until the total pressure equaled that at the start of the process. The whole procedure was then repeated. After N such cycles, the He^3 concentration was reduced by a factor $\left(\frac{V_1}{V_2}\right)^N$, while the total pressure remained constant. In Fig. 3 the log of the omegatron He^3 signal is plotted versus N . A straight line results, indicating a power law dependence to the omegatron response. The measured slope of the line is equal to the measured $\left(V_1/V_2\right)$ indicating that the power involved is 1 and the omegatron is linear under roughly operating conditions. ✓

IV. Low Temperature Thermometry and Temperature Regulation

Low temperatures are achieved by pumping on the He II bath surrounding the apparatus. Temperatures were measured by an oil manometer with observations taken with a cathetometer. The bath was maintained at a constant temperature by a mechanical "Walker regulator", which

consists of a latex condom in series with the bath pumping line. The condom expands or contracts, thus changing the pumping line impedance, as the bath vapor pressure is higher or lower than that in a surrounding volume. More precise regulation was achieved by adding an electronic servo system in which the signal from a bridge containing a resistance thermometer was amplified to drive a heater resistor in the superfluid bath. The circuit (see Fig. 4) consists of a d.c. bridge, an impedance matching voltage follower, a high gain amplifier, and a final emitter follower which drives the low impedance, 200 Ω evanohm wire heater. The power through the thermometer resistor in the bridge was about one microwatt. The bridge was set so that the output power from the heater was about 40 milliwatts.

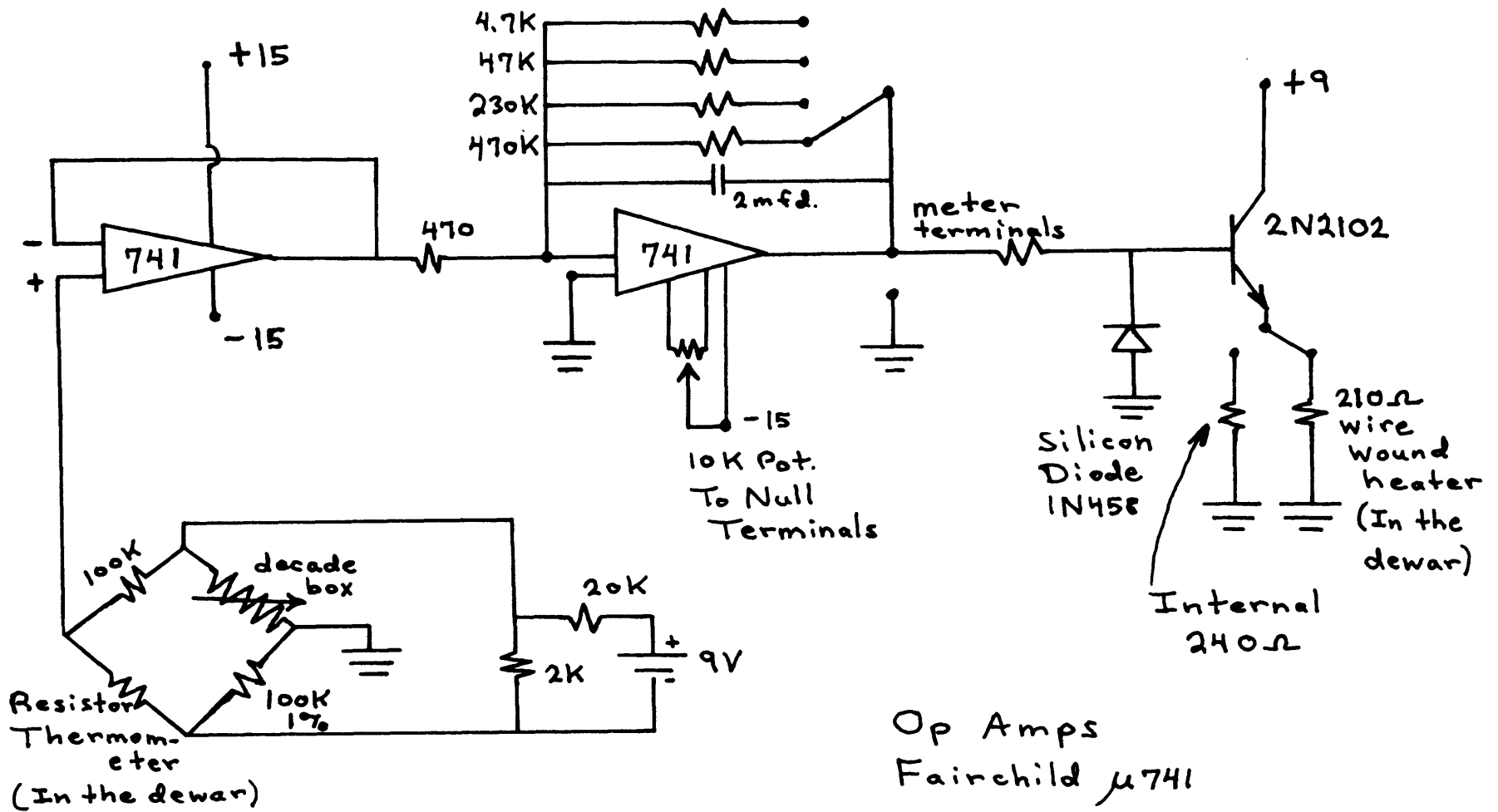
The apparatus was such that the ambient heat input from the main pumping tube was quite sensitive to the level of the bath; as the bath level dropped, the ambient heat input changed considerably. Using the regulator, (only the electronic regulator was used below 1.35°K) the temperature change of the bath was less than about 4×10^{-4} °K for the longer diffusion runs, and of the order of 1 to 2×10^{-4} °K for the shortest runs (low temperatures).

The resulting power input to the mixture can be estimated by computing $(NC\Delta T) / t$ where N=number of atoms in the mixture, c=specific heat per atom, about .2k to

1.0k in the experiment, $\Delta T = 4 \times 10^{-4} \text{ } ^\circ\text{K}$, $t = 80$ minutes. This gives about 2×10^{-7} watts, a negligible amount of power, about 10^{-3} of that applied to the chamber heater in the diffusion runs. Thus the temperature regulation for the experiment was adequate, and long term temperature changes did not produce significant error.

The sensitivity of the system to short term temperature fluctuations was tested several times by deliberately adjusting the decade resistor of the bridge to raise the bath temperature a few times $10^{-4} \text{ } ^\circ\text{K}$ for about 15-20 seconds, and then reducing the temperature to its initial value. After about 20 seconds, the omegatron signal returned to tracing out a curve identical with that extrapolated before the perturbing temperature change was applied. The perturbing temperature fluctuation introduced was the amount estimated to have occurred over a long period about 60 to 90 minutes: the actual short term temperature fluctuations were much smaller.

Figure 4 - Temperature Regulation Unit



Some of the procedures used have already been discussed. The complete procedure for a given run is presented for clarity:

1. Transfer liquid helium into the dewar.
2. Cool to about 1.7°K by pumping on the He⁴ bath.
3. Condense about 2 cc of liquid He⁴ into the well contained at the bottom of the "vacuum space" between the diffusion chamber and the outer shell.
4. Condense the He³ and He⁴ into the diffusion chamber. This was done in 3 steps, condensing 20 liters at about 160 Torr of He⁴ gas in each step. Before the last step, a 30 cc volume of about 45 Torr of He³ was condensed into the chamber.
5. Pump out the liquid He⁴ contained in the "vacuum space". This took about 15-20 minutes at 1.7°.
6. Cool the bath to the desired temperature and regulate, using both the Walker regulator and the electronic servo. (Only the electronic regulator was used at the lower temperatures.)
7. Monitoring the He³ signal, wait until the system is near equilibrium, i.e. until a nearly uniform He³ concentration is reached. This took from about 20 minutes to about an hour. The initial deviation from equilibrium was produced by a "heat flush" effect inherent in cooling the bath. The effect was reduced by cooling below the desired temperature and then warming. Since an excess

concentration at the bottom of the chamber was reduced by natural convection ($\rho_3 < \rho_4$), while an excess at the top of the chamber is reduced only by diffusion.

8. Turn on the heater and monitor the build up of the He^3 signal. The times for the complete build up were of the order of $L/2v_n$, where v_n is the normal fluid velocity $v_n = Q/\rho_s \tau$.

9. Turn off the heat and monitor the decay of the He^3 signal.

About 6 to 7 hours were available from the beginning of step number (1) until the bath level was near the top of the diffusion chamber. If all of the components in the apparatus were functioning properly, from 1 to 3 runs were made, depending on the temperatures involved. Note that the liquid had to be pumped out of the diffusion chamber (through the fill capillary) before the bath was depleted to avoid the danger of explosion.

References for Chapter 2

1. C. T. Lane, H. Fairbank, L. Aldrich, and A. O. Nier,
Phys. Rev. 75:46 (1949).
2. D. H. N. Wansink, K. W. Taconis, and F. A. Staas
Physics 22:449 (1956). (See p. 450.)
3. J. G. Daunt, R. E. Probst, and H. L. Johnston,
J. Chem. Phys. 15:759 (1947).
4. See for example: K. Mendelssohn, and G. K. White,
Proc. Phys. Soc. (London) A63:1328 (1950).
5. R. J. Warnecke Jr., Ann. de Radioelectricite
12:258 (1957).

CHAPTER 3

Formal Solution to the Diffusion Problem, and Consideration
of Experimental Conditions

The diffusion problem is determined by the following considerations: The diffusion chamber is one dimensional. The heater is at the bottom of the diffusion chamber, and the thermal path for the current of excitations is through the mixture to the copper block at the top of the chamber. The resulting steady state distribution of He^3 atoms is approximately $n \sim \exp(+\alpha Z)$ for $0 < Z < L$. This represents the initial He^3 distribution in the diffusion problem.

No He^3 atoms can flow through the bottom of the apparatus, and since the amount of He^3 in the vapor is at all times much smaller than that of the liquid, relatively very small amounts of He^3 are involved in flow to or from the vapor. Thus, the boundary conditions for the problem are $J=0$ at $Z=0$, and $J=0$ at $Z=L$, where L = the distance from the bottom of the chamber to the copper block. The solution to the diffusion equation:

$$D \frac{\partial^2 n}{\partial z^2} = \frac{\partial n}{\partial t}$$

subject to the above boundary conditions is:

$$n(z, t) = n_{\infty} + \sum A_m \cos \frac{m\pi z}{L} \exp(-\nu_m t)$$

where

$$\nu_m = D \left(\frac{m\pi}{L} \right)^2$$

The coefficients A_m are determined by the initial distribution:

$$n(z=0) = n_1 \exp(\alpha z)$$

and are found in the usual way.

Integrating

$$\int_0^L \cos\left(\frac{m\pi z}{L}\right) n(z, t=0) dz$$

and using the orthogonality of the cosines, one gets:

$$A_m \int_0^L \cos^2\left(\frac{m\pi z}{L}\right) dz = n_1 \int_0^L e^{\alpha z} \cos\left(\frac{m\pi z}{L}\right) dz$$

and

$$A_m = \frac{2\alpha L n_1 [(-1)^m e^{\alpha L} - 1]}{(\alpha L)^2 + (m\pi)^2}$$

At the surface of the liquid, the cosine terms each give $(-1)^m$, so that

$$n(z=L, t) = n_\infty + 2\alpha L n_1 \sum_m \frac{e^{\alpha L} - (-1)^m}{(\alpha L)^2 + m^2 \pi^2} e^{-\gamma_m t}$$

The constant n_1 is determined by conservation of He^3 :

$$n_\infty L = \int_0^L n_1 e^{\alpha z} dz \Rightarrow n_1 = \frac{\alpha L}{e^{\alpha L} - 1} n_\infty$$

The observed enhanced initial He^3 concentration is related to the equilibrium concentration (uniform concentration n_∞) by

$$n_0 = e^{\alpha L} n_1 = \frac{\alpha L e^{\alpha L}}{e^{\alpha L} - 1} n_\infty$$

(The distributions at $t=0$, and $t=\infty$, are shown in figure 5 below). Thus the approximate value of αL for a given run could be estimated from the steady state enhanced He^3 signal. In the experiment $(\alpha L)^2$ was about $.25^2$. Hence the coefficients A_m decreased rapidly with m . This together with the fact that the time constant for the decay of

the m^{th} mode $\gamma_m = \frac{L^2}{\pi^2 D^2} \frac{1}{m^2}$ means that except near $t=0$, only the first term in the series is important.

Thus for t sufficiently large

$$(n(z=L, t) - n_\infty) \sim \exp\left(-\frac{\pi^2}{L^2} D t\right)$$

and the diffusion constant is determined by the slope of the time dependence of $\log(n - n_\infty)$.

II. Correction to the Ideal Case - Geometry

Corrections due to geometry are due to 1) the fact that the heater is not exactly at $Z=0$, but is located a small but finite distance from the bottom of the apparatus; 2) the finite thickness of the copper block, and a small uncertainty in the liquid level. Conditions 1) and 2) imply that there are thin layers of liquid at the top and bottom of the diffusion chamber through which there is no heat flow, and thus the initial concentration distribution when the heat is just turned off, will be given by $n=n_1$ for $0 < Z < Z_1$, $n=n_1 e^{\alpha(Z-Z_1)}$ for $Z_1 < Z < Z_2$, and $n=n_1 e^{\alpha Z_2}$ for $Z_2 < Z < Z_3$, where Z_1 and $(Z_3 - Z_2)$ are both much smaller than Z_3 , (See Fig. 5), and $Z_3=L$.

Since the boundary conditions are the same as for the ideal problem, the general solution is the same

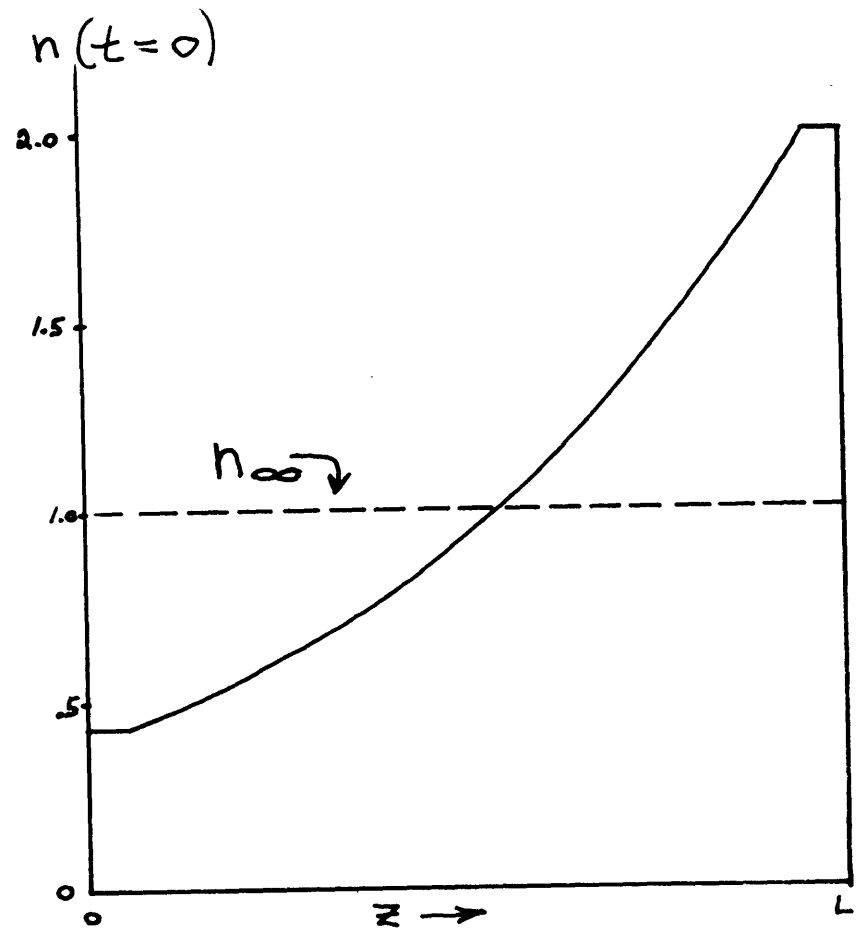
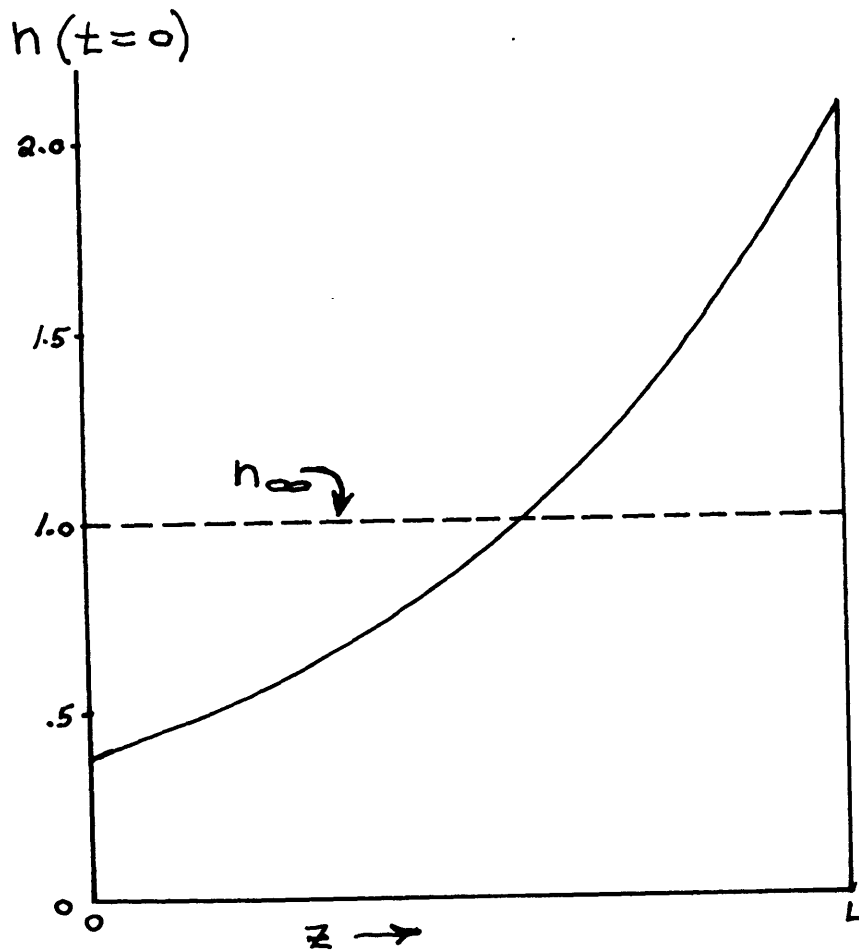
$$n = n_\infty + \sum A_m \cos \frac{m\pi z}{L} \exp\left(-\frac{m^2 \pi^2 D t}{L^2}\right)$$

only the A_m are different. Since the difference between this initial condition and the pure exponential initial

Figure 5 - Initial Concentration Distributions
For a Typical Run

a. Ideal Geometry

b. Non-ideal (actual) Case



condition is a flattening at the beginning and end, one 35
 would intuitively expect that the corrected solution would
 contain more of the principal mode $\text{Cos}\left(\frac{\pi z}{L}\right)$ and less of
 the higher frequency terms. A detailed solution to the
 problem verified that this is indeed true. The solution
 is obtained as for the ideal case. The result is a clumsy
 expression which is simplified by treating z_1/z_3 and
 $(z_3-z_2)/z_3$ as small quantities and expanding trigonometric
 and exponential functions accordingly.

Writing

$$n_3(z=L, t) \approx A_1 e^{-\gamma_1 t} + A_2 e^{-4\gamma_1 t} + A_3 e^{-9\gamma_1 t}$$

and assuming reasonable estimates for z_1, z_2, z_3 , the
 following relative values are obtained for A_1, A_2, A_3 in
 both the ideal and corrected cases:

	A_1	A_2	A_3
ideal case	1	.20	.14
non-ideal geometry	1	.17	.12

Thus the net effect is a small decrease in the magnitudes
 of the higher order modes relative to the principal mode,
 which for purposes of the data analysis is desirable
 although insignificant in magnitude. The important point
 is that the characteristic length for the problem is
 still L , the distance from the bottom of the chamber to
 the liquid level. The fact that there are small regions

at the top and bottom of the chamber where there is no initial concentration gradient, only produces changes in the relative sizes of the various modes, and does not affect their decay frequencies.

III. The Effect of the Finite Diffusion Time in the Vapor

A. Preliminary Discussion

The diffusion coefficients for gaseous He³-He⁴ mixtures at pressures equal to the saturated vapor pressures for the temperatures of the experiment are about 40 to 75 times the values derived for the liquid.*

* The gaseous diffusion coefficient for dilute He³-He⁴ mixtures has been measured⁽¹⁾ over a range of temperatures and pressures, but the lowest temperature data is at 1.74°K. However, the data indicates that the quantity $(nD\mu / T^{1/2})$ (where n =no. density of atoms, μ =He³-He⁴ reduced mass) proportional to $1/\sigma_{\text{eff}}$, is a weakly varying function of temperature. The experimental values for $(nD\mu / T^{1/2})$ are very close to theoretical calculations based on a Lennard-Jones potential^(2,3), and to calculations based on other potentials⁽⁴⁾. Thus the behavior of the gaseous diffusion constant seems to be fairly well understood, and the theoretical extension of the experimental values for the gas diffusion constant are used at the lower temperatures. (Only numerical estimates for D_g are desired; the exact shape of the potential is not of interest.)

Since the distance from the sniffer to the liquid surface was slightly less than L , the characteristic distance for the liquid diffusion problem, one might at first think that the effect of the diffusion in the vapor is completely insignificant, and that sniffer response time would depend on quantities on the order of $\exp(-60t/\tau_L)$, where τ_L is the decay time for the principal liquid mode. In fact the problem is not quite this simple. The diffusion depends on the total length of the vapor region of the chamber, and since the vapor boundary condition is different from the liquid case, the frequencies of the various modes are different from the liquid frequencies.

B. Solution to the Vapor Diffusion Problem

Consider the vapor portion of the diffusion chamber as a cylinder terminating at the liquid surface, having an effective length slightly smaller than the actual length, due to the volume occupied sniffer mount. Since the diffusion arises from the changes in concentration at the liquid surface, and such changes occur uniformly over the surface, radial diffusion modes will be unimportant, and the problem will be treated as 1-dimensional. The problem is determined by the boundary and initial conditions:

- 1) $J=0$, at $Z=0$, the top of the chamber.
- 2) At the liquid surface, $n_{3g}(t) = Cn_{3L}(t)$
- 3) $n_{3g}(t=0) = n_{g0}$ uniform throughout the chamber.

Taking the first three terms of the series solution for n_L , the boundary conditions 1) and 2) determine the general form of the solution:

Let D_2 =gas diffusion coefficient

D_1 =liquid diffusion coefficient

L_2 =effective length of the vapor region of the chamber

L_0 =length of the liquid diffusion region

Then, from 2)

$$D_2 \left. \frac{\partial^2 n_g}{\partial z^2} \right|_{z=L_2} = - \left[\gamma_L a_1 \exp(-\gamma_L t) + 4\gamma_L a_2 \exp(-4\gamma_L t) + 9\gamma_L a_3 \exp(-9\gamma_L t) \right]$$

This equation, and conditions (1,3) are simultaneously satisfied by:

$$n_g = n_{g\infty} + (n_{g0} - n_{g\infty}) \left[a_1 \frac{\cos\left(\frac{\pi}{L_0} \sqrt{\frac{D_1}{D_2}} z\right)}{\cos\left(\frac{\pi}{L_0} \sqrt{\frac{D_1}{D_2}} L_2\right)} \exp\left(-\frac{\pi^2 D_1 t}{L_0^2}\right) + a_2 \frac{\cos\left(\frac{4\pi}{L_0} \sqrt{\frac{D_1}{D_2}} z\right)}{\cos\left(\frac{4\pi}{L_0} \sqrt{\frac{D_1}{D_2}} L_2\right)} \exp\left(-\frac{4\pi^2 D_1 t}{L_0^2}\right) + \dots \right] + f(z, t)$$

where $f(z, t)$ is chosen to satisfy the initial condition 3),

and where $f(L_2, t)=0$, and $\left. \frac{\partial f}{\partial z} \right|_{z=0} = 0$

to satisfy the boundary conditions. This implies that:

$$(5) \quad f = \sum B_m \cos\left(\frac{2m+1}{2} \frac{\pi z}{L_2}\right) \exp\left[-\left(\frac{2m+1}{2}\right)^2 \frac{\pi^2 D_2 t}{L_2^2}\right]$$

where the B_m are determined by integrating

$$\int_0^{L_2} \cos\left[\left(\frac{2m+1}{2}\right) \frac{\pi}{L_2} z\right] n_g(t=0) dz$$

and using the orthogonality of the cosines, and the initial condition 3).

Thus the solution consists of a series of "transient" terms which decay with frequencies $D_2 \left(\frac{2m+1}{2} \right)^2 \frac{\pi^2}{L_2^2}$ and terms proportional to those of the ideal solution for the liquid.

Since the diffusion coefficient is determined from the slope of the principal liquid mode, the relative magnitude, and the decay frequencies of the other terms must be considered. All of the transient terms except for the first decay very quickly compared to the liquid terms. The decay frequency of the first transient term is

$$\nu_{1g} = \frac{\pi^2 D_2}{4 L_2^2} \quad (m = 0)$$

compared with

$$\nu_{1L} = \frac{\pi^2 D_1}{L_0^2}$$

for the principal mode of the liquid. In the experiment $L_2/L_0=2$, so that the ratio of the two frequencies is

$$\nu_{1g}/\nu_{1L} = D_2/16D_1$$

At the lowest temperatures of the experiment D_2/D_1 is lowest, and the effect of the first transient mode will be largest. Using $D_2/D_1 \approx 40$, $\nu_{1g}/\nu_{1L} \approx 2\frac{1}{2}$,

and thus the effect could be noticeable. (Note that the frequency of the second transient mode,

$$\nu_{2g} = 9\nu_{1g} \approx 22\frac{1}{2}\nu_{1L},$$

and except near $T=0$ is completely insignificant). To calculate the relative magnitudes of the various terms, $n_3(Z,t)$ defined in 4) and 5) must be evaluated at the

sniffer, $Z=L_1$, $\simeq .6L_2$. A detailed calculation shows that the magnitude of the lowest transient mode (at the lowest temperatures) is less than about .07 of that of the principal liquid mode, and that the determination of the slope of the decay of the liquid mode is unaffected.

The solution 4), as written, looks as though singularities can occur, as for example when

$$\cos\left(2\pi\sqrt{\frac{D_1}{D_2}}\frac{L_2}{L_0}\right) \simeq 0$$

However, when this occurs

$$\sqrt{\frac{D_1}{D_2}}\frac{L_2}{L_0} = 1/4, \quad \text{and} \quad \nu_{2L} = \frac{4\pi^2 D_1}{L_0^2} = \frac{\pi^2 D_2}{4 L_2^2} = \nu_{1g} \quad (m=0)$$

i.e. the second order liquid mode has the same frequency as the zero gas mode, and the large magnitude of the coefficient of the $\exp(-\nu_{2L}t)$ term is almost completely cancelled by the coefficient B_0 , the net magnitude is thus quite small, and the principal liquid mode still dominates.

The result for the diffusion problem in the vapor can be understood in physical terms as follows: initial changes in the He^3 vapor concentration at the liquid surface produce a gradient at the surface. When the gradient "propagates" back to the sniffer, a change in the He^3 signal is detected. But a decrease in concentration at the sniffer causes flow of He^3 from the region above the sniffer, and the full effect of a change in the concentration at the surface is not felt until the gradient has propagated throughout the chamber. Further changes of

the surface concentration propagate much more quickly 41

since a gradient, and hence a current $J = D_2 \frac{\partial n_{3g}}{\partial z}$, has already been established. Thus the solution consists of a "transient" part whose characteristic length is that of the chamber, and a second part which readily responds to changes at the liquid surface. The higher order liquid terms enable the initial gradient to be established much more rapidly than if the principal liquid made were present alone, and the result is that the transient modes do not substantially contribute to the signal except near $t=0$.

IV. The Effect of the Finite Amount of He³ in the Vapor.

In obtaining the "ideal" solution, it was assumed that $J=0$, at the liquid surface. However the presence of a small, but finite, amount of He³ in the vapor (proportional to the He³ liquid concentration at the surface) means that there will be small fluxes of He³ passing between the liquid and the vapor as the liquid concentration at the surface changes. Although the vapor density is much smaller than that of the liquid, the ratio $\frac{c_v}{c_L} = \frac{P_3}{P_4} \frac{N_{3L}}{N_{4L}}$ is quite large (see Appendix) and the net effect is that the He³ number density in the vapor is about 3% of that for the liquid, ranging from .027 to .044 over the temperature range of the experiment.

To derive the effect of the small flux from the vapor to the liquid on the solution to the diffusion equation, the composite liquid-gas diffusion problem must be considered. The diffusion equation must be solved for the two regions simultaneously, with:

- 1) $D=D_1$ in the liquid, $Z < 0$
- 2) $D=D_2$ in the vapor, $Z > 0$
- 3) $J_1=J_2$ at the liquid surface, $Z=0$
- 4) $n_{3V}=\alpha n_{3L}$ at $Z=0$

The solution will be similar to the separate liquid and gas solutions, except the wave numbers and, hence the frequencies, will be shifted slightly.

Considering only the principal "liquid" mode, and ignoring the transient vapor modes, which are unimportant except near $t=0$, ~~and~~ the solution is:

- 5) liquid, $Z < 0$ $n_1 - n_{1\infty} = \sum a_n \cos k_n(z+L_1) \exp(-D_1 k_n^2 t)$
- 6) vapor $Z > 0$, $n_2 - n_{2\infty} = \sum b_n \cos K'_n(z-L_2) \exp(-D_2 K_n'^2 t)$

where L_1 , and L_2 define the boundaries of the diffusion chamber. Conditions 3) and 4) can be satisfied simultaneously if:

- 7) $D_1 k_n^2 = D_2 K_n'^2$ and
- 8) $\tan(k_n L) = -\alpha \left(\frac{D_2}{D_1}\right)^{1/2} \tan(K_n' L)$

The diffusion constant is determined from the principal liquid mode $n=1$, which dominates the solution except at

very small times, so that it is only necessary to determine k_1 . Note that $\alpha(D_2/D_1)^{1/2}$ is small, so

that $k_1 L_1 \approx \pi$ as expected. Let $\sqrt{D_1/D_2}$, also small, = ϵ_1 , and $k_1 L_1 = \pi - \epsilon_2$, and put $L_2/L_1 = 2.0$.

Then equation (8) after expanding the tangent, becomes:

$$9) \quad \tan \epsilon_2 = \frac{\alpha}{\epsilon_1} \frac{\tan 2\pi\epsilon_1 - 2\epsilon_1\epsilon_2}{1 + 2\epsilon_1\epsilon_2 \tan(2\pi\epsilon_1)}$$

Values for α are obtained from section IIC of the Appendix, ($\alpha \approx .03$ as mentioned above), initially, ϵ_1 , is obtained from the values of D gotten by assuming $k_1 L = \pi$, the "ideal" solution. The transcendental equation (9) is then solved for ϵ_2 , a new ϵ_1 obtained, and the process is iterated until a self consistent solution is obtained. The frequency of decay $\nu = k_1^2 D_1$, so that the diffusion constant for the liquid,

$$D_1 = \frac{\nu}{k_1^2} = \frac{\nu L_1^2}{(\pi - \epsilon_2)^2} = D_1' \frac{1}{\left(1 - \frac{\epsilon_2}{\pi}\right)^2}$$

where D_1' is the diffusion constant obtained assuming that $k_1 L = \pi$.

The above correction was computed using a programmed electronic calculator. The result was that the "ideal" diffusion coefficients were all shifted about the same amount, from 17 1/2% to 22% over the temperature range of the experiment.

In summary, the vapor correction can be understood as

follows: after a short period during which transient effects occur, the solution in the vapor follows the solution in the liquid, decaying with the same frequency. But in order for this to occur small currents flow from the vapor to the liquid across the surface. The liquid mode accomodates this by making $k \cdot L$ slightly less than π

so that $D_1 \frac{\partial n_{3L}}{\partial z} \Big|_{z=0}$ just matches the

vapor current. The shift derived above, is about the same over the entire temperature range, the largest shift being only about 4% more than the smallest.

V. Effects Due to the "Sniffer" Capillary

A. Pumping Effects.

1. In several runs the system was allowed to come into equilibrium and a steady He^3 signal obtained and observed as a function of time. The resulting decay (or lack of it) is then due to omegatron fluctuations, and any pumping effect due to the sniffer. Observations at about 1.5°K , near the middle of the temperature range, indicate that an upper limit for such an effect is about 1% in an hour. As the diffusion times are all smaller than this, the direct effect of the sniffer on the He^3 signal is insignificant.

2. Most of the flow through the sniffer is due to the He II film. The total flow rate can be estimated from the pressure measured by the ion gauge. This was

nominally about 1.4×10^{-5} mm of mercury which when corrected for the relative ionization efficiency of helium⁽⁵⁾ gives about 6×10^{-5} mm. The pumping speed at the ionization gauge is determined primarily by the flow resistance of the pump tube. For free molecular flow of a gas of molecular weight M in a tube of radius a, and length L, the flow conductance is⁽⁶⁾

$$F = 30.5 \frac{a^3}{L} \sqrt{\frac{T}{M}} \quad \text{liters per second}$$

$$\text{or } \dot{N} = \left(30.5 \frac{a^3}{L} \sqrt{\frac{T}{M}} \right) \left(\frac{9.6 \cdot 10^{21} P_{\text{mm}}}{T} \right)$$

atoms/second into the vacuum system.

Putting T=room temperature about 290°K, $P=6 \times 10^{-5}$ mm and the relevant dimensions, the flow rate is about 3×10^{16} atoms/second. This is equivalent to 1.5×10^{-6} cc of liquid per second. The sniffer radius was 1 mil, and the perimeter about .016cm. The flux divided by the perimeter is then about 10^{-4} cc per cm. Values for the film transfer rate given in the literature⁽⁷⁾ range from about 7×10^{-5} to about 17×10^{-5} cm³/cm, the higher values presumably resulting from surface contamination. The magnitude of the total pressure is thus consistent with the film flow rate of the sniffer. The transfer rate of 1.5×10^{-6} cc/second, when considered as a fraction of the total amount of liquid in the chamber-about 14cc, implies a change in liquid level of about a few mils per hour, clearly a negligible effect.

3. The pumping of the helium vapor produces a net evaporation rate at the surface of the liquid, and therefore a small cooling effect. However, the surface of the liquid is in direct thermal contact with the exterior bath via the copper block in the diffusion chamber, so that there can be no heat flow through the mixture itself, and no heat flush effect. As it turns out, the amount of heat withdrawn is negligible anyway--the heat flux is the flux of atoms times the latent heat per atom, about 7°K for He⁴. The vapor flow is at most 10% of the total flux of atoms, so that

$$Q \lesssim (1.4 \times 10^{-23})(7^\circ)(3 \times 10^{15}) \approx 3 \times 10^{-7} \text{ watts}$$

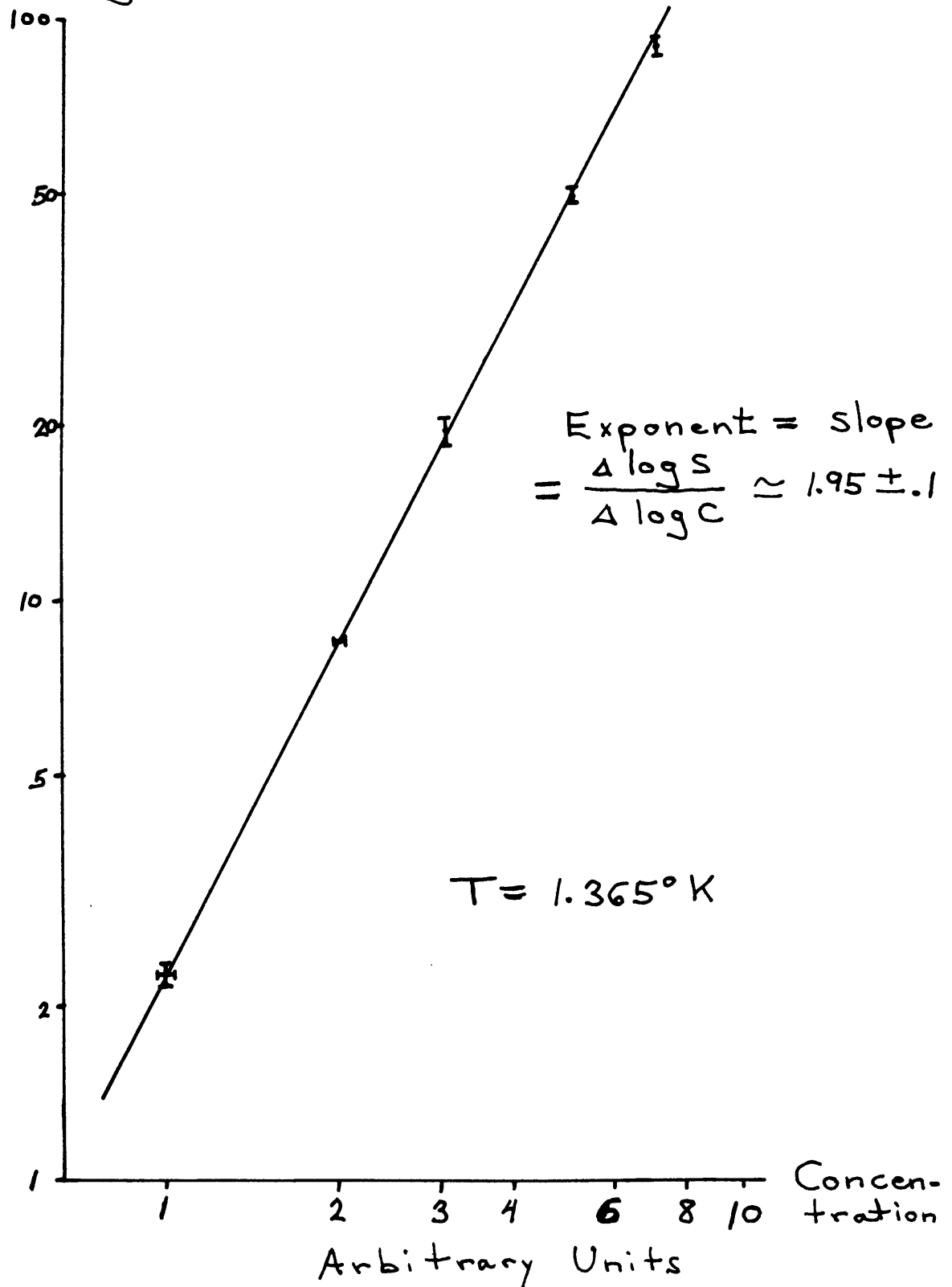
which is less than 1/400 of the power applied to the heater in the actual runs.

B. Transmission of the Vapor

It was observed that at a given temperature, the omegatron signal increased nonlinearly with He³ concentration. Since it has been well established that for dilute He³-He⁴ mixtures, the He³ partial pressure varies linearly with liquid concentration, this effect must be due to the flow properties of the sniffer in the presence of the superfluid film. If the flow were strictly the viscous flow of gas through a tube, the pressure gradient and the average pressure would be determined by the total pressure in the chamber $\approx P_4$. The He³ flow would be the $P_3/P_4 \cdot f(P_4)$, and the flow would be linear in P_3 . However,

in the experiment film flow was also present; in fact it was of the order of 10 times that measured when only helium gas was present in the chamber. Although the flow of gas under these conditions is quite complicated, the reason for the nonlinearity of the He^3 flow can be qualitatively understood. In order for the film flow to transport such relatively large numbers of atoms through the sniffer, most of the evaporation of the film and thus most of the pressure drop must occur near the end of the sniffer. He^3 does not participate in superfluid flow⁽⁸⁾ so that the pressure near the beginning of the sniffer is approximately P_{40} , (the pressure of pure He^4), while the pressure in the diffusion chamber is $P_3 + P_4$. Thus, the initial pressure gradient will be determined at least in part by P_3 , so that the net flow of He^3 to the vacuum system will depend on P_3 both through the vapor concentration, and through a pressure gradient which in part determines the total gas flow rate. This indicates that the He^3 flow rate is a nonlinear function of P_3 .

The details of the mechanism for producing the nonlinearity were not explored since the effect could be corrected for by determining the relationship between signal and concentration empirically. Measurements taken at two temperatures indicate that to a good approximation the signal S varies as: $S \sim n_3^P$ where P is a function of temperature. Figure 6 shows $\log S$ plotted versus $\log n_3$

Figure 6 - Sniffer FunctionHe³ Signal

for $T=1.365^\circ\text{K}$, the straight line indicating the power law relationship. Further, less detailed, data were taken over the entire temperature range of the experiment. The range of P was from about 1.2 to 2.4.

The diffusion constant is determined from the slope

$$\Delta \log [n_3(t) - n_{3\infty}] / \Delta t$$

Let the signal S be determined from a power law $S \sim n^g$.

Then for n not too far from n_∞ , the above slope is insensitive to the precision to which g is known. Suppose it is assumed that $S \sim n^P$, then $n \approx \bar{n}$ will be assumed to be $S^{1/P} = An^{g/P}$.

$$\begin{aligned} \text{Then } (\bar{n}(t) - \bar{n}_\infty) &= A(n^{g/P} - n_0^{g/P}) \\ &= An_0^{g/P} \left[\left(\frac{n}{n_0} \right)^{g/P} - 1 \right] \end{aligned}$$

$$\log \bar{n}(t) - \bar{n}_\infty = \text{const.} + \log \left[\left(\frac{n}{n_\infty} \right)^{g/P} - 1 \right]$$

putting $n = n_\infty + \Delta n$, this becomes

$$\log (\bar{n} - \bar{n}_\infty) = \text{const.} + \log \left[\left(1 + \frac{\Delta n}{n_\infty} \right)^{g/P} - 1 \right]$$

$$\approx \text{const.} + \log \frac{\Delta n}{n_0} \left(1 + \frac{1}{2} \left(\frac{g}{P} - 1 \right) \frac{\Delta n}{n_0} \right)$$

after expanding $\left(1 + \frac{\Delta n}{n_\infty} \right)^{g/P}$ and keeping the first

3 terms. For $\frac{\Delta n}{n_\infty} \ll 1$, $\log [\bar{n}(t) - \bar{n}_\infty]$ is

independent of P. For larger Δn , P need only approximate g for precise values of $\log(\bar{n}(t) - n_\infty)$ to be obtained. In the experiment the error in g is estimated at about $\pm .15$, and the resulting error in D at less than 1%.

VI. Method for Determining D

The diffusion coefficient is determined from the measurements of the decay of the He^3 signal by computing the slope: $\Delta \log(n(t) - n_\infty) / \Delta t$, after

waiting a short time until the transient vapor modes, and the higher order liquid modes have damped out. The discussion of this chapter indicates that the details of the experimental configuration—the geometry of the diffusion chamber, the presence of the sniffer capillary, and the monitoring the diffusion in the liquid via the vapor concentration—do not affect the general validity of this method. However, n is derived from the signal S by $n \sim S^{1/P}$ where P varies from 1.2 to 2.4, and D is related to the measured slope by: $D = (\text{slope}) / k^2$, where $k = \frac{\pi}{L} (1 - \epsilon)$, and ϵ varies from .077 to .095 over the temperature range of the experiment.

References for Chapter 3

1. Philip J. Bendt, *Phys. Rev.* 110:85 (1958).
2. E. G. D. Cohen, M. J. Offerhaus, and J. DeBoer, *Phys. Rev.* 20:501 (1954).
3. L. Monchick, E. Mason, and R. Munn, and F. Smith, *Phys. Rev.* 139:A1076 (1965).
4. R. A. Buckingham, and R. A. Scriven, *Proc. Phys. Soc. (London)* A65:376 (1952).
5. Saul Dushman, *The Scientific Foundation of Vacuum Technique*, John Wiley, (N.Y., 1962) p. 319.
6. Ibid. p. 89.
7. See for example:
 - a. R. K. Waring, *Phys. Rev.* 99:1704 (1955).
 - b. G. R. Hebert, K. L. Chopra, and J. B. Brown, *Phys. Rev.* 106:391 (1957).
8. J. G. Daunt, R. E. Probst, and H. L. Johnston, *J. Chem. Phys.* 15:759 (1947).

CHAPTER 4

Some Theoretical Considerations

I. Relation of the Diffusion Coefficient to the Cross Section

To extract information from the diffusion measurements, the relationship between D and more fundamental quantities, such as the cross section, must be known. For a dilute mixture of two classical gases, simplified kinetic theory gives:

$$(1) \quad D = \frac{\bar{v}\lambda}{3} = \frac{\bar{v}_3}{3\sqrt{2}n_r\sigma}$$

where the mean free path λ in a Maxwell-Boltzmann gas is

$1/\sqrt{2}n_r\sigma$. More rigorous theory gives⁽¹⁾:

$$(2) \quad D = \frac{3\pi}{32} \frac{\bar{v}_3}{\sqrt{\beta}n_r S}$$

where

$$\beta = \mu_r / (\mu_r + m_3^*)$$

$$(3) \quad \text{and} \quad S = 2\pi \int \sigma\left(\sqrt{\frac{2\mu r}{\mu}} x, \theta\right) (1 - \cos\theta) d(\cos\theta) x^5 e^{-x^2} dx$$

$(\mu = \beta m_3^*)$

S is an effective cross section which takes into account the velocity distribution of the gas, and the fact that diffusion is produced mainly by large angle scattering.

The diffusion problem in a dilute He^3 - He^4 solution involves particles having a nearly classical energy spectrum interacting with particles having the roton and phonon energy spectra. This problem is more complicated than the problem of classical particles, and requires solving the Boltzmann equation, in the presence of a concentration gradient, for rotons, phonons, and He^3

quasi-particles. This has been done by Khalatnikov, and Zharkov⁽³⁾ (referred to subsequently by "KZ"), who consider the more general problem with both concentration and temperature gradients present, and present solutions for various simplifying circumstances. In deriving their solution, KZ observe that:

1. Above .6°K, the phonons play no part in transport processes. Although this point is not discussed at length in their article, it would appear that this is due in part to kinetics. At the lowest temperatures of the experiment, where phonons would play the largest role, the average phonon momentum $\bar{k}_{ph} \approx 3kT/\hbar c$ is about 1/4 of the average He³ momentum $\bar{k}_3 \approx \sqrt{\frac{3m^* k_B T}{\hbar^2}}$, so that very few of the phonons can effect large momentum transfers required for large angle scattering of the He³ atoms. Since diffusion is determined primarily by large angle scattering, this means that phonons play a much smaller role than is suggested by their number density which is almost as large as the roton density at 1.27°K.

2. If the number density of He³ atoms is much smaller than the number density of rotons, then the roton distribution can be taken to be the equilibrium distribution.

3. Inelastic processes, such as the creation of phonons, when a He³ atom is decelerated in a collision, are improbable and can be neglected.

4. Thermal diffusion is negligible when n_3 is much less than n_r .

The solution for the diffusion coefficient in the high temperature regime, $T > .6^\circ\text{K}$, obtained by KZ is:

$$(4) \quad D = \left(\frac{\rho_{no}}{\rho_n} \right) \frac{kT}{n_r m_3} \overline{\left(\frac{1}{\sigma_{3r}^* V_3} \right)}$$

where: ρ_{no} = normal density contribution from the He^4 excitations,

ρ_n = total normal density,

$$(5) \quad \overline{\left(\frac{1}{\sigma_{3r} V_3} \right)} = \frac{\int p_3^2 d^3 p_3 \frac{n_3(p_3)}{\sigma_{3r}^* V_3}}{\int p_3^2 d^3 p_3 n_3(p_3)}, \quad \text{and}$$

where $n_3(p_3) \sim \exp[-(\epsilon_0 + p_3^2/2m_3^*)/kT]$, and

$$(6) \quad \sigma_{3r}^* = \frac{1}{2} \int_{-1}^1 \sigma_{3r}(\theta) (1 - \cos\theta) d(\cos\theta)$$

and σ_{3r} has been assumed to be independent of p_r .

II. Temperature Dependence of D

A. Khalatnikov and Zharkov Calculation of the Cross Section⁽²⁾

KZ calculate the roton- He^3 cross section by assuming that the interaction can be approximated by $V(\vec{r}_r, \vec{r}_3) = V_0 \delta(\vec{r}_3 - \vec{r}_r)$. (No physical reason for this choice is given.) The cross section is then determined by calculating the transition rate from the "Golden Rule" of perturbation theory:

$$(7) \quad dw = \frac{2\pi}{h} |V_{12}|^2 \delta(E_r + E_3 - E_{r'} - E_{3'}) \frac{\Omega^2}{(2\pi)^6} d^3k'_3 d^3k'_r$$

where the primed quantities refer to the final state in the collision, and V_{12} is the matrix element of the potential evaluated between the initial and final states.

The kinetics for roton-He³ collisions are complicated. For example, the magnitude of the relative velocity, when viewed from the center of momentum frame, is not conserved as for particles having classical spectra, and the usual simplification resulting from putting the problem into the "center of mass" frame does not seem to apply here. The choice of the delta function potential simplifies the calculation, but integrating the final densities of states, which first must be written in terms of the initial momenta, and angles of incidence, is still quite tedious. After some work, ∇_{3r} is derived in terms of V_0 , u_r , and m_3^* . The important point is that ∇_{3r} is independent of the He³ and roton energies.

B. Evaluation of (ρ_{nr}/ρ_n)

The roton contribution to the normal density can be written $\rho_{nr} = n_r (p_0^2/3kT)$, a result which was pointed out by Landau. Numerically, this is $\rho_{nr} \approx \left(\frac{15 m_H}{T}\right) n_r$. (Note that

$p_0^2/3kT$ refers to an effective mass for convective transport, since the normal density is defined in terms

of the momentum density of a heat current, Q ,

$$\frac{|\vec{P}|}{V} = \rho_n |\vec{v}_n| = \rho_n (Q / \rho_s T) .)$$

The normal density contribution of the He^3 atoms is $n_3 m_3^* (2)$. In the experiment, the He^3 concentration was about $1.4-1.5 \cdot 10^{-4}$, equivalent to a He^3 number density of about $3.0 \cdot 10^{18}$. The number density of rotons (see Appendix) varied from about $7.0 \cdot 10^{19}$ at the lowest temperature, to $5.1 \cdot 10^{20}$ at the highest temperature.

Thus, $n_3 \ll n_r$ and $\rho_{n3} / \rho_{nr} = (n_3 m_3^*) / (n_r \frac{p_3^2}{3kT}) \simeq \frac{n_3}{n_r} \frac{8.1T}{60} \simeq 0$

making $\frac{\rho_{ne}}{\rho_n} \simeq 1$. If higher concentrations had been used, this would not have been true; for a 1% He^3 solution at 1.27° , ρ_{n3} / ρ_n is about 1/3.

Thus, for conditions of the experiment

$$(8) \quad D = \frac{kT}{n_r m_3} \left(\frac{1}{\overline{v_{3r}^* v_3}} \right)$$

If the delta function approximation is valid, that is if the roton- He^3 potential is like that of a hard sphere of very small radius, then $\overline{v_{3r}^*}$ is independent of p_3 , the momentum of the He^3 atom. Then, since $v_3 \sim T^{1/2}$, and $n_r \sim T^{1/2} \exp(-\Delta/T)$, the temperature

dependence of the diffusion constant is given by: $D \sim \exp(\Delta/T)$

where Δ is the roton energy gap.

III. Spatial Distribution of Rotons

The quasi-equilibrium achieved after the heater has been on for a long time implies a time independent exponential He^3 distribution, and a steady normal fluid current of excitations. Since the entropy is dominated by the roton contribution, and since it is roton- He^3 collisions which are of interest for diffusion, only the roton distribution will be considered.

The spatial distribution of rotons is derived from the condition that there is no acceleration of the superfluid. This is equivalent to setting the net gradient produced by the fountain pressure, the osmotic pressure, and the hydrostatic pressure equal to zero. The hydrostatic pressure accounts for a small effect, which is present whether or not the heater is on, and so will be ignored. (It is interesting to note, though, that the equations imply a thermomechanical effect in pure He II in a column of liquid, even without the presence of a "superleak".) Then ΔP_f equals ΔP_{os} . In Appendix I, it is shown that: $\Delta P_f = \rho_s \Delta T = \Delta(n_r kT)$ for the roton gas. Thus the condition on the superfluid becomes:

$$(9) \quad \Delta(n_3 kT) = \Delta(n_r kT)$$

$$\text{or} \quad kT \Delta n_3 + n_3 k \Delta T = kT \Delta n_r + n_r k \Delta T$$

Since $n_3 \ll n_r$, the second term on the left hand side is negligible. Also the second term on the right hand side

is about 15% of the first so that to a first approximation

$$\Delta n_r \simeq \Delta n_3 \quad .$$

The initial roton gradient is thus about the same as the initial He^3 gradient. In the experiment, the He^3 gradients were of the order of n_3/L , and since $n_3 \ll n_r$, $\Delta n_r/n_r$ must be very small, i.e. the initial roton number density is approximately spatially uniform.

IV. Concentration Effects in Mixtures

In a number of experiments with He³-He⁴ solutions, the purpose of the He³ atoms is to act as probes to study the nature of the He⁴ excitations. In such experiments it is desirable to know what effect the presence of the solute atoms has on the excitation spectrum and on the excitation number density.

A. Estimate of Magnitude

The magnitude of such an effect can be estimated from the following considerations:

1. The neutron scattering data indicate that as the number of excitations gets to be large and the mean free path for an individual roton gets to be small, the linewidths of the individual excitations become large and the energy gap decreases.
2. The data for this effect at intermediate temperatures are sparse but the level at which the effect becomes noticeable, on the order of a few tenths of a degree, is at about 1.7° where $Nr=5 \times 10^{20}/\text{cm}^3$. (See Appendix I).
3. The magnitude of the cross section for He³-roton interactions as derived from the present experiment (in approximate agreement with the value obtained from thermal conductivity measurements) is from 1.6 to $24 \times 10^{-14} \text{cm}^2$. The roton-roton interaction estimated⁽³⁾ from viscosity data is about $5 \times 10^{-15}/T^{1/2} \text{cm}^2$. Thus He³ solute atoms are more effective than other rotons in limiting the roton mean free path, by a factor of about 5. (Phonons play a very small role in limiting the roton mean free path.)
4. Thus, if the variation of the roton energy parameters with the

temperature is primarily a mean free path effect, one can estimate the He^3 number density at which the effect is important at about $10^{20}/\text{cm}^2$. This corresponds to a concentration of about 5×10^{-3} .

B. Some Experimental Data

The above effect of He^3 solute atoms on the roton spectrum has been generally ignored in many of the papers on He^3 - He^4 solutions. The effect has been observed by Esel'son et al.⁽⁴⁾ in measurements of positive ion mobilities in dilute He^3 - He^4 mixtures. Esel'son et al. find that for pure He^4 $\mu^+ \sim \exp(\Delta/T)$ where $\Delta = 8.8^\circ$ (in good agreement with Rief and Meyer⁽⁵⁾ indicating that the mobility is determined by ion-roton scattering. The reason for the exact value of Δ obtained is not understood. At finite He^3 concentrations, Esel'son et al. find that at sufficiently low temperatures or sufficiently high enough concentrations the mobility becomes independent of temperature, and inversely proportional to the concentration. In this region the mobility is dominated by He^3 -ion interactions which are apparently independent of temperature. Since $1/\mu$ is proportional to the cross section, and the scattering centers are presumably independent, the roton contribution to the mobility is: $1/\mu_r^+ = 1/\mu^+ - 1/\mu_3^+$

The authors find that μ_r^+ calculated in this way varies as $\exp(\Delta/T)$, where Δ varies with He^3 concentration. At $c = 7.5 \times 10^{-3}$, Δ is about 7.7° with an upper limit of about 8.2° to 8.3° . At $c = 6.3 \times 10^{-2}$, Δ is below 6° . Additional results are presented at higher concentrations which agree with data from 4th sound measurements⁽⁶⁾.

The above data together with the order of magnitude calculation, suggest that the roton energy spectrum and hence the number density are

altered in He^3 solutions having concentrations of about 1/2% or more. The effect on the number density for a change in Δ , $\Delta(c) - \Delta(o)$, is a factor of $\exp[(\Delta(c) - \Delta(o))/kT]$. This effect can be substantial. At 1.2°K, a difference in Δ of .4°K, leads to a factor of $e^{.3}$ or about a 35% change in number density. However, in the present work, $c = 1.45 \times 10^{-4}$, and the effect should be negligible.

References for Chapter 4

1. E. H. Kennard, Kinetic Theory of Gases, McGraw Hill (New York, 1938) p. 194.
2. I. M. Khalatnikov, and V. N. Zharkov, Soviet Physics JETP 5:905 (1957).
3. J. Wilks, The Properties of Liquid and Solid Helium, Oxford Press, (Oxford, 1967), p. 177. Also, L. D. Landau, and I. M. Khalatnikov Zh. E. T. F. 19:637 (1949) (in Russian).
4. B. N. Esel'son, Yu. Z. Kovdrya, and V. B. Shikin, Soviet Physics JETP 32:37 (1971).
5. F. Rief and L. Meyer, Phys. Rev. 119:1164 (1960). ✓
6. N. E. Dymnikov, B. N. Esel'son, E. Yu. Rudavskii, and I. A. Serbin, Sov. Phys. JETP 29:406 (1969).

CHAPTER 5

Data and Data Analysis

I. General Observations

Using the apparatus and procedure described in previous sections, measurements of the decay time of the applied concentration gradient were made. Thirty four runs were analyzed at 17 temperatures between 1.274°K and 1.693°K. Most of the runs were made at concentrations of about $1.45 \cdot 10^{-4}$. Five runs were made at concentrations 2 to 4 times higher. The power applied to the heater was $1.3 \cdot 10^{-4}$ watts, equivalent to about 30 microwatts/cm². In a few of the runs larger amounts of power were applied up to twice this amount. Some general observations follow:

1. At a given temperature, the He⁴ signal remained constant, independent of whether the heater was on or off.

2. The He³ signal increased by a factor of from 2 to 5, depending on temperature, when the heat (lower power) was applied.

3. After correcting for the "sniffer function" $n = S^{1/P}$, plots of $\log [n(t) - n_{\infty}]$ versus time indicate a fast decay near $t=0$ becoming an almost pure exponential at later times, as expected.

4. The slopes derived were independent of the power applied to the heater.

Plots of $\log [n(t) - n_{\infty}]$ appear on subsequent pages. The points at large times, near the end of the curves have a relatively large amount of scatter since a small error in n produces a large error in $\log(n - n_{\infty})$ when n is near n_{∞} . At small times, the pure exponential form has

Figures 7 through 17 - Data from 11 of the 35 runs is shown on pages 60 through 76. The data include runs at 10 temperatures covering the entire temperature range of the experiment. In the plots $\log (n - n_{\infty})$ is plotted versus time. A few error brackets for the run indicate the estimated uncertainty in reading the recorder, and that due to short term fluctuations.

Figure 7 $T = 1.693^{\circ}\text{K}$ (Run No. I26-A)

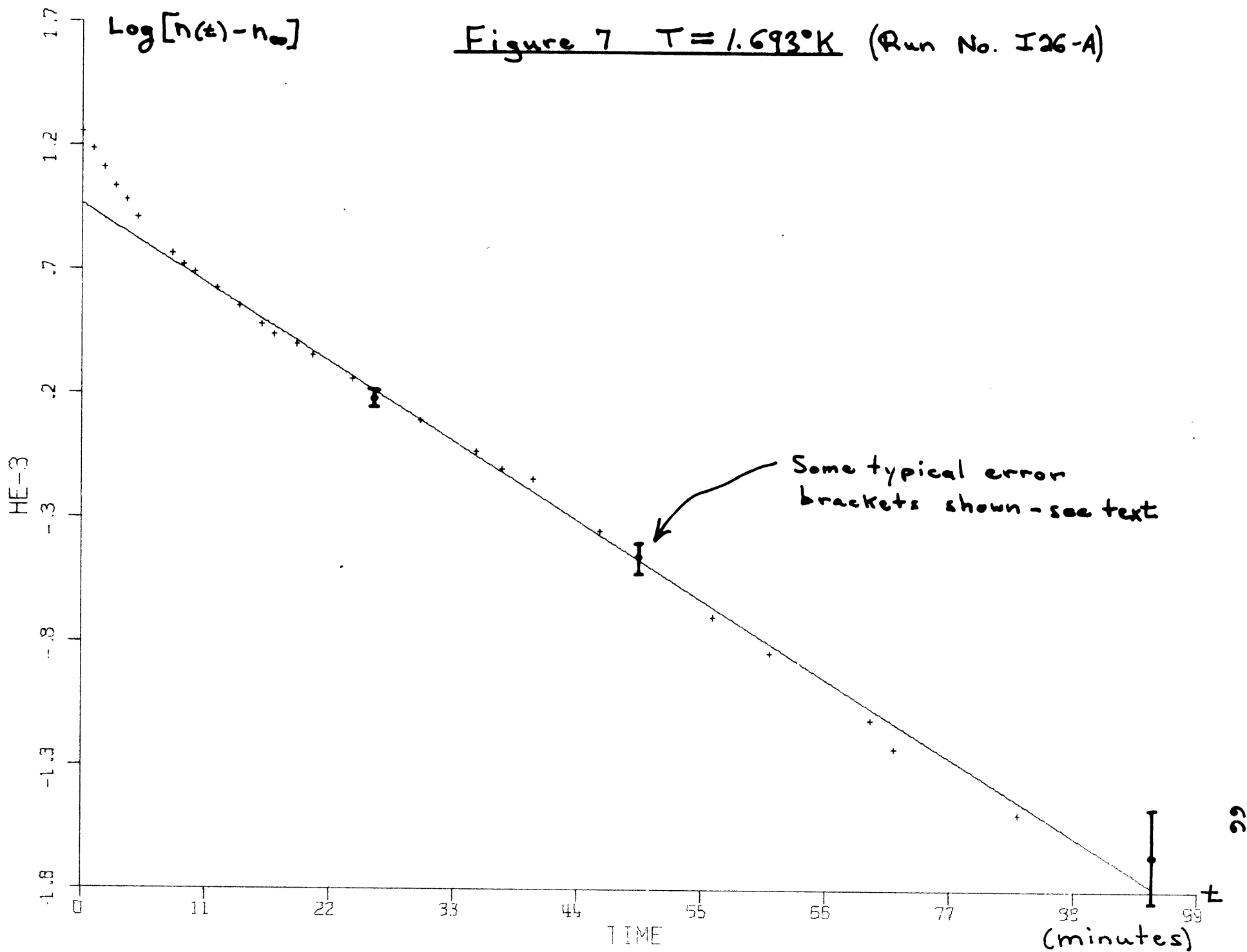


Figure 8 - $T = 1.611^\circ\text{K}$
(Run # I-24A)

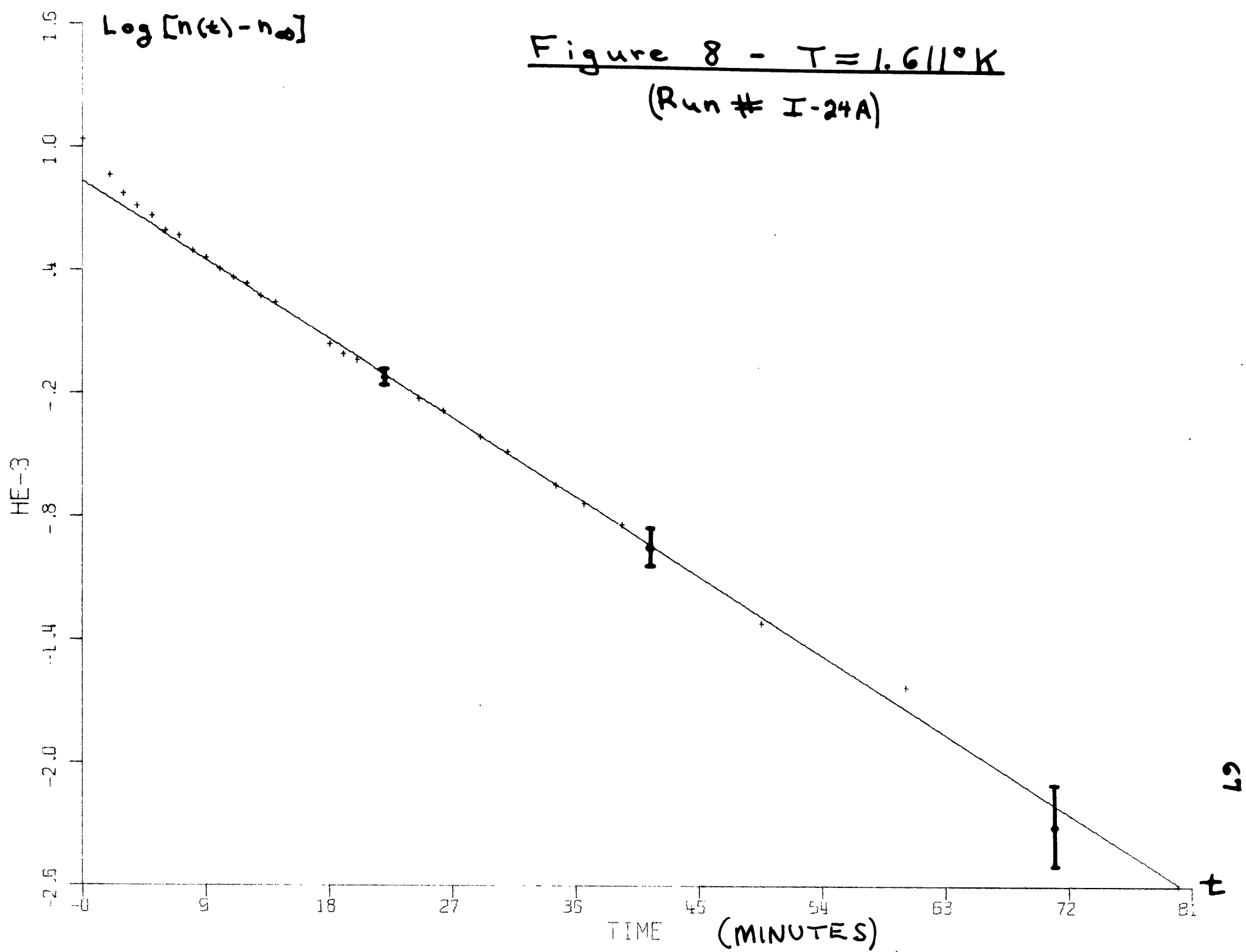


Figure 9 $T = 1.580^\circ\text{K}$
(Run #J-9)

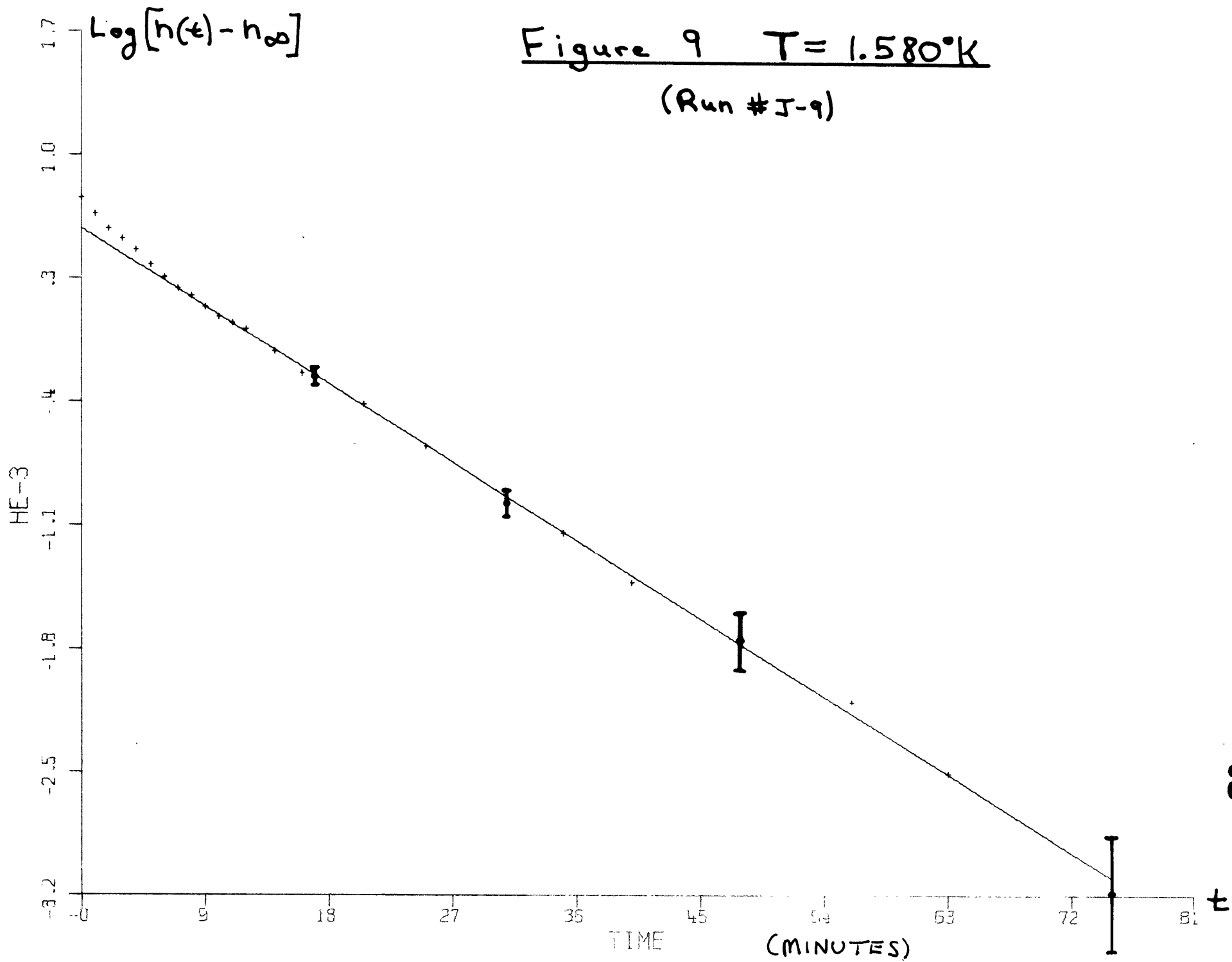


Figure 10 - $T = 1.565^{\circ}\text{K}$
(Run # K-5A)

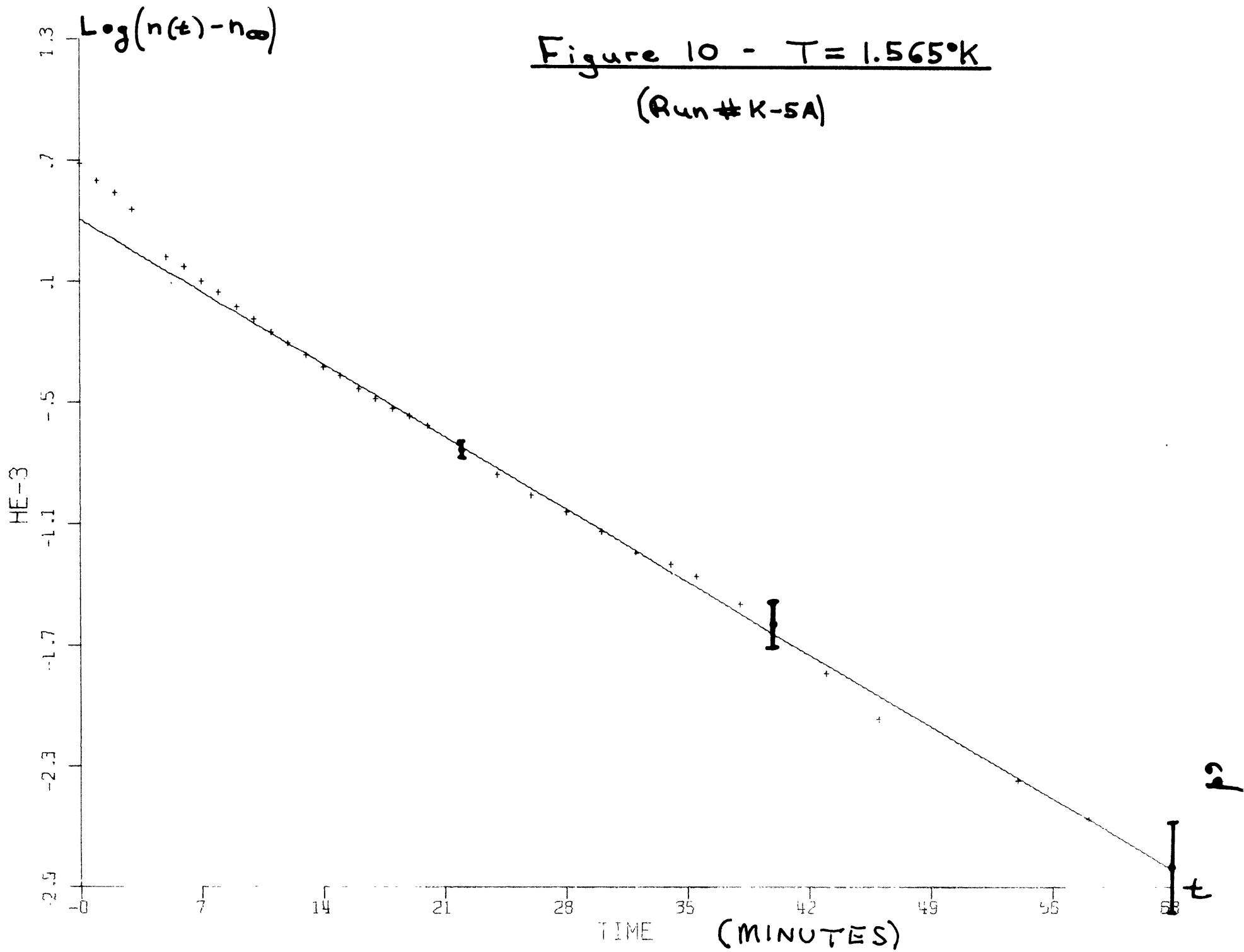


Figure 11 - 1.530°K
(Run # I-4B)

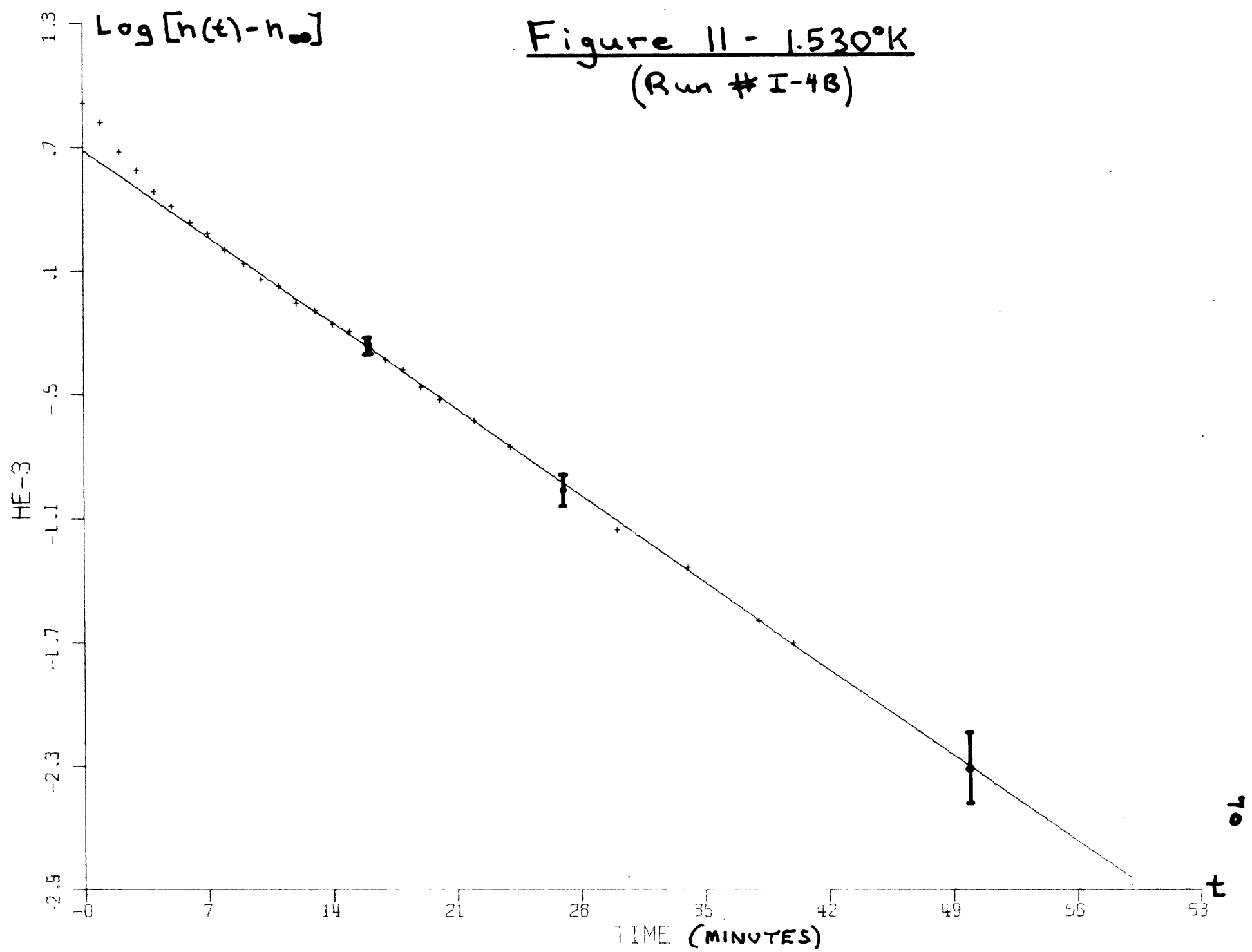
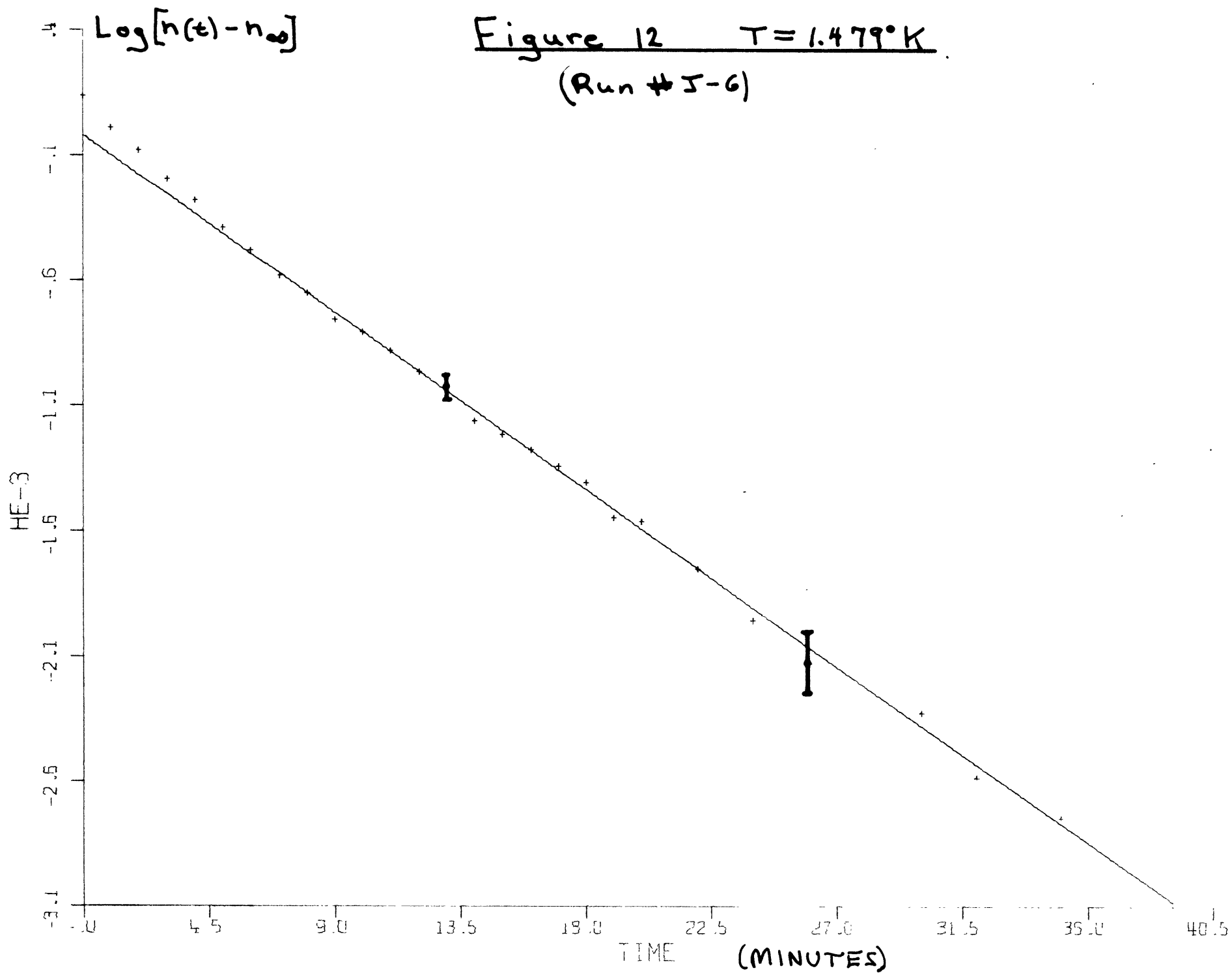


Figure 12 $T = 1.479^\circ\text{K}$
(Run # J-6)



71
4

Figure 13 - $T = 1.437^\circ\text{K}$
(Run # K-5B)

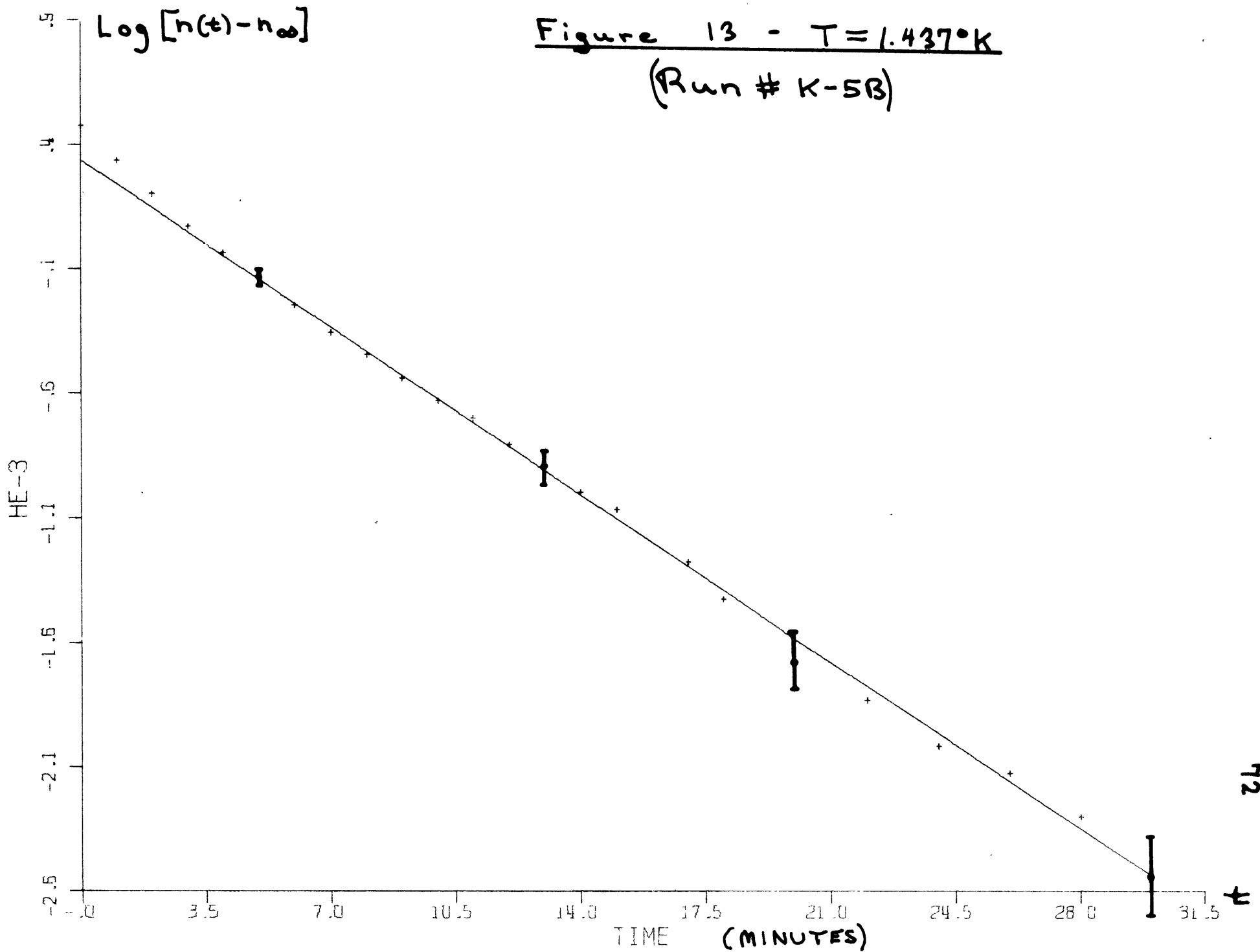


Figure 14 - $T = 1.409^\circ\text{K}$
(Run # J-4)

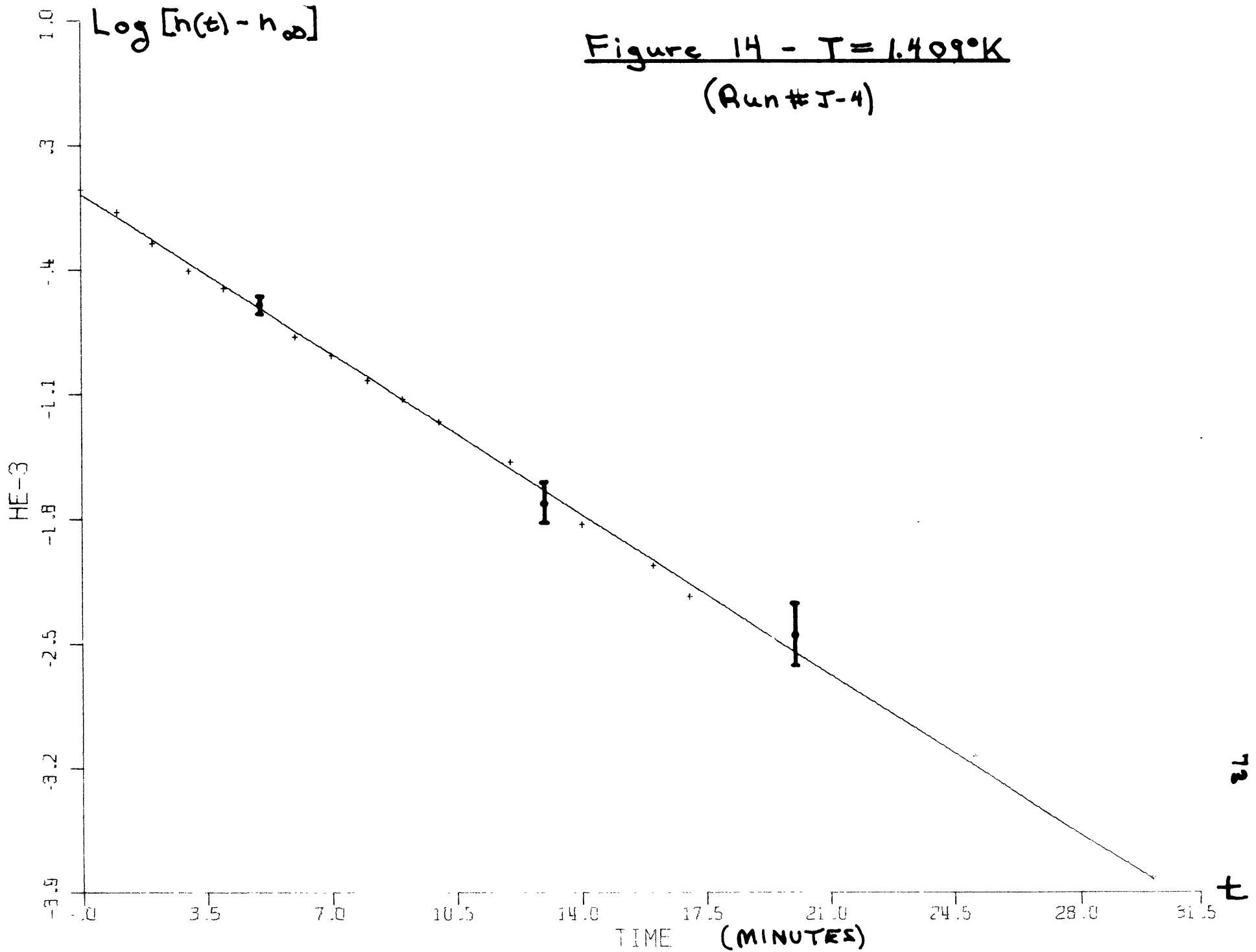


Figure 15 - $T = 1.360^\circ\text{K}$
(Run # K-3A)

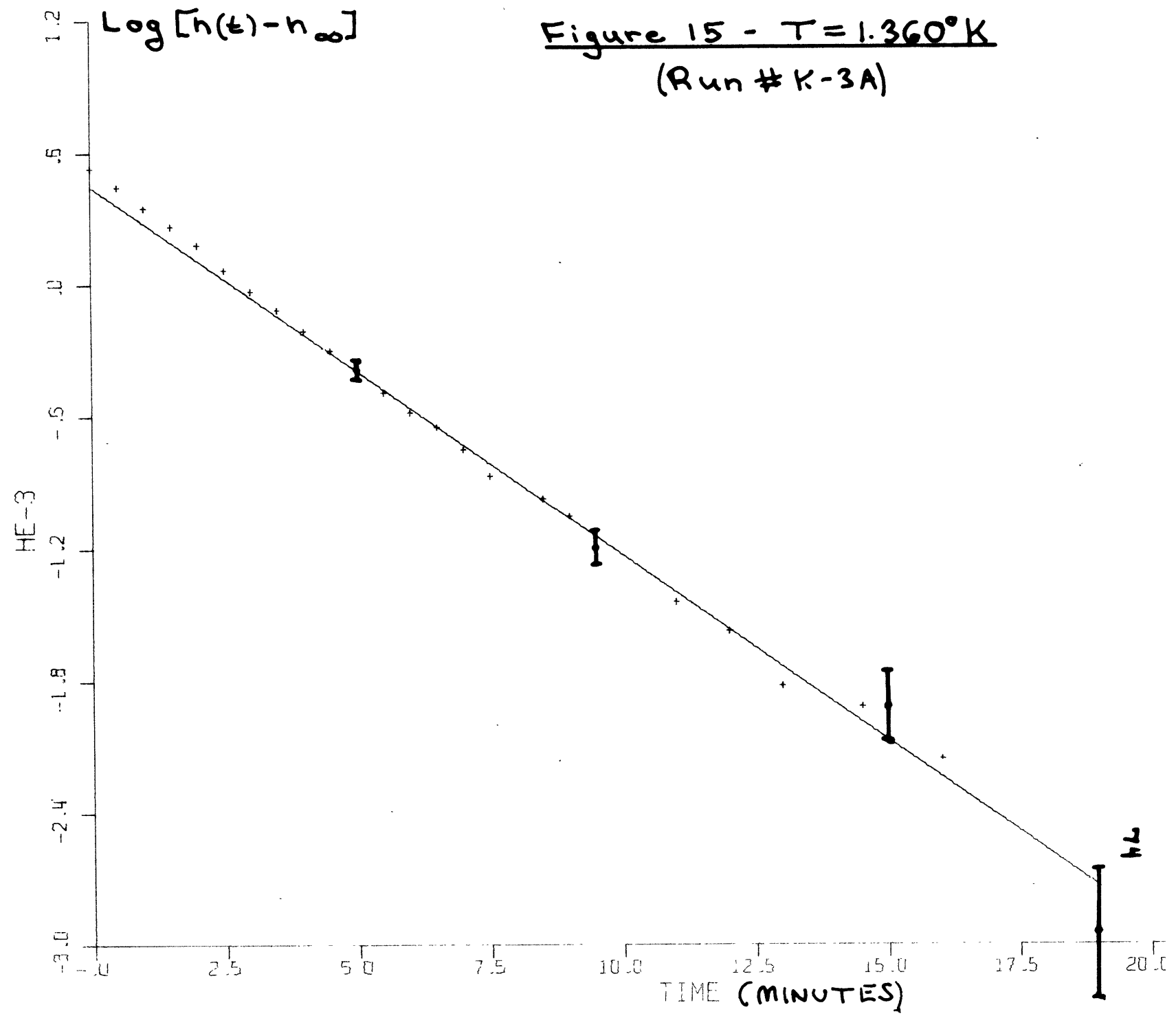
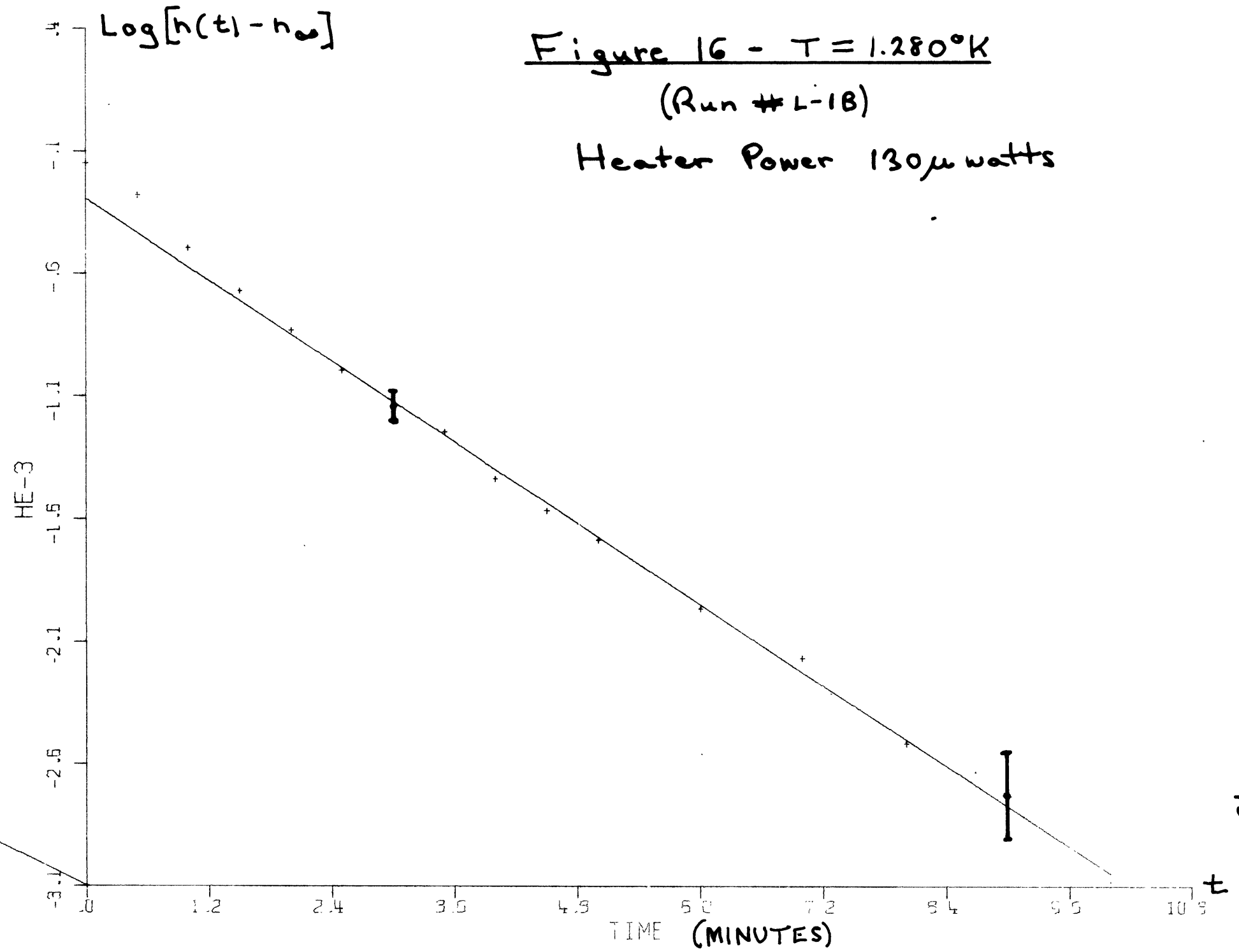


Figure 16 - $T = 1.280^{\circ}\text{K}$

(Run # L-18)

Heater Power $130\mu\text{watts}$



75

7

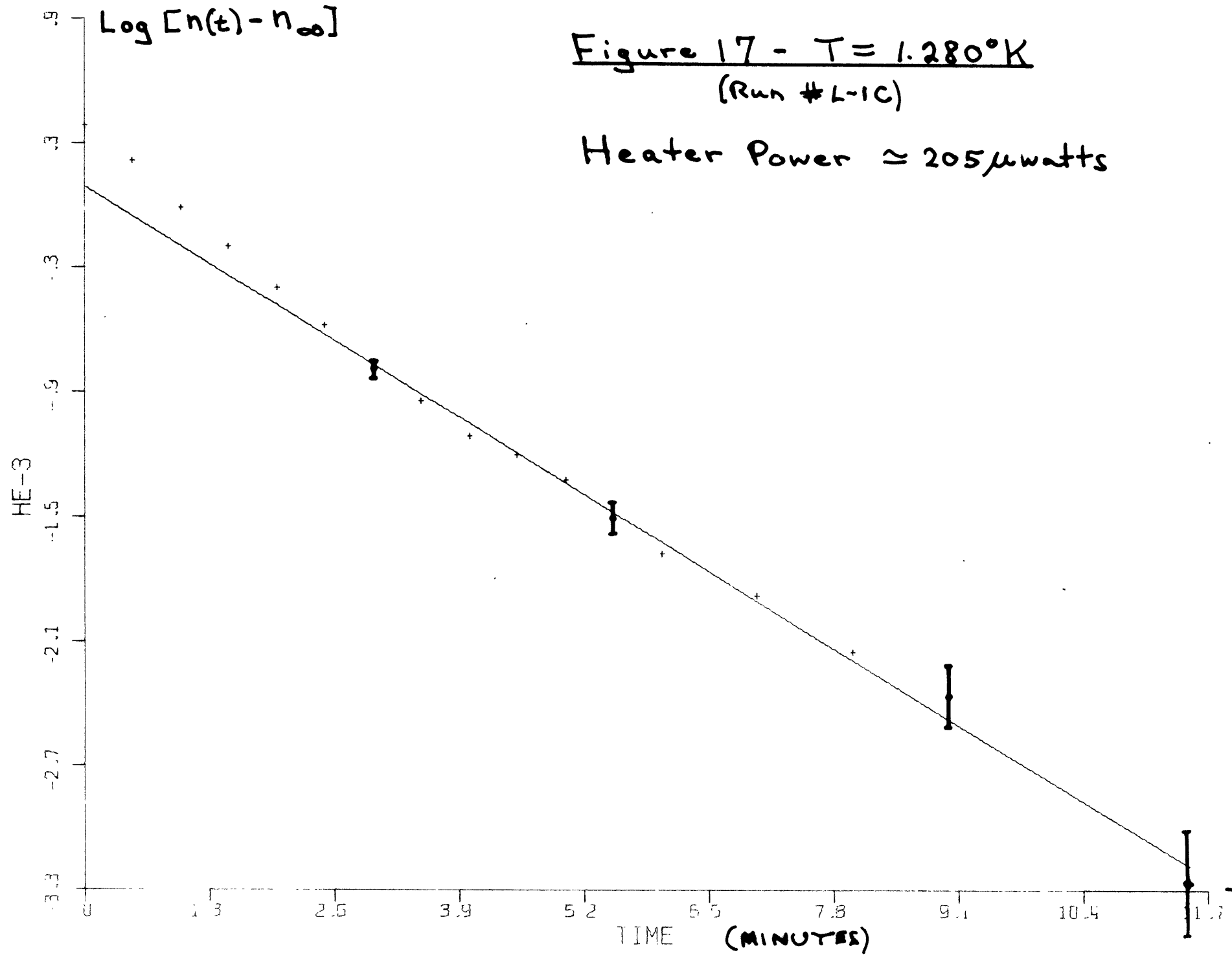


Figure 17 - $T = 1.280^{\circ}\text{K}$
(Run # L-1C)

Heater Power $\approx 205 \mu\text{watts}$

76
77

not yet been reached, so that most of the information regarding the diffusion coefficient is contained in the middle of the curves. In general the higher temperature runs took much longer to decay, but the signal levels were higher, and hence, less noisy.

The independence of the slope of the curves on the power applied to the heater is illustrated by the two runs at $T=1.28^\circ$ in figures 16 and 17. These graphs show decays at heater powers of 130 and 205 microwatts. The initial omegatron signals (uncorrected for the sniffer response) were about $4 \frac{1}{3}$ and $8 \frac{1}{2}$ times the final signals, for the lower power and higher power respectively. Least square fits to the two curves gave slopes which were identical to within the experimental error in either one. Thus, although the higher heater power produced an initial signal which was twice that produced by the lower heater power, the slopes of the asymptotic exponential decays were the same.

II. Determination Diffusion Constant, and Discussion of Sources of Error

A. Method For Determining D from the Data

The slopes of the exponential curves were derived from least square fits to the curves. In fitting the data, the sniffer response function, the equilibrium level n_∞ , and the time t_1 after which the higher order modes in the decay could be ignored had to be known. The sniffer

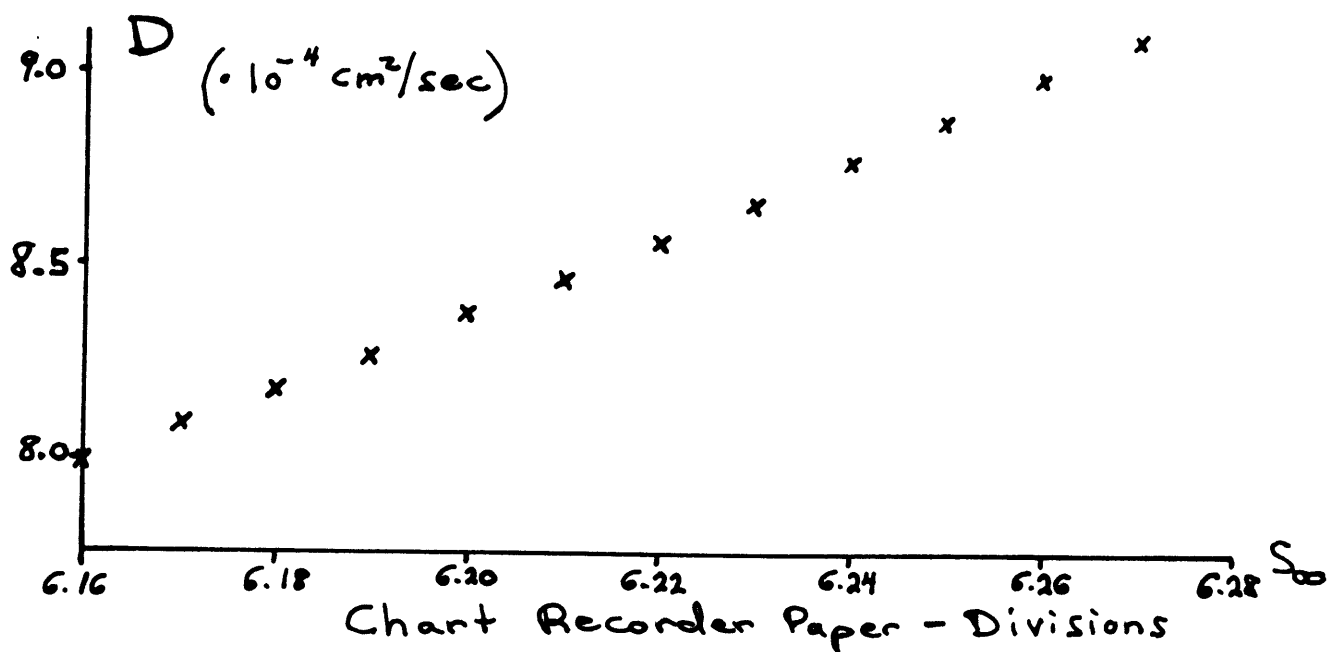
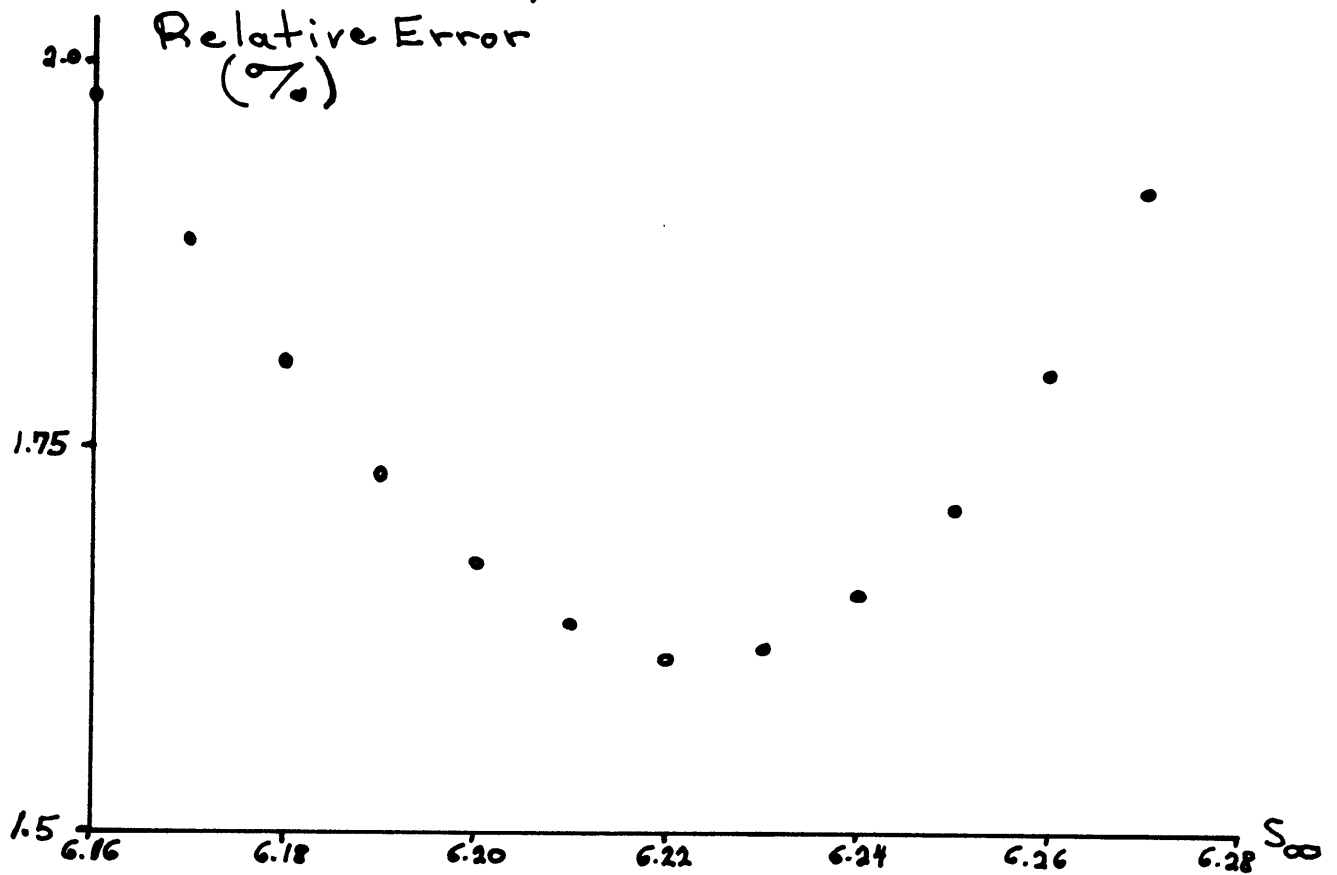
response function, as explained in detail in Chapter 3, was determined by measuring the signal level at various concentrations and temperatures. At the lower temperatures, n_{∞} could be determined experimentally, while at the intermediate and high temperatures this required an inordinate waiting time, and was known only approximately. The time t_1 , was estimated from the time necessary for the second liquid mode to damp out. For a crude estimate for t_1 , let the ratio of the magnitudes of the two modes be $a_2/a_1 \approx .2$, and $\gamma_2 = 4\gamma_1$, $\tau_2 = \tau_1/4$. Then the ratio $.2 \exp(-4t/\tau_1) / \exp(-t/\tau_1) = .2 \exp(-3t/\tau_1)$ is down to a few percent after a time $t_1 \approx \tau_1/2$. Thus if τ_1 is known approximately, t_1 can be estimated.

More precise values for the variables discussed above were obtained by fitting the data on a computer. Least square fits to the data were derived for various values of the parameters t_1 , n_{∞} , and p , the exponent characterizing the sniffer function. Values for t_1 were chosen by fitting to the exponential form with progressively fewer points and noting the values of the derived slopes. The effect of uncertainties in p , was found empirically, and proved to be quite small, in general less than about 1%. For example in run no. K-5-A at $T=1.565^\circ$ (at a zero level of 6.22) $D=8.50 \cdot 10^{-4}$ for $p=1.55$, and $D=8.55 \cdot 10^{-4}$ for $\hat{p}=1.40$.

The computer analysis indicated that the principal source of uncertainty in the slope was the uncertainty in the "zero level" n_{∞} . To reduce this error, n_{∞} was calculated from the data at finite times. This was done

Figure 18

Error Analysis - The Effect of Uncertainty in the Zero Level S_{00}



by computing a measure of the error of the fit for various values of n_∞ and choosing n_∞ to minimize the error. The quantity calculated was:

$$\Delta m = \frac{\Delta y}{t_2 - t_1}, \quad \text{where} \quad \Delta y^2 = \sum_{i=1}^N \frac{[y_i - (mt_i + b)]^2}{N},$$

m and b are the least square slope and intercept respectively, (t_i, y_i) are the measured pairs of time and He^3 concentration, and t_1 and t_2 refer to the end points of the fit. A plot of the relative error $\frac{\Delta m}{m}$, and the derived diffusion constant D versus S_∞ , the signal at $t = \infty$, $n_\infty = S_\infty^{1/p}$ for a given run (K-5-A, $T=1.565^\circ$) is shown in Figure 18.

The width of the curve gives an estimate of the error in D due to the uncertainty in S_∞ . In general the values of n_∞ obtained by minimizing the error curves were consistent with the approximate values obtained by waiting as long as possible and estimating n_∞ . In some of the more noisy runs there were differences between the two numbers, in these cases an average value was chosen.

The least square fits each involved points which differed in the precision to which the values of the ordinate $y = \log(n - n_\infty)$ were known. For this reason, the least squares slope was chosen to minimize:

$$\sum W_i [y_i - (mt_i + b)]^2$$

where W_i is a weighting factor added to the usual formula to take into account this variation in the size of the error bracket about each point. The factor W_i was chosen

as follows: If there were a uniform uncertainty δ in each point, then the relative error in y , would be

$$\text{Err} = \log(n_i' - n_\infty) - \log(n_i - n_\infty)$$

where $n_i' = (s_i + \delta)^{1/p}$, $n_i = s_i^{1/p}$. If

in addition there was a uniform density of points per unit time interval, then W_i would be $\text{Err}^2(n_1) / \text{Err}^2(n_i)$, having picked the error at t_1 as a normalizing factor. The actual data involved did not have a strictly uniform error since for t large, the signal was decaying more slowly and could be averaged over a larger time interval than for smaller t , and the effect of short term fluctuations was lower. In addition, the density of points used was lower at t large. The weighting factor was somewhat arbitrarily chosen as:

$$W(y_i) = \text{Err}(n_1) / \text{Err}(n_i),$$

a value between the two extremes of $W(y_i) = 1$, and the expression for uniform density of points and constant error given above.

D was determined by $D = (\text{slope}) / k^2$, as discussed in Chapter 3. Values for D as a function of temperature are given in the table on page 84. For many of the temperatures these values represent averages of 2 or more runs.

B. Additional Sources of Error

Sources of error in addition to those already discussed were the error in fitting the curve due to

scatter in the data, and uncertainties in the liquid level, the temperature, and in the correction for the finite flux of vapor at the liquid surface. The error due to scatter in the data, is given by the quantity Δm discussed above. The uncertainty in temperature was due mainly to the uncertainty in reading the oil manometer, which was about .01" of octoil "g", equivalent to about 3 millidegrees at 1.274°, and .6 millidegrees at 1.693°K. The absence of a temperature difference between the bath and the mixture was verified by independently measuring the pressure of the mixture with an oil manometer on the ~~the~~ gas handling system which connected to the chamber via the fill tube. The error in the correction of D due to the vapor flux was due principally to the uncertainty in the value of C_V/C_L at low concentrations as discussed in the appendix. The fractional error in the correction was estimated as less than 10%, when comparing a point at one temperature with that at another, and less than 20% on an absolute scale. Since the magnitude of the correction itself was about 20%, the net error was less than 2% on a relative basis, and 4% on an absolute scale. The uncertainty in the liquid level was about 1/2% to 1% when considering one run relative to another, and about 5% on an absolute scale.

An independent check of the total random error for a given run was gotten by taking 5 runs at the same temperature, 1.280°. At this temperature the signal was relatively small and somewhat noisy, and the estimated error in a particular run ranged from 5% to 10%. The first 4 runs were taken on the same day, the fifth a month earlier. The data and the mean and standard deviation follow.

Run Code No.:	L-1-A	L-1-B	L-1-C	L-1-D	I-26-B
$D(\cdot 10^{-3})$:	4.35	4.45	4.3	4.65	4.4

$$\bar{D} = 4.43 \cdot 10^{-3} \quad \sigma = \sqrt{\sum_{j=1}^5 (D_j - \bar{D})^2 / 4} \approx .14 \cdot 10^{-3}$$

The total relative error was estimated at each temperature from the considerations of the previous sections. The values obtained are indicated by the error bars on the graph in Figure 19. In addition, the absolute value of the curve as a whole has an uncertainty of about 12%.

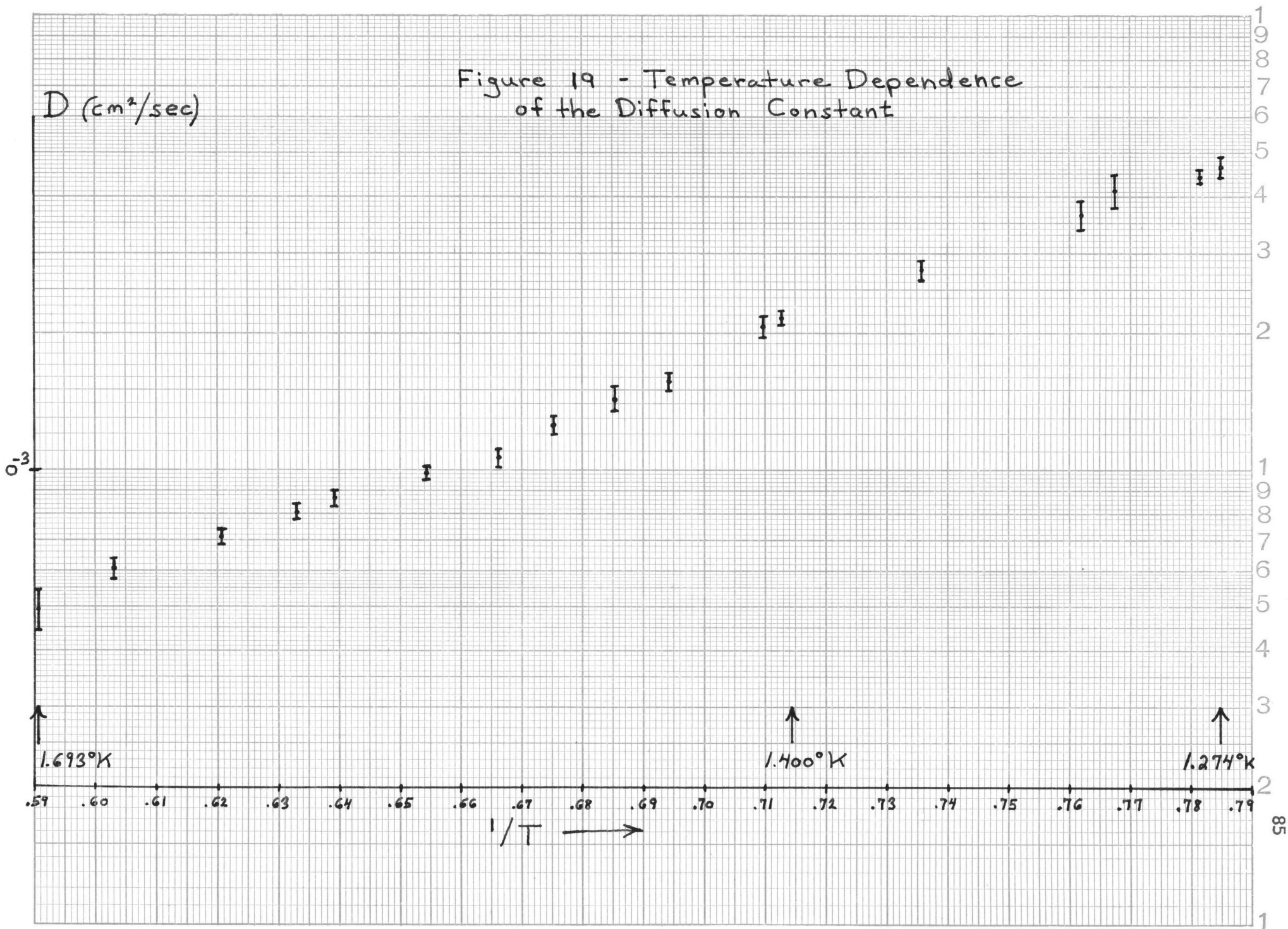
Values of D as a Function
of Temperature

He³ Concentration $C=1.4-1.5 \cdot 10^{-4}$

<u>T</u> (°K)	<u>D</u> (10^{-4} cm ² /sec)	<u>No. of Runs</u>
1.274	46.7	2
1.280	44.3	5
1.303	41.2	1
1.312	36.5	1
1.359	27.8	3
1.403	21.7	2
1.409	20.8	1
1.440	15.6	2
1.459	14.4	1
1.480	12.6	2
1.501	10.7	2
1.528	9.83	3
1.564	8.67	2
1.580	8.08	1
1.611	7.15	1
1.658	6.04	1
1.693	4.94	1

Figure 19 - Temperature Dependence of the Diffusion Constant

D (cm^2/sec)



III. Temperature Dependence of the Diffusion Coefficient and Effective Scattering Cross Section

A. Diffusion Coefficient

In analyzing the data, $\log D$ is plotted against $1/T$, since He^3 -roton scattering is assumed to predominate in the diffusion. Coincidentally diffusion in some "ordinary" solids and liquids is also described by plots of $\log D$ versus $1/T$, but in these cases the diffusion is characterized by the formation of lattice vacancies in a solid or holes in a liquid. ⁽¹⁾ The process of forming a hole or vacancy is determined by a given energy ϵ . (For the liquid case ϵ is equal to a fraction of the evaporation energy.) The diffusion is, thus, thermally activated, and $D \sim \exp(-\epsilon/KT)$. D , therefore, increases with temperature exactly opposite to the roton- He^3 case where $D \sim \exp(+\Delta/T)$.

The log plot is shown in Figure 19 on page 85. The following properties of the data can be seen:

1. D decreases with increasing temperature, unlike most "classical" substances.
2. The slope of the observed curve is not constant, but the curve as a whole is still close to being linear. If the data are fit to a single straight line, the least squares slope gives $\Delta = 11.7^\circ\text{K}$.
3. Neutron scattering data indicate that the roton energy gap Δ decreases slightly with temperature, at the higher temperatures, (see Appendix I), and a perfect straight line is not expected. But this effect is not enough to account for observed steepness of the curve, and an energy dependent He^3 -roton cross section is implied.

B. He³-Roton Scattering Cross Section

The energy dependence of the effective cross section can be obtained from the data by taking into account the temperature variation of the roton number density and the average velocity, i.e. by evaluating:

$$T^{1/2}/n_r D \sim \exp(\Delta/T)/D$$

where Δ is the roton energy gap. Plots of this quantity versus temperature are shown in Figure 20. In Figure 20A, the empirical relation of Yamell et al. ⁽²⁾, derived from neutron scattering data, $\Delta = 8.68 - .0084 T^7$ is assumed, while Figure 20B shows the effective cross section assuming a constant, Δ , equal to 8.65°. Error brackets, reflecting the uncertainty in D, are shown. The error associated with the empirical function of Yamell et al. is not known, but is probably substantial since it is based on only a few data points, as discussed in Appendix I. Nevertheless, even if a constant roton energy gap is assumed, as in Figure 20B, the general slope of the curve is the same; the cross section increases with increasing temperature, the high temperature values being about 50% higher than those at the lowest temperatures.

In equating the expression $\exp(\Delta/T)/D$ with the effective cross section, the Khalatnikov - Zharkov expression has been approximated as follows:

$$D = \frac{hT}{m_3 n_r} \left(\frac{1}{\overline{v_{3r}^* v_3}} \right) \approx \frac{hT}{m_3 n_r} \left(\frac{1}{\overline{v_{3r}^*}} \right) \left(\frac{1}{\overline{v_3}} \right)$$

(where the averages refer to weighted integrations over momentum space).

The above approximation can be used to evaluate the absolute value of the cross-section.

$$\text{Using: (a) } m_3^* = 2.7 m_3 \quad (4)$$

$$(b) \mu_r = .16 m_4 \quad (2)$$

$$(c) \Delta \simeq 8.68 - .0084 T^7 \quad (2)$$

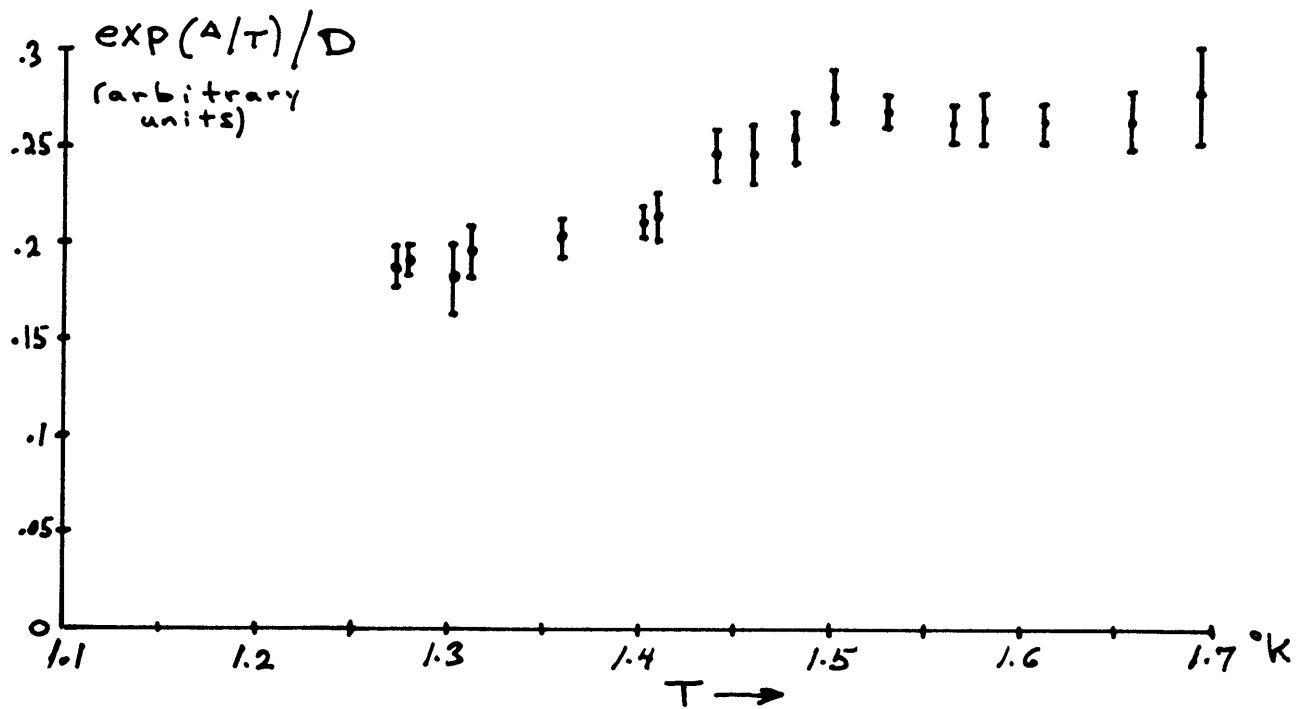
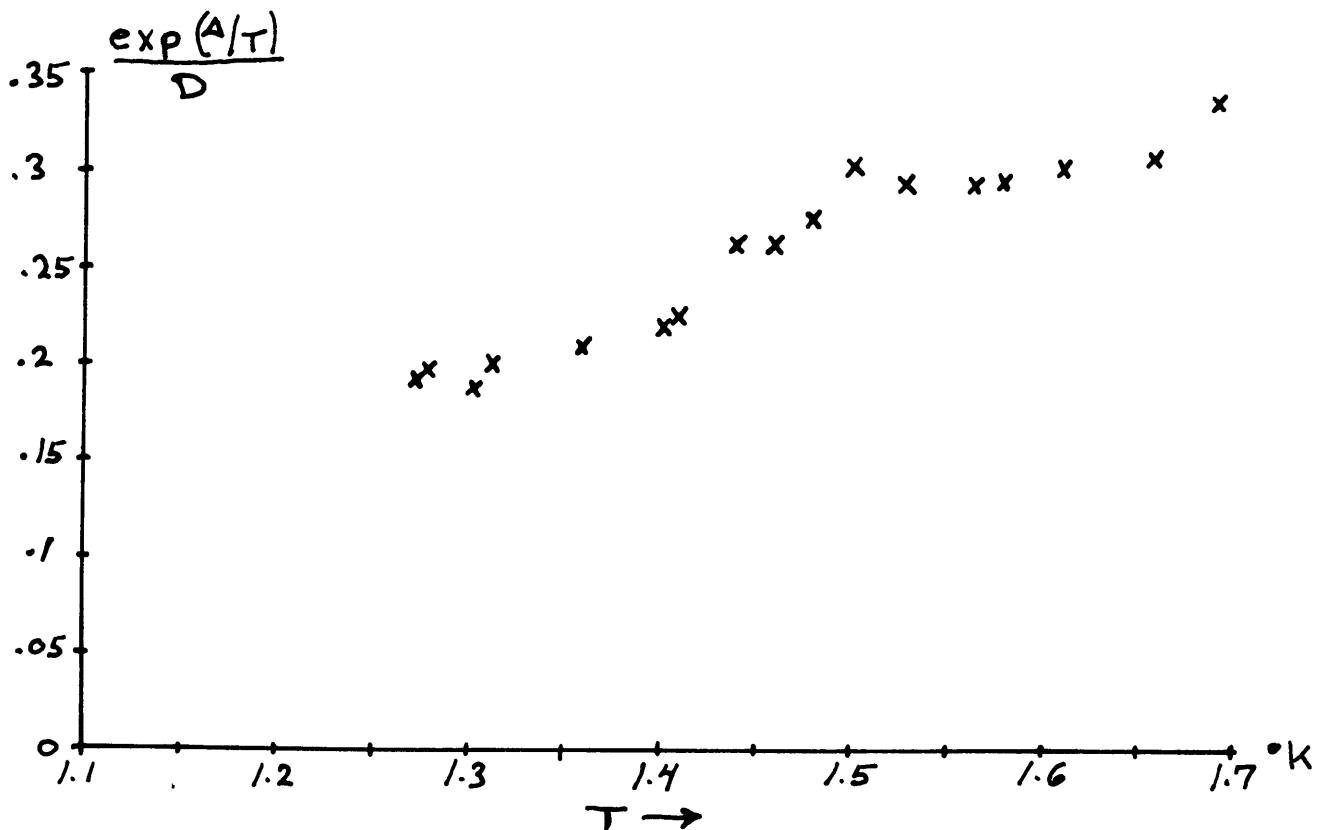
The He^3 -roton cross section ranges from:

$$\sqrt{\sigma_{3r}} \simeq 1.6 \times 10^{-14} \text{ cm}^2 \text{ at } T = 1.27^\circ$$

$$\text{to } \sqrt{\sigma_{3r}} \simeq 2.4 \times 10^{-14} \text{ cm}^2 \text{ at } T = 1.69^\circ$$

If it is assumed that $\Delta = 8.65^\circ$, independent of temperature, then the higher temperature cross sections are somewhat larger, the value at $T = 1.69^\circ$ being about 20% greater.

Figure 20 - Effective Cross-Section

Figure 20-A $\Delta = (8.68 - .0084 \cdot T^7)^\circ$ Figure 20-B $\Delta = \text{constant} = 8.65^\circ$

IV. He³ Concentration Dependence

Data were taken at higher He³ concentrations - from 2 to 4 times higher than the low concentration data where $C = 1.45 \times 10^{-4}$. The purpose was primarily to check that indeed D was approximately independent of concentration, that no anomalies were present. Also, the presence of the slight concentration dependence predicted by the Khalatnikov-Zharkov expression was sought, although a detailed study was not made. The He³ concentration enters the KZ expression for D in the factor (ρ_{no} / ρ_n) . This expression was derived assuming that $n_3 \ll n_r$, where $\rho_{no} / \rho_n \approx 1$. An expression is also derived for the (high temperature) case where $n_3 \gg n_r$. This case leads to several curious results which are not relevant to the experiment. However, the high He³ concentration expression leads KZ to present an "interpolation formula" covering the whole concentration range in which D is proportional to $(\rho_{no} / \rho_n)^2$.

The data, shown on page 92, indicate that D is approximately independent of He³ concentration as expected. Only at the lowest temperatures can a weak concentration dependence be seen. Quantitatively:

$$\frac{\rho_{no}}{\rho_n} = \frac{\rho_{nr}}{\rho_{nr} + \rho_{n3}} \approx 1 - \frac{\rho_{n3}}{\rho_{nr}} \equiv 1 - \epsilon$$

for $T = 1.274^\circ$, and the lower concentration, $\epsilon \approx .0074$. For a mixture having a He³ concentration 4 times higher, the quantity (ρ_{no} / ρ_n) would be about 2.2% lower, and $(\rho_{no} / \rho_n)^2$ would be about 4 1/2% lower. The observed values for D indicate a small shift with increasing concentration, but the error brackets of about 5% for this pair of runs are too large to distinguish between the two expressions,

although the squared expression gives better agreement. At the higher temperatures ϵ is smaller, $\epsilon \simeq .0033$ at 1.45° , and the data indicate little if any concentration dependence, as expected.

It is interesting to note that for a classical gas, no observable concentration dependence would be expected (see page 53), while the KZ expression involving (ρ_{n0} / ρ_n) is independent of concentration only at very low He^3 concentrations. The reason for this is that there is an additional term proportional to the concentration gradient in the Boltzmann equation for $\text{He}^3\text{-He}^4$ mixtures. This term is not present in the usual Boltzmann equation and arises out of the fact that in a He II mixture, the normal fluid as a whole can move, and this motion is governed by the temperature and concentration gradients in the mixture - equivalent to the He^3 and roton kinetic pressures previously discussed. The coefficient relating the collision integral to the concentration gradient in this extra term involves the total normal density $\rho_n = \rho_{n0} + \rho_{n2}$ which except for very dilute solutions, involves a He^3 concentration dependence.

Concentration Dependence of D

<u>T</u> (°K)	<u>He³ Conc.</u> ($\cdot 1.45 \cdot 10^{-4}$)	<u>D</u> ($\cdot 10^{-4} \text{cm}^2/\text{sec}$)
1.274	1	46.7 (avg. of 2 runs)
1.274	4	44.0
1.312	1	36.1
1.312	3	34.2
1.479	1.6	12.4
1.481	.8	12.8 1/2
1.437	2	15.6
1.439	3	14.9
1.440	1	15.0
1.441	1	15.9

The relative error in each of the above runs was about 5% to 7%.

V. Steady State Data

The discussion in Chapter 1 indicates that, in principle, D can be derived from the steady state magnitudes of the He^3 signal both with and without the heater on, and that the ratio of the two signals would be:

$$(1) \quad \frac{n_3(\text{heat})}{n_3(\text{no heat})} = \left(\frac{v_n L}{D}\right) \exp\left(\frac{v_n L}{D}\right) / \left[\exp\left(\frac{v_n L}{D}\right) - 1\right]$$

where v_n = normal fluid velocity, related to the applied heat current by $v_n = Q / \rho S T$, and L is the length of the chamber.

An analysis of these "static" data was not undertaken, primarily because:

1) Unlike the "dynamic" method of measurement, this method is sensitive to non-idealities in the geometry of the sample chamber. Correcting equation (1) for geometrical effects leads to a clumsy expression, which requires precise knowledge of the chamber geometry.

2) The sniffer function, too, must be known precisely, for this type of measurement, while this has shown not to be true for the time decay method.

In addition the static method is complicated by the following:

1) In He^3 - He^4 mixtures heat is transported by irreversible diffusion in the normal fluid, as well as by the convective transport process assumed in equation (1). For the He^3 concentrations of this experiment, this process is dominant below about 1.1°K ,⁽³⁾ and still may play a finite role at the lower temperatures of the experiment. The exact magnitude of the effect is not known at these temperatures,

since thermal conductivity experiments measure the total heat transport due to both processes.

2) The static method also requires the assumption that:

$J_3 = v_n n_3$, i.e., that the He^3 atoms move exactly at the normal fluid velocity.

Neither of the above enter the analysis in the dynamic method of measurement.

References for Chapter 5

1. J. O. Hershfelder, C. F. Curtiss, and R. B. Bird, Molecular Theory of Gases and Liquids, John Wiley (New York, 1954). p. 624.
2. J. L. Yarnell, G. P. Arnold, P. J. Bendt, and E. C. Kerr, Phys. Rev. 113:1379 (1959).
3. T. P. Ptukha, Sov. Physics JETP 13:1112 (1961).
4. R. De Bruyn Ouboter, K. W. Taconis, C. Le Pair and J. J. Beenakker, Physica 26:853 (1960).

CHAPTER 6

Comparison of Results with
Other Methods of Measurement

I. Thermal Conduction Measurements

A. Relation of the Effective Thermal Conductivity to D

As has been previously shown, a thermal current applied to a He³-He⁴ mixture produces a He³ concentration gradient as well as an oppositely directed temperature gradient. In order for a steady state to be achieved, the osmotic pressure difference produced by the concentration gradient must exactly balance the roton kinetic pressure difference produced by the temperature gradient (see chapter 4, section III). In terms of thermodynamic quantities this is expressed as:

$$(1) \quad kT \nabla n_3 = - \rho S_0 \nabla T$$

(where n_3 is the He³ number density, and S is the entropy per unit mass of the pure He⁴). If it is assumed that the He³ atoms move with the

normal fluid, that (2) $\vec{J}_3 = \vec{V}_n n_3$

where (3) $\vec{V}_n = \vec{Q} / \rho S T$, $\vec{Q} =$ thermal current

then since (4) $\vec{J}_3 = - D \nabla n_3$

a relation between \vec{Q} and ∇n_3 is implied, which when put into equation (1) gives an expression for the effective thermal conductivity K_{eff} :

$$(5) \quad \vec{Q} = [(\rho S_0)^2 D / n_3 k] \nabla T \equiv K_{\text{eff}} \nabla T$$

Thus, the measurement of the effective thermal conductivity, and knowledge of the entropy should enable a determination of D .

This method is complicated by the fact that a liquid mixture can also transport heat via the (irreversible) diffusion of thermal excitations as in an ordinary solid. In addition, a more detailed consideration of the problem¹ gives an added factor $(\rho_n / \rho_{n0})^2$ to (5) so that

the full expression becomes:

$$(6) \quad \chi_{eff} = (\rho_n / \rho_{no})^2 \left(\frac{\rho^2 S_0^2}{n_3 k} \right) D + \chi'$$

B. Results of Measurements

The finite thermal conductivity of He³-He⁴ solutions was discovered by Beenakker et al.² The details of their results, however, have been superseded by the later work of Ptukha.³ The Beenakker apparatus relied on the measurement of the vapor pressures of a surrounding He⁴ bath and the mixture to determine temperature differences, while the Ptukha apparatus measured the temperature at four points along the thermal path and in addition corrected for the possibility of unwanted convective effects. The data of Beenakker et al. for D are rather sparse, but indicate a much steeper temperature dependence than either the data of Ptukha or the present work. The lowest temperature point at about 1.2° does not include the contribution from the irreversible conductivity process, and is probably in error. The only data point for D in the temperature range of the present experiment, at T = 1.49° agrees with the present results to within 10%.

Ptukha³ carried out thermal conductivity measurements at several concentrations at temperatures. The measurements indicated that the irreversible process dominated the heat transport below 1.1°, and thus results for D were obtained only above 1.2°K. Some of the measurements were taken in the temperature range of the present experiment. These are shown in Figure 21, along with the diffusion data of the present experiment. In the higher temperature region, 1.5° < T < 1.7°, the derived values for D agree quite well with the present measured values, while

at lower temperatures, the curves differ, the results of Ptukha curve being lower.

The reason for the discrepancy is not known. However, the following points should be noted:

1. In deriving D from the effective thermal conductivity at the lower temperatures of the curve, the small but finite contribution of the irreversible transport thermal process had to be subtracted out. Since only the total thermal conductivity can be measured, this contribution could not be known exactly but must have been extrapolated from thermal conductivity data at much lower temperatures, where the irreversible process dominated.

2. No statement as to the temperature dependence of the cross section is made in the Ptukha paper. If the data at 10^{-4} and 10^{-3} concentrations are considered as one curve, then regions of differing slope become apparent, although the average slope is between about 8° and 9° .

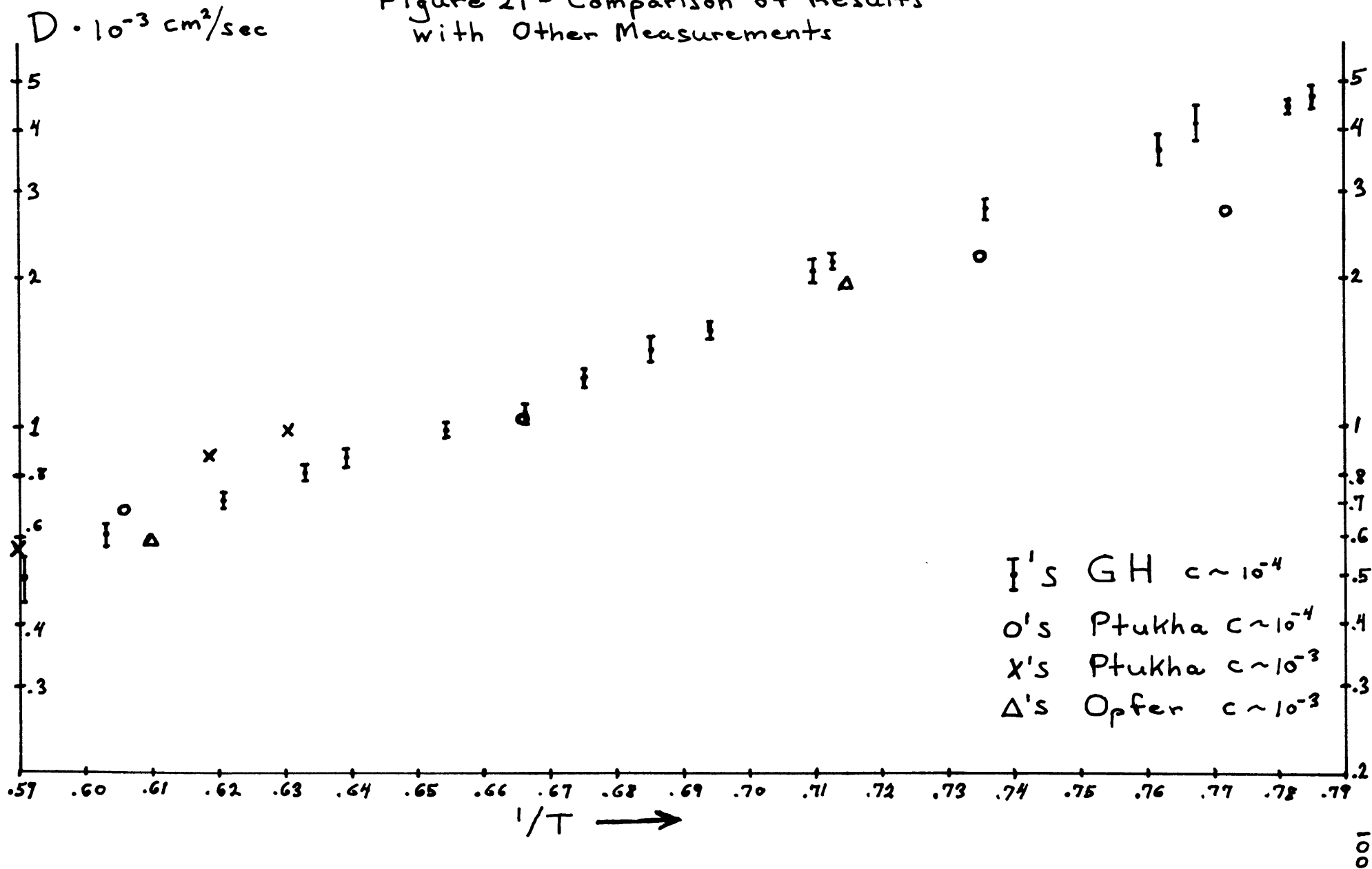
In general the data are not inconsistent with a constant cross section, but could be fit to a $\sigma_{3-r}(T)$ as well.

3. A numerical value for σ_{3-r} is given for the one point at $T = 1.5^\circ$ in the Ptukha paper. By coincidence this is the one point where the values for D given by the two methods agree to within a few per cent.

4. An assumption inherent in the above derivation of the diffusion coefficient is that the He^3 atoms move with the characteristic normal fluid velocity, v_n , that is

$$D \frac{\partial n_3}{\partial z} = v_n n_3 = \left(\frac{Q}{\rho S T} \right) n_3$$

Figure 21 - Comparison of Results
with Other Measurements



This assumption is not necessary in the present work and is not made.

II. Nuclear Magnetic Resonance Diffusion Measurements

A. Spin-Echo Measurements

1. Description of the Method - Classical Picture (for a more complete description see (4) and (5)).

In this method a liquid $\text{He}^3\text{-He}^4$ mixture is placed in a uniform magnetic field $H_0 \hat{z}$, on which is superposed a small field gradient $G_z \hat{z}$. A pulse of rf field at the Larmor precession frequency $\omega_0 = \gamma H_0$, having a magnetic field strength H_1 perpendicular to \hat{z} , is then applied. In a frame of reference rotating with the precessing He^3 spins, this appears as a nearly constant transverse field about which additional precession occurs. If the direction of the pulse is such that $\int (\gamma H_1 / 2) dt = \pi / 2$, then the net effect of the pulse is to cause a 90° nutation of the precessing spins. (The factor of 2 in the integral results from resolving a linear sinusoidal signal into two circular components, only one of which is rotating in the correct sense). After the nutation, spins which were initially oriented in the $+z$ direction begin to precess in the x - y plane. The applied magnetic field gradient implies a spatial variation in ω_0 , and thus the spins rapidly become dephased with respect to one another. The subsequent application of a 180° pulse causes another nutation, which has the effect of reflecting the spins about an axis in the x - y plane, causing the phase of the faster precessing spins to lag behind that of the slower spins. Eventually the faster spins overtake the slower spins, all of the spins become in phase again, and a pulse of magnetization, the so called

spin-echo, can be observed. If during the period between the application of the two rf pulses, diffusion is occurring, the spins will have changed position, and hence precession frequency, slightly. The original in-phase signal will not be fully recovered, and thus diffusion implies a decay in the echo signal.

Even if no diffusion is present, spin-spin interactions produce an irreversible dephasing process characterized by the "transverse relaxation time" T_2 , where the polarization signal is proportional to $\exp(-t/T_2)$. The time decay of the signal due to diffusion should vary as $\exp(-\alpha t^3)$, where α is a constant, so that the two effects should be separable. Note that unlike the "direct" method used in the present work, $\text{He}^3\text{-He}^3$ collisions contribute to spin diffusion. (A rigorous analysis shows that only collisions of spins having opposite spin are involved).

2. Experimental Results

The first spin diffusion measurements on $\text{He}^3\text{-He}^4$ solutions were carried out by Garwin and Reich⁶, whose data was taken at concentrations of 1% and 2% under 19 atmospheres pressure, and at 2% at 2 atmospheres. The data at 19 atmospheres indicated that above 1.4° D varied as $\exp(\Delta/T)$, with $\Delta \simeq 13.5^\circ\text{K}$. At low temperatures, below about .9°K, D was determined primarily by $\text{He}^3\text{-He}^3$ interactions. Garwin and Reich interpreted this result to be evidence of a large variation of the He^3 -roton cross section with energy. Part of this temperature dependence may be due to the temperature variation of the roton energy gap under pressure. At 19 atmospheres the gap (for pure He^4) is less than 7 1/2°K at $T=1.1^\circ$ implying a higher density of excitations. The temperature dependence of

the energy gap Δ under these conditions is not known, but even at saturated vapor pressure a decrease in the magnitude of Δ is noticeable above about 1.6° to 1.7°K. The presence of the 1% and 2% He³ concentrations may influence the roton spectrum as well. These considerations make exact comparison with the present data difficult. However, the general result of a large variation of D with temperature implying a temperature dependent cross section does agree with the present result.

Additional measurements were carried out nine years later (1968) by Opfer, Luszczynski, and Norberg⁷ who investigated spin diffusion over a wide range of temperatures, at concentrations from 3×10^{-4} to 3×10^{-2} . Unfortunately, no data above 1.1° were taken at the lowest concentration, and very little of the data were taken in the regime where D was concentration-independent. Two points which were taken at $C = 1.0 \times 10^{-3}$ fall in temperature range of the present experiment and are shown with present data and the Ptukha data in Figure 21. The two points show the same temperature dependence as the present data, and differ in absolute value from the present data by 10%.

Data over the full range of concentration and temperature were analyzed by the authors by fitting D to the form:

$$(7) \quad \frac{1}{D(C, T)} = \frac{1}{D_1(T)} + \frac{C}{D_2(T)}$$

on a computer. The result was that for $T > .8^\circ\text{K}$, D_1 varied as $\exp(\Delta/T)$ with $\Delta = 8.65^\circ\text{K}$ exactly. This results contrasts with the present data, and implies that the diffusion is dominated by He³-roton scattering with a cross section which is energy dependent. At temperatures less than .8°K, the values for D_1 lie lower than the exponential curve, indicating

either that phonon-He³ interactions are important or that the roton He³ cross section is energy dependent. But the Khalatnikov-Zharkov theory indicates that phonons do not play a significant role in limiting the He³ mean free path until much lower temperatures, so that the former assumption is not likely. The authors conclude that there may be a temperature dependence to the cross section, but that the experimental accuracy of these measurements is also questionable.

It should be noted that about half of the data presented in the paper of Opfer et al. was taken at concentrations of 1% and 3%. In fitting the data on the computer the effect of the He³ atoms on D is supposed to be completely accounted for by the term $C/D_2(T)$ representing the contributions of He³-He³ interactions to the diffusion. The considerations of Section IV of Chapter 4 indicate that at these concentrations, the solute He³ may have a substantial effect on the roton spectrum, and hence on the roton number density as well. This is not taken into account in the paper and may account for part of the discrepancy between the present data and the data of Opfer et al.

Later work on spin diffusion in mixtures under pressure was published recently by Biegelson and Luszczynski.⁸ This work was limited to $T < 1.15^\circ\text{K}$, at concentrations from 4×10^{-3} to 1.25×10^{-2} . In this regime D was dominated by the He³-He³ interaction. As in the previous paper the data for D were fitted to the form defined by equation (7) above. In carrying out the computer fit an exponential form was assumed for D_1 , $D_1 \sim \exp(\Delta/T)$, the value for Δ being determined by only two points at the highest temperatures. The result was $\Delta = 9.1^\circ$ at S.V.P., decreasing with increasing density. The above comment on the

effect of He^3 on the roton spectrum seems appropriate for this paper as well. The Biegelson et al. paper also deals at length with the results for $D_2(T)$ and the He^3 - He^3 interaction, results which are not relevant to the present work.

A paper by Husa, Edwards, and Gaines⁹ describes diffusion measurements at low temperatures at $c = 2\%$ and 12% . In analyzing the data, $1/D$ is plotted versus concentration, and at $T = 1.225^\circ\text{K}$, a straight line can be drawn through the 12% point, the 2% point and a point assumed to be at 0 concentration from the data of Ptukha. However, the error brackets are such that a value for D at $c = 0$ as much as $2\ 1/2$ times larger could also be fit on the same line. In addition, the effect of the relatively high He^3 number densities on the roton parameters is ignored in the analysis.

Other papers have appeared investigating diffusion in He^3 - He^4 mixtures, but these have been in the He^3 - He^3 regime, i.e. at low temperatures and relatively high concentrations. Some of the data has been taken well below the Fermi degeneracy temperature of the He^3 solute quasi-particle gas. These papers are quite interesting but not relevant to the present work.

B. Nuclear Relaxation

In principle, the diffusion constant can also be derived from the spin-lattice nuclear relaxation time T_1 . The theory of nuclear relaxation has been given by Bloembergen, Purcell, and Pound.¹⁰ The time T_1 can be shown to depend on the correlation time τ during which a spin sees a given local magnetic field. Taking into account that both a given spin and neighboring spins are diffusing, τ turns out to be $\tau \approx \frac{\langle r^2 \rangle}{12D}$

where $\langle r \rangle$ is the average distance between spins. The complete theory shows that T_1 is proportional to τ and is thus inversely proportional to D .

The principal difficulty in measuring T_1 in $\text{He}^3\text{-He}^4$ mixtures, and in pure He^3 for that matter, is that small amounts of paramagnetic impurities, such as oxygen, on the walls of the sample chamber and at the liquid surface are very effective in producing nuclear relaxation. Since

$\mu_N \ll \mu_B$ and the relaxation varies as the square of the impurity moment, concentrations of less than 10^{-6} are very important.

The papers referred to in the previous sections (6), (7), (8), all present T_1 data which indicate effects due to relaxation at the sample walls and other spurious effects. As yet no reliable measurements of the true bulk relaxation times have been presented for dilute $\text{He}^3\text{-He}^4$ solutions.

Chapter 6

References

1. I. M. Khalatnikov and V. N. Zharkov, op. cit., p. 905.
2. J. J. Beenakker, K. W. Taconis, E. L. Lynton, Z. Dokoupil, and G. Van Soest, *Physica* 18:433 (1952).
3. T. P. Ptukha, *Soviet Physics JETP* 13:1112 (1961).
4. E. L. Hahn, *Phys. Rev.* 80:580 (1950).
5. H. Y. Carr and E. M. Purcell, *Phys. Rev.* 94:630 (1954).
6. R. L. Garwin and H. A. Reich, *Phys. Rev.* 115:1478 (1959).
7. J. E. Opfer, K. Luszczynski, and R. E. Norberg, *Phys. Rev.* 172:192 (1968).
8. D. K. Biegelson and K. Luszczynski, *Phys. Rev. A* 3:1060 (1971).
9. K. L. Husa, D. O. Edwards, and J. R. Gaines, *Proceedings of the Tenth Conference on Low Temperature Physics LT-10, Moscow, 1966*, p. 345.
10. Bloembergen, Purcell, and Pound, *Phys. Rev.* 73:679 (1948).

CHAPTER 7
A Possible Model for the
He³-Roton Interaction

One of the principal results of the experiment is that the cross section for He^3 -roton interactions is energy dependent, and is not adequately described by a simple δ function potential. One way in which an energy dependent cross section might come about is through an interaction dependent on the finite extent of the He^3 atom and the roton excitation and the consequential backflow of the surrounding superfluid "ether". That is, instead of the infinitely narrow, repulsive hard core described by a delta function, the interaction might involve a hard core of finite extent, and a long range interaction due to backflow effects in the superfluid.

The backflow effects can be derived by applying hydrodynamics to the case of 2 spheres moving in an inviscid, irrotational background fluid. The velocity field is then characterized by a velocity potential, $\vec{v} = \nabla \phi$ where ϕ obeys Laplace's equation: $\nabla^2 \phi = 0$. The solution for a single sphere in an infinite medium is the familiar dipole flow pattern, similar in form to the dipole field pattern obtained for a conducting sphere placed in a uniform electric field. For two spheres, having velocities \vec{u}_1 and \vec{u}_2 , the boundary conditions at the surfaces of both spheres must be satisfied simultaneously: for sphere #1, v_1 at the surface must be $u_1 \cos \Theta$, where Θ is the angle between the radius at the surface of the sphere and \vec{u}_1 , a similar condition holding for sphere #2. The problem can be solved, as in electrostatics, by using the method of images. The resulting velocity field can be used to calculate the total kinetic energy of the background superfluid. The complete

calculation can be found in reference (1).

Letting u_1, u_2 represent components of velocity along the line of centers, and w_1, w_2 represent velocity components perpendicular to the line of centers, and expressing all distances in powers of R , the distance between the centers of the 2 spheres, the result for the kinetic energy of the fluid is:

$$T = \frac{A}{2} (u_1^2 + w_1^2) - B (u_1 u_2 - \frac{1}{2} w_1 w_2) + \frac{C}{2} (u_2^2 + w_2^2)$$

with:

$$A = \frac{1}{2} M_1 \left(1 + \frac{3a^3 b^3}{R^6} + \dots \right) \quad C = \frac{M_2}{2} \left(1 + \frac{3a^3 b^3}{R^6} + \dots \right)$$

$$B = \frac{2\pi \rho a^3 b^3}{R^3} \left(1 + \frac{a^3 b^3}{R^6} + \dots \right)$$

where a and b are the radii of the two spheres, ρ is the liquid density, and M_1 and M_2 are the masses of liquid displaced by the spheres.

Keeping the lowest order terms, this simplifies to:

$$T = \frac{M_1}{4} (u_1^2 + w_1^2) - \frac{2\pi \rho a^3 b^3}{R^3} (u_1 u_2 - \frac{1}{2} w_1 w_2) + \frac{M_2}{4} (u_2^2 + w_2^2)$$

In considering collisions between the two spheres, the terms involving the coefficients A and C are present even when the spheres are isolated (at $R = \infty$), and so can be ignored in determining the interaction. Also, most collisions occur when u_1 and u_2 have opposite signs, (i.e. when two particles are approaching one another), and when w_1 and w_2 have the same sign. Thus, the energy of interaction due to the influence of the background superfluid is:

$$T = \frac{2\pi\rho a^3 b^3}{R^3} (|\vec{u}_1| |\vec{u}_2| + \frac{1}{2} |\vec{w}_1| |\vec{w}_2|)$$

which in terms of the total velocities v_1, v_2 can be shown to be:

$$T = \frac{2\pi\rho a^3 b^3}{R^3} [\vec{v}_1 \cdot \vec{v}_2 - 3(\vec{v}_1 \cdot \hat{R}_1)(\vec{v}_2 \cdot \hat{R}_2)]$$

To get a rough estimate for the form of the cross section from this rather complicated velocity dependent expression, the interaction will be approximated by the potential:

$$U(R) = \infty \text{ for } R > a$$

$$U(R) = -\frac{U_0}{R^3} \text{ for } R \leq a$$

with the strength of the potential U_0 proportional to the average velocities \bar{v}_3, \bar{v}_r (assumed constant in calculating the matrix element of the potential). Calling the He^3 quasi-particle sphere #1, and noting that the mass of the displaced superfluid, $M_1 \approx m_3^* - m_3$ where m_3^* is the experimental ^{effective mass} and letting $\frac{4}{3}\pi b^3$ represent the effective volume of the roton, the strength of the interaction becomes:

$$U_0 = 2\pi\rho a^3 b^3 \bar{v}_3 \bar{v}_r = \frac{9}{8\pi} (m_3^* - m_3) V_{\text{rot.}} \bar{v}_3 \bar{v}_r$$

The cross section can now be estimated, using perturbation theory. Let the incident and final wave functions be plane waves (as was done in the Khalatnikov-Zharkov calculation).

$$\Psi_i = \frac{1}{\Omega} e^{i\vec{k}_3 \cdot \vec{r}_3} e^{i\vec{k}_r \cdot \vec{r}_r}$$

and:

$$\Psi_2 = \frac{1}{\Omega} e^{i\vec{k}_3 \cdot \vec{r}_3} e^{i\vec{k}_r \cdot \vec{r}_r}$$

The matrix element V_{12} for these wave functions is easily shown to be:

$$\begin{aligned} V_{12} &\equiv \langle \Psi_1 | V(\vec{r}_3 - \vec{r}_r) | \Psi_2 \rangle \\ &= \frac{1}{\Omega^2} \int d^3r_r \int d^3r_3 e^{i\Delta\vec{k} \cdot (\vec{r}_3 - \vec{r}_r)} V(\vec{r}_3 - \vec{r}_r) \end{aligned}$$

where:

$$\Delta\vec{k} = \vec{k}_3' - \vec{k}_3 = \vec{k}_r - \vec{k}_r'$$

For the above potential, this can be shown to be:

$$V_{12} = \frac{q}{2\Omega} (m_3^* - m_3) \nabla_{\text{rot}} \cdot \vec{v}_3 \vec{v}_r \underbrace{\left[\frac{\sin(\Delta ka)}{(\Delta ka)} - Ci(\Delta ka) \right]}_{f(\Delta ka)}$$

where $ci(x) \equiv \int_0^x \frac{\cos x}{x}$

is tabulated in collections of mathematical tables.

The transition rate is then:

$$\begin{aligned} dw &= 2\pi/\hbar |V_{12}|^2 \delta(E_3 + E_r - E_3' - E_r') \left[\frac{\Omega}{(2\pi)^3} \right]^2 d^3k_3' d^3k_r' \\ &= \frac{81}{8\pi^5} \frac{1}{\hbar} (m_3^* - m_3)^2 \nabla_{\text{rot}}^2 \vec{v}_3^2 \vec{v}_r^2 f^2(\Delta ka) d^3k_3' d^3k_r' \\ &\quad \cdot \delta(E_3 - E_3' + E_r - E_r') \end{aligned}$$

The cross section is then determined by dividing by the relative velocity. Noting that $\vec{k}_3' = \vec{k}_3 + \Delta\vec{k}$ and $\vec{k}_r' = \vec{k}_r - \Delta\vec{k}$, the expression can be reduced to a single integral over d^3k . The presence of the delta function indicates that the integral is over a 2 dimensional phase space area. Without carrying the details of the calculation further, the general result can

be seen. The cross section is proportional to:

$$\sigma \sim (m_3^* - m_3)^2 \frac{v_3^2 v_r^2 \nabla_{\text{roton}}^2}{v_3 v_{\text{relative}}} \overline{f(\Delta k a)}^2 \text{ (phase space area)}$$

The temperature dependence of the cross section is gotten by integrating σ over the Boltzmann distribution. The general form of the result can be derived by noting that:

$$v_3 = \frac{\hbar k_3}{m_3^*} \sim T^{1/2}$$

$$v_r \equiv \frac{\partial \epsilon_r}{\partial p} \sim \frac{\hbar(k_r - k_0)}{\mu} \sim T^{1/2}$$

The phase space area $\sim (\Delta k)^2$ increases with increasing temperature but at a rate less than T^2 . (To show this one calculates Δk in terms of k_3^3 and $k_r - k_0$, making the approximation that $(k_r - k_0) \ll k_r$.)

The temperature dependence of the integral of $f^2(\Delta k a)$ is that of an oscillating function which gradually decreases. The ~~net~~ temperature dependence is that of a cross section increasing at a rate slightly greater than T , on which is superposed an oscillating function, in qualitative agreement with Figure 20 of Chapter 5. The amplitude of σ will not be computed since the calculation is still quite crude. It has been seen, though, that σ is proportional to

$$(m_3^* - m_3)^2 \cdot \nabla_{\text{roton}}^2.$$

Thus, it has been seen that a plausible model for the He^3 -roton interaction, that of a hard sphere repulsion together with a long range $1/r^3$ attraction due to the dipole-dipole coupling of the superfluid backflow can, at least qualitatively, be fit to the observed data.

Note that the kinetics of the He^3 -roton interaction are quite

complicated, and for example the magnitude of the relative velocity in the center of momentum system is not conserved, and no simple way to reduce the problem to a 1-body problem is evident. For this reason phase shift methods for analyzing the cross section do not seem to apply here.

Chapter 7

References

1. A. B. Bassett, A Treatise on Hydrodynamics, Dover Publications (New York, 1961), (originally published: Deighton, Bell and Co., 1888), p. 229.

Appendix - 1

Some Properties of Liquid He^4 ,
and of Liquid He^3 - He^4 Mixtures

A. Roton Densities

Since the energy of a roton is large compared with temperature of He II, Maxwell-Boltzmann statistics apply, and:

$$N_r = \frac{V}{(2\pi)^3} 2\pi \int \exp\left\{-\left(\Delta + \frac{\hbar^2(k-k_0)^2}{2\mu_r}\right)/kT\right\} k^2 dk$$

Only a small error is introduced by extending the limits of integration to ∞ , since $\exp(-x^2)$ drops off rapidly. The result of the integration is:

$$\frac{N_r}{V} = \frac{K k_0^2}{(2\pi)^{3/2}} \exp(-\Delta/T) \left(1 + \frac{1}{2} \frac{K^2}{k_0^2}\right)$$

where $K = \sqrt{\frac{2\mu_r kT}{\hbar^2}}$. In most derivations, $k^2 dk$ is approximated by $k_0^2 dk$ and the second term is not present. The value of $\frac{\hbar^2 k_0^2}{2\mu_r}$

when expressed as a temperature is about 140°K, so that this second term contributes about 1/2% numerically and can be dropped. The error in replacing the Bose distribution function by the Maxwell-Boltzmann function is on the order of $\exp(-\epsilon/kT)$ or about e^{-5} to e^{-7} for the temperatures in the experiment and is numerically insignificant. Similarly the error in extending the $(k-k_0)^2$ parabola to ∞ can be estimated at about 1% from error function tables.

The neutron scattering data,^{(1), (2)} on which the roton parameters are based, indicate that the energy gap Δ is not constant but a weak function of temperature for the temperature range of the experiment, 1.27° to 1.69°. The low temperature roton parameters are known to a relatively high precision. The energy gap $\Delta = 8.65 \pm 0.04^\circ\text{K}$, at 1.12°K. However for the temperature range of the experiment, the data are sparse, and the precision is not high. Nevertheless, empirical functions for $\Delta(T)$ have been derived by Bendt et al.⁽³⁾ which fit their neutron scattering data⁽¹⁾ below about 1.8°, and are consistent with similar data of Henshaw and Woods.⁽²⁾ Bendt et al. also calculate the entropy of He II, including contributions from all portions of the dispersion curve, and find good agreement for temperatures less than about 1.8°K. An empirical fit which agrees with both the entropy and neutron scattering data is $\Delta = 8.68 - .0084T^7$. There is no physical basis given for this expression, and ab initio one would expect Δ to be a function of the number of excitations already present. However in the absence of better neutron data or a better model, the above expression is used in tabulating roton densities and other properties. Some numerical data for a few of temperatures in the experiment are given below.

<u>T</u>	<u>$\Delta = 8.68 - .0084 \cdot T^7$</u>	<u>N_r/V</u>
(°K)	(°K)	(1/cm ³)
1.274	8.63	$7.0 \cdot 10^{19}$
1.409	8.59	$1.45 \cdot 10^{20}$
1.564	8.49	$3.0 \cdot 10^{20}$
1.693	8.35	$5.1 \cdot 10^{20}$

B. Numbers of Phonons

Phonons in liquid helium presumably represent density fluctuations and the number density, and thermodynamic functions are calculated in a manner similar to that for solids, except that no transverse modes can exist in the liquid. The number density is

$$N_{\text{ph}} = \frac{6}{5\pi^2} (kT/kc)^3$$

$$N_{\text{ph}} = 4.2 \cdot 10^{19} \quad \text{at } 1.27^\circ$$

$$= 1.0 \cdot 10^{20} \quad \text{at } 1.69^\circ$$

C. Fountain Pressure in Liquid Helium as a Roton Kinetic or Osmotic Pressure*

The "fountain pressure" is a hydrostatic pressure which develops between two vessels connected by a fine channel "superleak" across which a small temperature is applied.

* This elementary derivation may be well known, but the author has never seen a similar exposition.

This pressure is well understood in terms of two fluid hydrodynamics, and is given by: ⁽⁴⁾

$$\Delta P_f = \rho S \Delta T$$

where S is the entropy per unit mass. Consider the roton contribution to this pressure. The entropy per unit volume of the roton gas is given by: ⁽⁵⁾

$$\rho S_r = \frac{(2K\mu)^{1/2} \rho_0^2 \Delta}{(2\pi)^{3/2} h^3 T^{1/2}} \left(1 + \frac{3}{2} \frac{KT}{\Delta}\right) e^{-\Delta/KT}$$

But this is just:

$$\begin{aligned} \rho S_r &= n_r \left(\frac{\Delta}{T} + \frac{3}{2} k \right) = n_r k + kT \frac{dn_r}{dT} \\ &= \frac{d}{dT} (n_r kT) \end{aligned}$$

Thus: $\frac{dP_f}{dT} = \frac{d}{dT} (n_r kT) \quad \text{or} \quad P_f = n_r kT$

Thus the thermomechanical pressure is just the kinetic pressure of the roton gas. The form is the same as Vant Hoff's Law for an "osmotic pressure" arising from considering the rotons as solute atoms in the superfluid.

II. Dilute He³-He⁴ Mixtures

A. Phase Separation ⁽⁶⁾

For the temperatures of interest in the experiment He³ dissolves in He⁴, and there is no phase separation. In fact no phase separation occurs at all above .9°K

B. Osmotic Pressure ⁽⁷⁾

The He³ solute atoms exert an osmotic pressure:

$$P_{os} = n_3 kT$$

C. Vapor - Liquid Equilibrium⁽⁸⁻¹⁴⁾

The solution is not "ideal" in the sense that the partial He³ and He⁴ vapor pressures are related in a complicated way, and in particular, the ratio of the concentration in the vapor to that in the liquid:

$$\frac{C_V}{C_L} \neq P_{30}/P_{40}$$

where P_{30} , P_{40} are the vapor pressures of pure He³ and pure He⁴ at the given temperature. For sufficiently dilute solutions, however, "Henry's Law" is satisfied,

the amount of He³ in the vapor is proportional to the liquid concentration. The available data indicate that this relationship holds for $C_L \lesssim .02$, that is

$$\frac{P_3}{P_4} / \frac{N_{3L}}{N_{4L}} \equiv \frac{C_V}{C_L} \quad \text{is independent of concentration}$$

for liquid concentration less than about 2%. (Note

that P_4 is very close to P_{40} for dilute solutions, and

it is P_3 not $\frac{P_3}{P_3 + P_4}$ which is independent of concentration.

in the above relationship.) Numerical values of the

He³ vapor concentration were desired to determine the

effect of the flux of He³ which passed from the vapor

to the liquid as the diffusion progressed. (See Chapter 3

Section IV.)

There are a number of papers in which measurements of C_V/C_L or of related quantities are presented. The values presented therein are not in total agreement with one another, so that data had to be obtained by averaging the various measurements. The work of Essel'son and

and Berezniak,⁽⁸⁾ which covered a wider range of concentrations than the other papers, was combined with that of Sommers⁽⁹⁾, Sreedhar and Daunt⁽¹⁰⁾, and a small portion of that of Roberts and Sydorik⁽¹¹⁾ who worked at higher concentrations. The discussions contained in several books and a review article (Peshkov⁽¹²⁾, Atkins⁽¹³⁾, and Wilks⁽¹⁴⁾) were also considered. Data from the various sources were reduced to the form C_V/C_L (in some of the papers, P_{total} , or X_V/X_L , where $X_V = N_{3V}/(N_{3V} + N_{4V})$, was given).

Results for two temperatures are tabulated in figure 22. The composite curve for C_V/C_L extrapolated to zero concentration is plotted versus temperature in figure 23. C_V/C_L varies from about 20 to about 75 over the temperature range of the experiment. The precision of the extrapolated values is about 10%, and is adequate for the analysis done in the experiment.

D. Spectrum⁽¹⁵⁾

Measurements of the specific heat of solutions, and the velocity of sound are consistent with thermodynamic quantities calculated assuming that the He^3 solute atoms behave like an ideal gas of "quasi particles", each having an energy spectrum:

$$E = - \epsilon_0 + \frac{\hbar^2 k^2}{2m_3^*}, \quad \text{where}$$

$$m_3^* \approx 2.7 m_3.$$

Figure 22 Vapor Enhancement

Summary of Data for 2 Temperatures

o's Essel'son & Berezniak
 x's Sreedhar & Daunt
 Δ's Sommers
 +'s Roberts & Syderiak

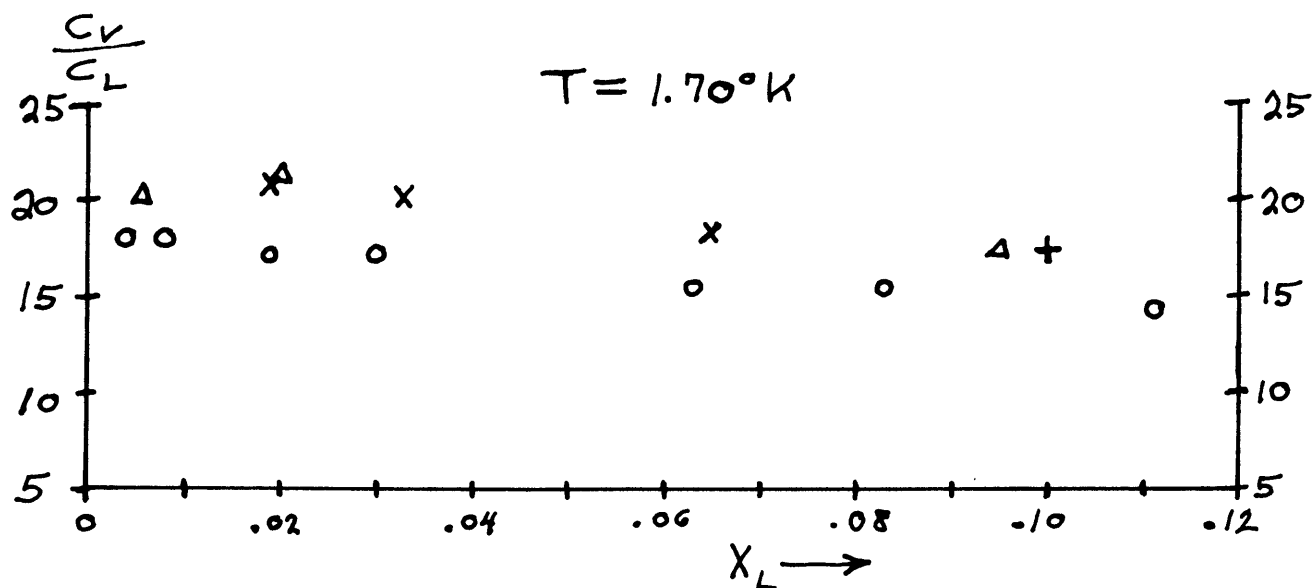
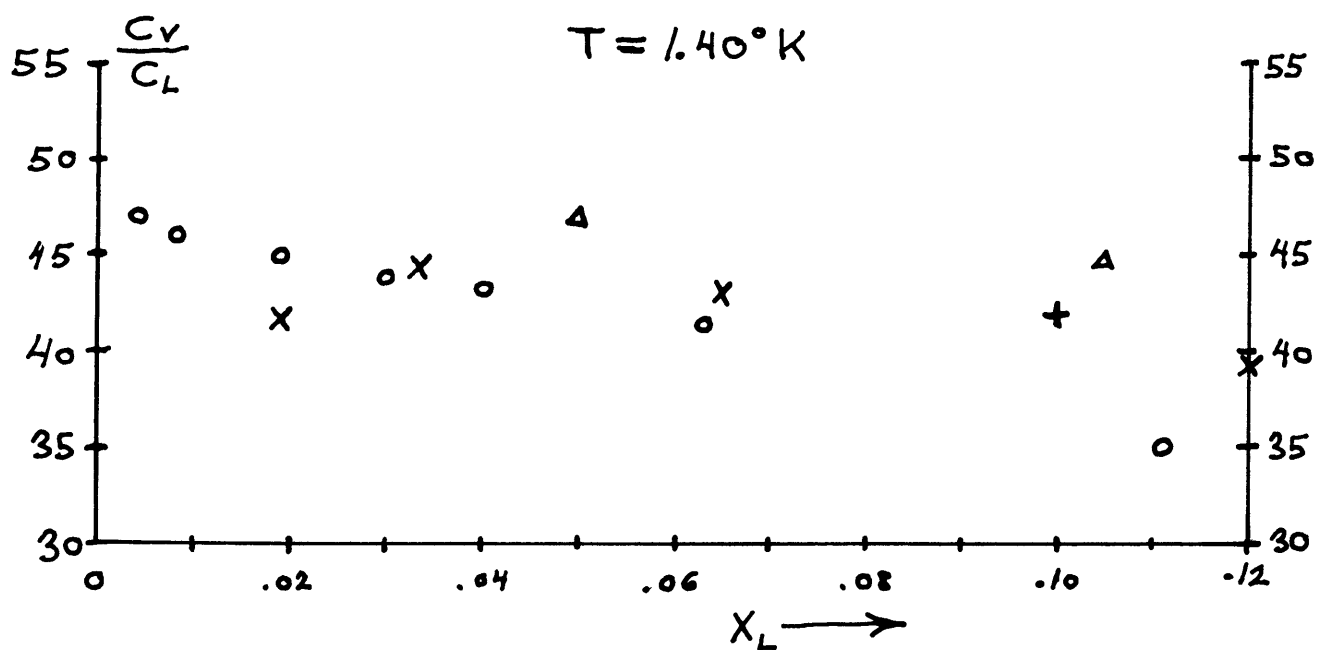
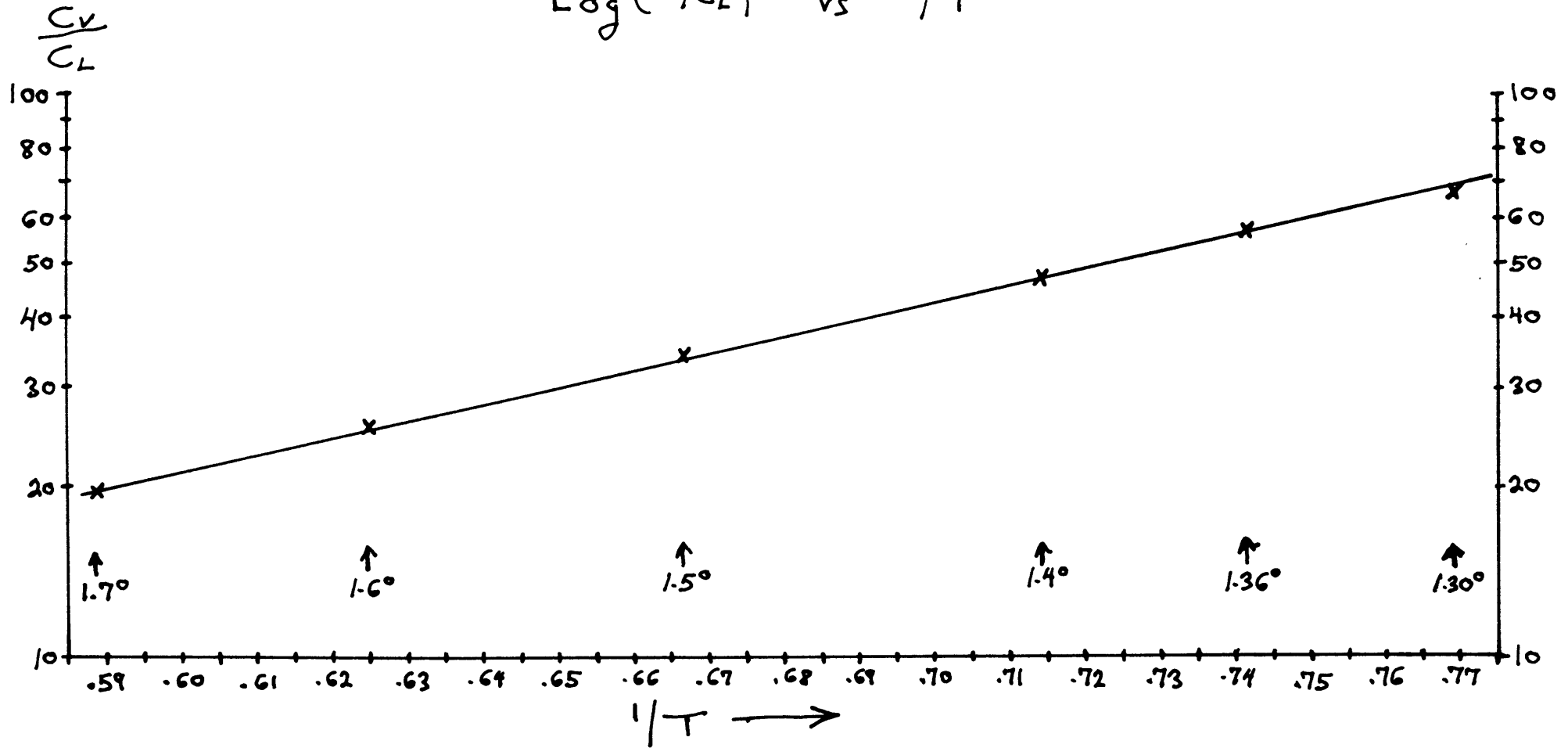


Figure 23 - Composite Vapor Enhancement Data
At Low Concentration

$\text{Log}(C_V/C_L)$ vs $1/T$



The presence of a thermal current in a $\text{He}^3\text{-He}^4$ mixture implies a flow of thermal excitations. Since the excitations interact with the He^3 solute atoms, these atoms are "dragged along" by the thermal current, producing an increase in the He^3 concentration near the coldest part of an apparatus. This phenomenon, has been referred to many times in the literature and has been used to extract He^3 from a mixture of the two isotopes⁽¹⁶⁾. It is usually present as an unwanted side effect, and some papers describe apparatus which are equipped with mechanical stirrers to avoid this "heat flushing" effect.

1. J. L. Yarnell, G. P. Arnold, P. J. Bendt, and E. C. Kerr, Phys. Rev. 113:1379 (1959).
2. D. G. Henshaw, and A. D. B. Woods, Phys. Rev. 121:1266 (1961).
3. P. J. Bendt, R. D. Cowan, and J. L. Yarnell, Phys. Rev. 113:1386 (1959).
4. H. London, Proc. Roy. Soc. A171:484 (1939).
5. I. M. Khalatnikov, An Introduction to the Theory of Superfluidity, Tr. Hohenberg, Benjamin (New York, 1965), p. 12.
6. See for example: J. Wilks, Properties of Liquid and Solid Helium, Oxford Press, (Oxford 1967) p. 228.
7. D. H. N. Wansink, and K. W. Taconis, Physics 23:125 (1957).
8. B. N. Essel'son and N. G. Berezniak, Sov. Physics JETP 3:568 (1956).
9. H. S. Sommers, Phys. Rev. 88:113 (1959).
10. A. K. Sreedhar, and J. G. Daunt, Phys. Rev. 117:891 (1960).
11. S. G. Sydoriak and T. R. Roberts, Phys. Rev. 118:901 (1960).
12. V. N. Peshkov, Sov. Phys. Uspekhi 11:209 (1968).
13. K. R. Atkins, Liquid Helium, Cambridge Univ. Press (Cambridge, 1959), Chapter 9.
14. J. Wilks, op. cit. , p. 226.
15. I. Pomeranchuk, Zh. E. T. Fiz. 19:42 (1949).
16. C. Reynolds, H. Fairbank, C. T. Lane, B. McInteer, and A. Nier, Phys. Rev. 76:64 (1949).

BIOGRAPHICAL NOTE

George Arthur Herzlinger, of Milburn, New Jersey, was born on June 16, 1943. In June of 1965, he received a Bachelor of Science degree from the Massachusetts Institute of Technology, in Cambridge, Massachusetts. His undergraduate thesis was entitled "Diffraction Patterns of Lunar Occultations."

In the period from 1965 to 1967, he was a teaching and research assistant at the University of Maryland. Since that time, he has been a Ph.D. candidate in the Department of Physics at the Massachusetts Institute of Technology. He has worked on the present research since October, 1968.

He is married to the former Regina Elbinger, of New York City, an Assistant Professor of Business Administration at Harvard University, in Cambridge, Massachusetts.